Stellingen

behorende bij het proefschrift
Quantum phenomena in networks of Josephson junctions
van Wiveka Elion

1. De hoge waarde van de barrière voor thermisch geactiveerd transport van vortices gemeten in een array door Tigh et. al. wordt niet, zoals gesuggereerd veroorzaakt door inhomogeniteiten in het array maar is een systematisch verschijnsel dat optreedt in arrays dicht bij de supergeleider-isolator overgang.
   T. S. Tighe, A. T. Johnson and M. Tinkham, Phys. Rev. Lett. 44, 10286 (1991) en hoofdstuk 2 van dit proefschrift.

2. Een klein array waarop een geschikt magneetveld wordt aangelegd, vormt een quantum dot voor vortices.

3. Voor het uitvoeren van akoestische metingen aan gesteentes is vloeibare honing het beste contactmiddel tussen de samples en de akoestische plaat. Voor longitudinale golven, die ook voor medische toepassingen gebruikt worden voldoet de in de kliniek gebruikte gel.

4. Thermospanningsmetingen zijn niet geschikt voor het bepalen van het teken van de ladingsdragers in een vaste stof.

5. Voor de in het laboratorium gebruikelijke toepassingen kan GE varnish verdund worden met alcohol, in plaats van met het gebruikelijke mengsel van alcohol en de giftige stof tolueen.

6. Het thema noodlot is belangrijk in de werken van Van Schendel alsook in die van Couperus. Waar bij de eerste het accent op 'nood' ligt, is bij de laatste het 'lot' het belangrijkste.

7. Aan natuurkundigen die in hun onderzoek het geluk steeds lijken aan te trekken, schrijft men een goede fysische intuïtie toe.

8. Een goede strijkersgroep in een symfonieorkest wordt aangevoerd vanuit de achterste lessenaars.

9. In Guatemala zijn de universele rechten van de mens een relatief begrip.

10. Het meest vernieuwende element uit de authentieke uitvoeringspraktijk van barokmuziek is de her-introductie van de improvisatie binnen de klassieke muziek.

11. Het antwoord op de aan een sollicitant gestelde vraag ,,Wat zijn uw slechte eigenschappen ?" levert voornamelijk informatie over haar of zijn ervaring met solliciteren.

12. Het programma van de International Conference of Low Temperature Physics leent zich uitstekend voor het aanmaken van een kampvuur.

Delft, maart 1995

Quantum phenomena in networks

of Josephson junctions

Quantum phenomena in networks

of Josephson junctions

Proefschrift

ter verkrijging van de graad van doctor
aan de Technische Universiteit Delft,
op gezag van de Rector Magnificus Prof. ir. K. F. Wakker,
in het openbaar te verdedigen ten overstaan van een commissie,
door het College van Dekanen aangewezen,

op donderdag 13 april 1995 te 13.30 uur

door

Wiveka Jacoba ELION

doctorandus in de natuurkunde,
geboren te Leiden

Dit proefschrift is goedgekeurd door de promotor:

Prof. dr. ir. J. E. Mooij

Promotie commissie:

Prof. dr. G. B. J. Schön

Prof. dr. C. W. J. Beenakker

Prof. dr. C. van Haesendonck

Prof. dr. J. van Himbergen

Prof. dr. G. E. W. Bauer

Dr. D. Estève

Preface

The most well-known property of a superconductor is that it conducts extremely well. It is not so clear what will happen if two pieces of superconducting material are separated with an insulating barrier. In our everyday world, no system is stronger than its weakest link and one would expect a superconductor-insulator-superconductor junction to be insulating. Only thirty years ago physicists knew, that because electrons are quantum-mechanical particles, there is a finite probability that they hop, or tunnel, through an insulating barrier. In a superconductor however, charge carriers are paired, forming Cooper pairs, and the probability that the two particles constituting a pair would tunnel together seemed to be too small to cause an observable current. This belief was so strong that when supercurrents were actually observed in fabricated junctions, the current was attributed to shorts in the insulating barrier. In his Nobel prize lecture, Brian Josephson tells how he, as a 19 year old graduate student, proved that these ideas were wrong. Because of the macroscopic coherence within a superconductor, tunneling rates for Cooper pairs can be much larger than those for electrons. The supercurrent depends on the difference between the 'phases' of the superconductors, which is a variable that was theoretically defined but until then did not seem to be observable.

Since the discovery of the Josephson junction, many experiments have been performed and theories checked. An interesting question was raised by Anderson, who considered the fact that a junction also forms a capacitor. When a Cooper pair tunnels onto a superconductor that is connected to the outside world with junctions only, the junction capacitors will be charged. What happens when the required energy, the charging energy, is not available? He proposed that when junctions are small and the temperature is low enough, the flow of current will be blocked. In this case the phase difference is no longer a meaningful variable. According to the laws of quantum mechanics it will strongly fluctuate.

In this thesis several experiments on vortices in two-dimensional arrays of junctions, and also on smaller networks will be reported on. All networks consist

of junctions in the intermediate regime, where phase fluctuations are strong but the Cooper pairs still flow through the junctions. The "Quantum phenomena" in the title of this thesis refers to the quantum interference, phase transitions, tunneling and the Heisenberg uncertainty relation that are observed in this regime. This illustrates how the word 'quantum' in our field has become equivalent to 'new' or 'interesting', as it is impossible to explain classical superconductivity, let alone Josephson currents, without using the framework of quantum mechanics.

Wiveka Elion
February 27, 1995

Contents

Chapter 1

Introduction

1.1 Phase and charge as non-commuting variables

An essential property of the superconducting state is that charge carriers can be described with one macroscopic wavefunction [1]. The amplitude of this wavefunction is easily interpreted as the density of paired charge carriers, Cooper pairs. The physical importance of the phase of the superconducting wavefunction became clear with the discovery of the Josephson effect [2]. When two pieces of superconducting material are connected via a thin insulating barrier, as shown in Fig. 1.1, a supercurrent will flow that depends on the difference between the phases φ_1 and φ_2 as $I = I_c \sin(\varphi_1 - \varphi_2 - \int_1^2 \mathbf{A} dl)$. Here $\mathbf{A}$ is the magnetic vector potential integrated over the distance between the two superconductors. The term $(\varphi_1 - \varphi_2 - \int_1^2 \mathbf{A} dl)$ is known as the gauge-invariant phase difference ϕ. I_c is the critical current, which is the maximum supercurrent that can theoretically flow. It depends on the energy gap in the superconductors and the resistance of the barrier [3].

$$\psi = |\psi| e^{i\varphi_1} \qquad \psi = |\psi| e^{i\varphi_2}$$
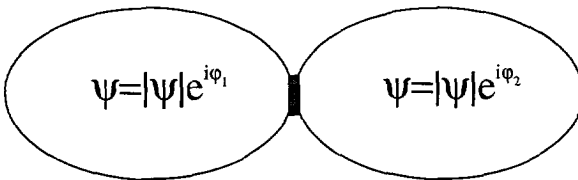
Figure 1.1: *The original system considered by Josephson and Anderson, two superconducting grains coupled by an insulating barrier.*

Anderson [4] was the first to realize that also the total capacitance C_Σ of a piece of superconductor plays an important role. When a Cooper pair tunnels onto the superconductor, the electrostatic energy of the system is increased by an amount $(2e)^2/2C_\Sigma$. At that time it was not possible to fabricate junctions with such small capacitances that this electrostatic energy is smaller than the thermal fluctuations. It was however realized that because the charge on the island and the phase of the superconducting wavefunction are non-commuting variables a Heisenberg uncertainty relation holds of the form $\Delta Q \Delta \phi \geq e$ If the electrostatic energy involved is small compared to the Josephson coupling energy $E_J = (\Phi_0/2\pi)I_c$, the phase is a well defined variable and Cooper pairs will flow freely. If the electrostatic energy is large the number of Cooper pairs is fixed and the phase is undetermined.

With present day nano-technology it is possible to fabricate junctions in both regimes and experimentally study the competition between Josephson and charging effects. A complete treatment of junctions in the superconducting regime can be found in ref. [5]. An overview of the physics in the charging regime is given in ref. [6]. While these regimes are often referred to as "classical" and "quantum" regime respectively, we will reserve the word quantum for quantum fluctuations of either phase or charge in the regime where both energy scales are comparable. Here we will discuss one example in this intermediate regime in some detail to illustrate the importance of the Heisenberg uncertainty relation between charge and phase.

Consider the system shown in Fig. 1.2. Two junctions in series are connected to a voltage source. On the island in between the junctions a charge Q_g can be induced by applying a gate voltage U to a small capacitor C_g. The island is coupled with a third junction to a large superconducting reservoir. This third junction has a variable Josephson coupling energy $E_J(\Phi)$.

Setting the bias voltage V, the gate voltage U and the variable coupling energy of the third junction all equal to zero the Hamiltonian becomes:

$$H = \frac{Q^2}{2C_\Sigma} - E_J \cos(\varphi_l - \varphi) - E_J \cos(\varphi - \varphi_r), \qquad (1.1)$$

where Q is the charge on the island, C_Σ is the total capacitance of the island, φ is the phase on the island and φ_l and φ_r are the phases of the left and the right contact respectively. Due to the low impedance of the leads to the voltage source the phases of the superconducting contacts will be classical [6]. As the phase difference is the only physically relevant variable we can define $\varphi_r = -\varphi_l$ and
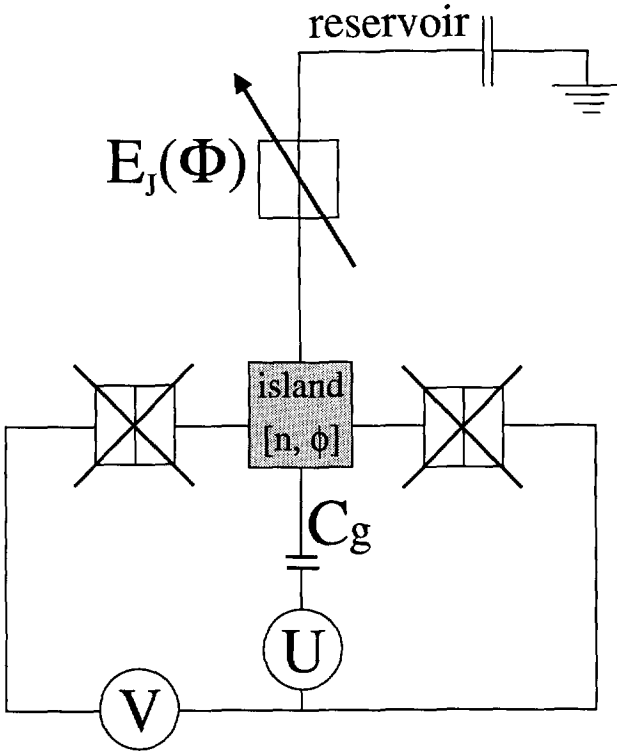
Figure 1.2: *Two small Josephson junctions in series are connected to a voltage source V. The superconducting tunnel junctions are drawn as two rectangles that represent the junction capacitor and a cross to represent the Josephson channel. The "island" in between both junctions is coupled with a small capacitor to a gate voltage source U. A junction with variable Josephson coupling $E_J(\Phi)$ couples the island to a superconducting reservoir with a phase that does not fluctuate quantum mechanically.*

separate out the quantum mechanical phase of the island in the Hamiltonian.

$$H = \frac{Q^2}{2C_\Sigma} - E'_J \cos\varphi, \tag{1.2}$$

where $E'_J = 2E_J \cos(\frac{\varphi_l - \varphi_r}{2})$

This Hamiltonian is similar to that of a single junction. For small E_J the second term can be treated as a perturbation that couples charge eigenstates. The strength of the coupling depends on the phase difference between the contacts. If the coupling is strong enough, quantum fluctuations in the charge variable lead to a supercurrent through the device.

Fluctuations in the charge variable can be enhanced by applying a voltage U to the gate that is coupled with a small capacitance C_g to the superconducting island. The influence of the gate is often expressed in terms of the induced charge on the capacitor to the gate $Q_g = UC_g$. If the gate capacitance is small, this induced charge does not change significantly when Cooper pairs tunnel on and off the island, and can be treated as a control variable [7]. The energy required to add a Cooper pair to the island will be lowered to the value of $(Q - Q_g)^2/C_\Sigma$. When the induced charge $Q_g = 2e$, the energy with and without an extra Cooper pair on the island is the same which enables resonant tunneling of Cooper pairs.

The amplitude of the quantum fluctuations in the charge on the island can also be changed by tuning the Josephson coupling of the junction that connects the island to a large superconducting reservoir (Fig. 1.2). Because the reservoir is otherwise unconnected, no DC current can flow through this third junction and the time averaged phase difference across it must be zero. However, the energy cost of quantum fluctuations of the phase φ of the island will be increased by the Josephson coupling energy of this third junction. In chapter 5 we will show how two junctions in parallel, a DC SQUID, can be used as a junction with a tunable effective Josephson coupling energy. Strong coupling means a decrease in the quantum fluctuations of φ. The corresponding increase in charge fluctuations leads to a easily measurable increase in the supercurrent though the double junction [8].

An alternative way to explain the influence of the fluctuations of the phase on the supercurrent is the following. For a given phase difference between the contacts, the energetically most favorable value of the phase on the center island is the one that corresponds to the largest supercurrent. Fluctuations around this equilibrium value will reduce the supercurrent. Changing fluctuations of the phase by tuning the Josephson coupling of the third junction will result in changing the supercurrent.

This experiment provides a clear example of how phase fluctuations correspond to localization of charge carriers. The wavefunctions of the simple system discussed above can be calculated exactly. In Fig. 1.3 we show the probability amplitude, which is the square of the wavefunction, for the variables φ and Q. The solid line gives the probability distribution for the case that the gate voltage is zero and the island is decoupled from the reservoir. The dashed line gives the distribution when the island is coupled to the reservoir with a Josephson coupling of approximately twice that of the other junctions. This coupling clearly enhances the probability of one additional or one missing Cooper pair on the island, while
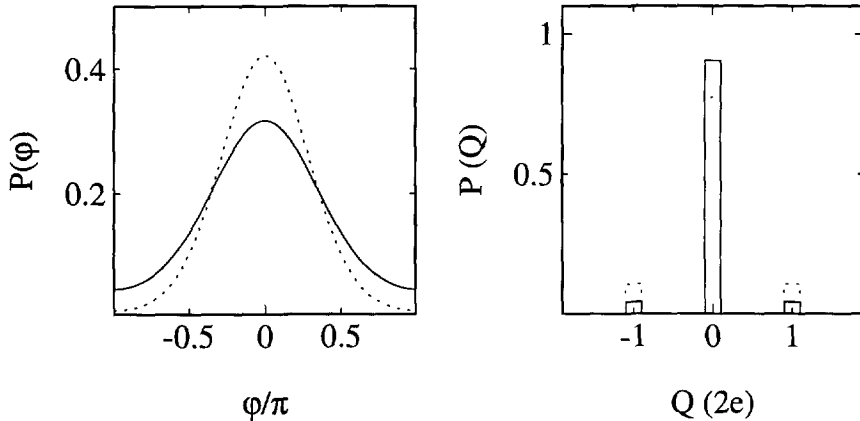
Figure 1.3: *Probability amplitude for the phase φ (left) and the charge Q (right) on the island. The solid line represents the case where there is no coupling between the island and the reservoir. The dashed line corresponds to a coupling of twice that of the other junctions.*

the distribution for the phase variable becomes more sharply peaked around its equilibrium value of zero.

The competing influence of phase and charge fluctuations also leads to interesting effects in two-dimensional networks of Josephson junctions in the regime where the Josephson coupling energy is only slightly larger than the charging energy. In section 2 we will discuss the Josephson and the charging regime in these arrays and the superconductor-to-insulator phase transitions that separate the regimes. We will then concentrate on the superconducting regime where vortices are the relevant excitations. In section 3 we will recapitulate the classical dynamics of vortices. Still in the superconducting regime, but close to the charging regime the behavior of vortices show interesting effects that will be discussed in section 4. We have observed quantum tunneling of vortices and quantum interference of vortices around an induced charge, which is a manifestation of the generalized Aharonov-Casher effect. Section 5, the discussion, deals with the similarities and differences between the dynamics of vortices in the quantum regime and the dynamics of the phase difference in small systems, like the double junction discussed above. We conclude with an overview of the remaining chapters of this thesis.
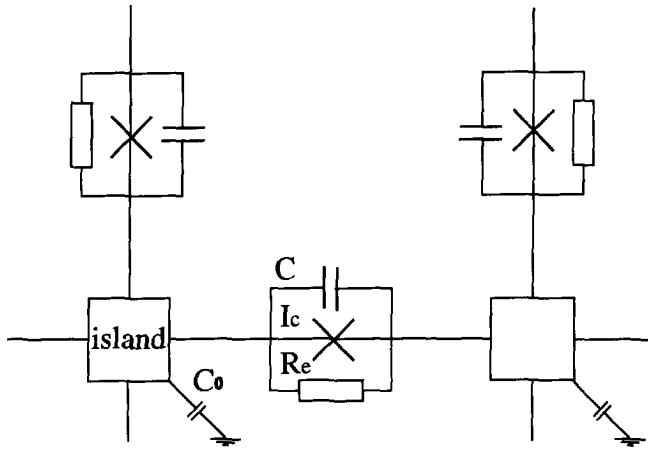
Figure 1.4: *Schematics of a Josephson junction array. Each junction can be represented as a ideal junction with critical current I_c in parallel with a capacitance C and a, voltage dependent shunt resistance Re. Each island has a small capacitance to ground.*

1.2   Phase transitions and duality in 2D arrays

The arrays that we use consist of a lattice of superconducting islands that are coupled with Josephson junctions. The schematic representation of such an array is shown in Fig. 1.4.   The junctions are underdamped $Al - Al_2O_3 - Al$ junctions. Typical values of the McCumber parameter $\beta_c = 2\pi I_c(T)CR_e^2/\Phi_0$ of the junctions vary between 1 and 50 for different samples, if it is assumed that the normal-state resistance is the effective R_e shunting the junction. The quasiparticle or sub-gap resistance at low temperatures however, is about four orders of magnitude larger. The Josephson penetration depth is of the order of the array size and shielding or self-field effects are not taken into account. Arrays are fabricated with the now standard method of shadow-evaporation that is outlined in the appendix to this chapter. In chapter one we will further discuss experimental details, here we will focus on the general physics of such a system.

Starting point for a discussion on the behavior of Josephson junction arrays is the zero-field phase diagram [9], shown in Fig. 1.5.   At zero temperature the superconducting and the charging regime are separated by a superconductor-to-insulator phase transition. Approaching from the superconducting side, the transition marks the point where fluctuations become so strong that the phase is completely delocalized and the behavior should be evaluated in terms of the num-
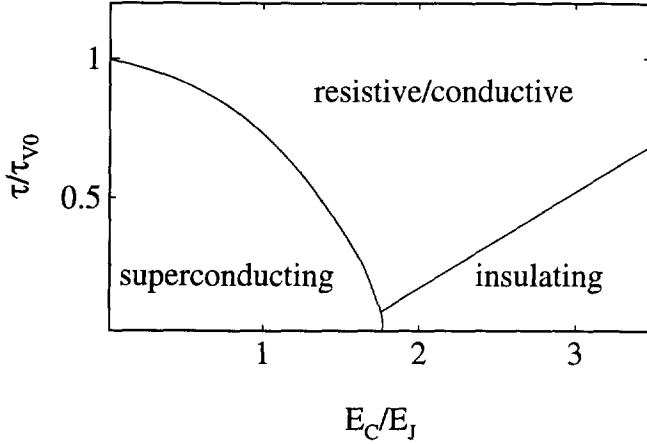
Figure 1.5: *The phase diagram as a function of the ratio of E_C/E_J and $\tau = k_B T/E_J$ in zero field. The superconducting to resistive boundary is scaled to the vortex-KTB transition temperature in the classical limit τ_{V0} as will be discussed in detail in chapter 2.*

ber of Cooper pairs on the islands. At this transition the supercurrent vanishes and the current-voltage characteristic shows a Coulomb gap. We note that this transition is well defined, in contrast with the double junction system discussed above where charging and Josephson effects coexist for a large range of E_C/E_J values.

The possible excitations in the superconducting regime are spin waves, oscillating modes of the phases around their equilibrium value, and vortices, of which an example is shown in Fig. 1.6. The vortex position is defined as the cell around which the sum of the gauge-invariant phase differences equals 2π. A sum of -2π signifies the presence of an antivortex. These excitations can be induced by thermal fluctuations or by applying a magnetic field perpendicular to the array. When raising the temperature, first bound vortex-antivortex pairs will form. At high enough temperatures these pairs unbind following the rules of the Kosterlitz-Thouless-Berezinsky (KTB) transition [10]. Apart from a short discussion of the measured KTB temperatures in chapter two, this thesis reports on experiments that are performed at low temperatures where vortices are induced by a magnetic field.

A magnetic field applied perpendicular to the array will cause vortices of one
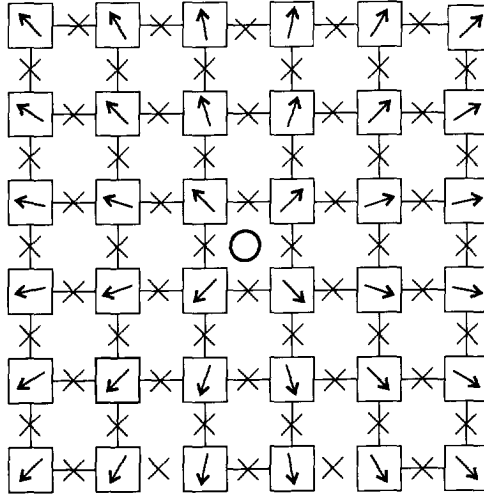
Figure 1.6: *The phase configuration that corresponds to a vortex in the arctan approximation. The arrows represent angles between 0 and 2π that correspond to phases of the superconducting wavefunction on the islands. The open circle shows the position of the vortex.*

sign to enter the array from the sides. In an infinite array the number of vortices will equal the total number of flux quanta applied to the array. The applied magnetic field is usually given in units of frustration f which is the number of flux quanta per unit cell. If there is one vortex present in every cell it can easily be verified that all currents cancel. The system is therefore periodic in f with period one. At certain values of the magnetic field, like $f = 1/2, 1/3$ and $1/4$, the vortices form a lattice that is commensurate with the underlying junction network. These commensurate states are more stable than the non-commensurate ones.

At low temperatures the vortices are generally pinned in the periodic lattice of the junction network and the array is superconducting. When current is applied to the array, vortices experience a force perpendicular to the current direction. Vortex motion will occur when the applied current exceeds the depinning current. The corresponding time-dependent phase differences across the junctions lead to finite voltages over the array. In the arrays that we have fabricated, current can be injected through superconducting busbars as shown in Fig. 1.7 . A vortex that crosses the array in a time Δt will give rise to a voltage of $\Phi_0 2\pi/\Delta t$ across the busbars.

In the charging regime excitations are formed by an extra Cooper pair, that is
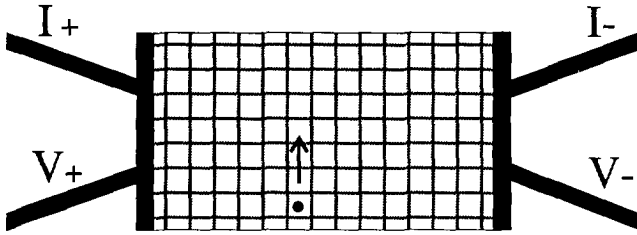
Figure 1.7: *An array that is, as in the experiment, connected to superconducting busbars to inject current and to measure the voltage. The black dot represents a vortex that moves perpendicular to the applied current.*

present on an island in addition to the equilibrium number [9]. If the capacitance to ground is smaller than the junction capacitances, a Cooper pair that resides on one island will not only charge the junctions connected to it but also junctions further away. This Cooper pair excitation is the two-dimensional analogue of a soliton [11] that occurs in systems where a number of junctions is connected in series. Like vortices in the superconducting regime, Cooper pair excitations are induced by thermal fluctuations. If all islands are connected by a small capacitance C_g to a gate, additional Cooper pairs can be induced on the islands also at zero temperature. The dynamics of these excitations in arrays in the charging regime have been predicted to be dual to the motion of vortices in the regime for large E_J. In the Josephson regime pinned vortices will be mobilized when the current exceeds the depinning current and the array changes from superconducting to resistive behavior. In the charging regime a transition from insulating to resistive behavior occurs when Cooper pairs are delocalized by applying a voltage larger than a certain threshold voltage. The experimental study of Cooper pair dynamics is hindered by the fact that there will be random offset charges present on the islands, due to charged defects in the substrate or in the junction barrier. It has so far not been possible to obtain a uniform charge frustration.

For arrays with an E_C/E_J ratio slightly smaller than the zero-field critical value a superconductor-to-insulator transition occurs as a function of magnetic field. This transition is explained using the fact that vortices are bosons and that they may exhibit quantum properties. When the density of vortices exceeds a critical value, they will Bose-condense. The resultant superfluid of vortices leads to an infinite array resistance. This transition has been observed in arrays [12] and agrees well with scaling theory [13]. From the duality of vortices and charges one expects an insulating to superconducting transition as a function

of charge frustration [14]. This charge-tuned transition has not been observed experimentally.

The field-tuned transition is a result of quantum mechanical properties of vortices. Generally one expects the dynamics of the vortices to be influenced by phase fluctuations in arrays that have an E_C/E_J ratio close to the critical value. Before discussing results of these quantum properties we will briefly summarize the relevant classical vortex dynamics.

1.3   Classical dynamics of vortices

Typical for underdamped arrays is that the junction capacitance plays an important role in the array dynamics. The voltages that are induced by the moving vortex will charge these capacitors. The corresponding electrostatic energy is proportional to the vortex velocity squared, and can be viewed as the vortex kinetic energy.

For a single vortex in an infinite array it has been proposed [15, 16, 17] that its motion along the x-axis of the array can be described by the following equation.

$$M_v \ddot{x} + \eta \dot{x} = \gamma E_J \sin(2\pi x) + I \tag{1.3}$$

Here M_v is the vortex mass, x is the vortex position in units of its cell-to-cell distance, γ is a constant that depends on the lattice geometry, η is a phenomenological damping term and I is the bias current. This equation resembles the equation of motion for the phase difference across a single underdamped junction. Instead of the relevant one-dimensional washboard potential in the case of a single junction, one can think of a two-dimensional 'egg-carton' potential in the case of an array. Just like in a single junction the mass term is proportional to the junction capacitances.

Fabricated arrays are never infinitely large and in a typical experiment there will always be more vortices present in the array. Still the single vortex model has proved useful to explain experimental results [18]. In Fig. 1.8 a typical measured *I-V* characteristic is shown of an array in the classical regime. The supercurrent corresponds to the situation where the vortex is pinned in one of the holes of the egg-carton. Above the so-called depinning current the vortex moves through the array at a speed that is determined by the damping present. This resistive regime is called the flux-flow regime. Not shown in the figure, is that there is a certain limiting vortex velocity above which the array switches to the superconducting gap voltage. If the current is still further increased, steps occur in the voltage
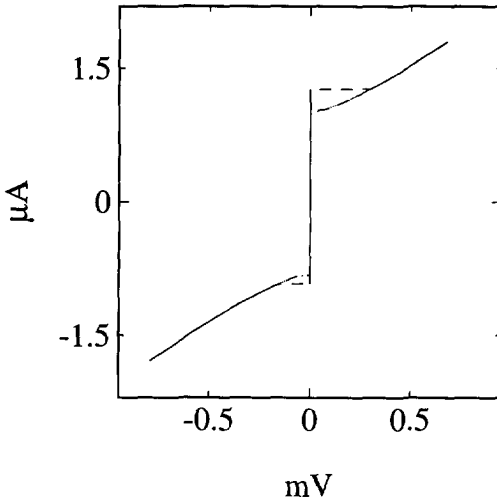
Figure 1.8: *Typical current-voltage characteristic in the superconducting regime*

corresponding to the rows of the array switching one by one. We will focus on the part of the *I-V* shown in Fig. 1.8 and will discuss the different terms of the equation of motion and their correspondence with experimental results in some more detail.

The egg carton potential has been calculated in ref. [19] in a quasi-static approach. For a square lattice, where all islands are coupled to four neighbouring islands, the cell to cell barrier is 0.2 E_J, and for a triangular lattice 0.04 E_J. The depinning currents consequently become 0.1 I_c and 0.02 I_c. In measurements on square arrays, values between 0.4 and 0.7 have been found [17, 20]. These values depend on the frustration and possibly the system size, which signifies that edge barriers or interactions between vortices do play a role. No systematic investigation of these effects has so far been carried out. Measured depinning currents for both the square and the triangular lattice agree with the predicted values for $f = 0.1$ and $\beta_c \approx 1$. For higher β_c the depinning current decreases [21].

Eckern and Schmidt [15] have calculated the vortex mass in the continuum approach. Their result is $M_v = \Phi_0^2 C/2p^2$, for a square lattice and $M_v = \Phi_0^2/3p^2$ for a triangular lattice [22] where p is the distance between vortex positions in nearest neighboring cells. Later work shows that the dynamical band mass can be up to an order of magnitude larger [23]. In the measured *I-V* characteristic hysteresis is visible around the depinning current that, just as in a single junction,

signifies the presence of the mass term in the equation of motion. In a specially shaped sample ballistic motion of vortices over 40 triangular lattice cells has been reported [24].

In simulations and analytical work on underdamped systems it has been found that moving vortices generate oscillating modes of the junctions [25, 26, 27, 28, 29, 30]. These so called spin waves provide a damping mechanism for the moving vortex even at high β_c. There is still some discussion about the possibility of a window just above the depinning current for which vortices do not couple to these spin waves, and also about the influence of the discreteness of charge already in this regime [31]. The fact that the resistance shunting the fabricated junction is frequency, or voltage, dependent is not taken into account in the theoretical work. In experiments on samples with β_c around 1 the resistance of the flux flow branch is found to be of the order of the normal-state resistance of the junctions. In these samples the single junction plasma frequency is close to the gap frequency and quasiparticles might be generated as the vortex moves. For samples with higher β_c the flux-flow resistance becomes significantly lower than the normal state resistance which indicates that spin-wave damping becomes important.

1.4 Quantum dynamics of vortices

At the superconducting side, but close to the transition, we expect to find the influence of the phase fluctuations on the dynamics of magnetically induced vortices. It has been proposed that as long as the fluctuations are not too strong, the dynamics of vortices can still be described within the single vortex model and the vortex behaves as a macroscopic quantum particle [15, 32, 33, 34]. The vortex is predicted to exhibit zero point fluctuations in this potential well in close analogy to a single junction, with a vortex plasma frequency that is $\sqrt{\gamma}\,\hbar\omega_p$ in a square array and $\sqrt{2\gamma/3}\,\hbar\omega_p$ in a triangular array, where $\hbar\omega_p = \sqrt{8E_J E_C}$ is the single junction plasma frequency. These fluctuations are expected to reduce the depinning current and also quantum tunneling of vortices through the potential barriers has been predicted.

The experiments reported in chapter two clearly show these features. In samples close to the S-I transition the depinning current is strongly suppressed. The branch below this apparent depinning current is no longer perfectly superconducting but shows a finite resistance even at the lowest measuring temperature of 10 mK. Although results can qualitatively be explained within the single junction model, quantitatively there are discrepancies that will be discussed in chapter

two.

Another clear signature of the fact that vortices have quantum mechanical properties is the observation of vortex interference around an induced charge that is shown in chapter three. It has been predicted that charge, induced on an island with a gate, plays the role of a charge vector potential for a vortex, similar to the magnetic vector potential for a charged particle. The existence of a charge vector potential can be derived in a ring shaped array [35] and from the duality between vortices and charges [36, 37]. The resulting definition for the charge vector potential is $\oint A_q dl = Q_g$.

In a ring-shaped array this vector potential can lead to quantum interference analogous to the Aharonov-Bohm [38] effect for an electron in a magnetic field. If a vortex is a macroscopic quantum particle, it will have a wavefunction of which the phase is sensitive to this vector potential. When a vortex moves around a loop that encloses an induced charge Q_g, it experiences a phase shift in this wavefunction that is equal to $\sigma = 2\pi Q_g/2e$. When a vortex moves along a doubly connected path enclosing a charge, the same phase shift is imposed on the two parts of the wavefunction. As a function of this induced charge quantum interference occurs. This phenomenon is a generalized form of the Aharonov-Casher effect, that has first been predicted for a particle with a magnetic moment [39], or a flux line in a superconductor [40], moving around an infinite line charge.

We have probed this interference in a specially designed sample shown in Fig. 3.2. Vortices can cross the sample along a doubly connected path that encloses an island on which a charge can be induced with a gate. Interference should manifest itself as an periodic changing of the number of vortices that pass at a fixed bias current. When the current is biased above the depinning current we observe an e-periodic modulation of the flux-flow resistance as a function of gate voltage. The oscillation is e instead of 2e periodic due to the presence of a finite number of quasi-particles that we will discuss in more detail in chapter three.

1.5 From double junction to two-dimensional array

In the course of this work we have investigated both small systems, such as the double junction, and 2-D arrays of different sizes. There are several connections but also differences that will be discussed here.
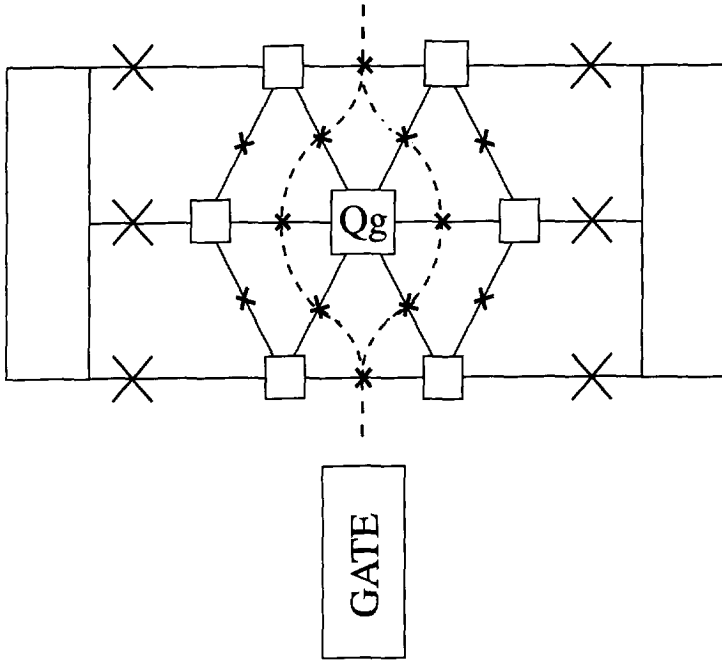
Figure 1.9: *Layout of the sample used to measure quantum interference, or the Aharonov-Casher effect, for vortices.*

A vortex crossing an array induces a phase slip of 2π and consequently a voltage difference across the busbars. Although the vortex carries no local magnetic flux, the crossing of a vortex corresponds to the crossing of a flux quantum. A phase slip across a single junction also corresponds to the crossing of a flux quantum. This is most easily shown by connecting the junction in a superconducting loop. Assuming that any electric field will be confined in the junction, a phase slip of 2π in a time Δt corresponds to a change in flux through the loop that is given by Faradays law:

$$\int_0^{\Delta t} \frac{\partial \Phi}{\partial t} = \int_0^{\Delta t} \oint \mathbf{E}.dl = \int_0^{\Delta t} \frac{\Phi_0}{2\pi} \frac{\partial \phi}{\partial t} = \Phi_0 \qquad (1.4)$$

The fact that a 2π phase slip across a junction always corresponds to the motion of a flux quantum implies that instead of the phase difference one can use a variable that has the dimensions of magnetic flux. However while the phase difference is periodic in 2π, the flux in a loop is in principle a measurable quantity

and it is not obvious that the behavior of the junction is periodic in this flux. It has been shown [42, 43, 44] that as soon as a junction is coupled to a low impedance electromagnetic environment, states differing by a phase of 2π will in principle be distinguishable. For instance if the environment is inductive the flux, and if it is resistive the dissipated energy, is at least theoretically a measurable quantity. However, if the environment impedance is higher than the quantum resistance $R_q = e^2/h$, the periodic phase variable is sufficient to describe the system. In this case the charge has to be treated as a discrete variable [44].

The supercurrent through a double junction can be described as the current at which the phase difference between the external contacts starts to move, or equivalently as the current at which flux quanta start crossing the junctions. The two possible ways for a flux quantum to cross, over the left or over right junction, effectively form a doubly connected path. We show in chapter four that the influence of a charge induced on the island between the junction can be attributed to interference of flux quanta that resembles the Aharonov-Casher effect for vortices.

An important difference between the motion of a vortex through an array and a flux quantum across a junction is that in an array a flux flow branch is present in the *I-V* characteristic. In a double junction, current can only flow at low voltages when Cooper pairs can transfer energy to the electromagnetic environment. Specific current resonances are present below the gap. In arrays that are larger than three by three cells a resistive flux flow branch is visible above the depinning current. In some smaller samples we have also observed the intermediate situation, where the current resonances are enlarged and broadened so that they exceed the depinning current and can be mistaken for a "bumpy" flux flow branch.

1.6 Thesis outline

We have tried to give the background information to the rest of this thesis as well as an overview of the physics to be discussed. Unlike in this introduction, the chapters hereafter will be presented in the order in which the described experiments were performed. In chapter two we give details of the experimental arrays and results on phase transitions and first evidence for quantum tunneling of vortices. In chapter three we discuss the experimental observation of quantum interference of vortices or the Aharonov-Casher effect. Motivated by work on the supercurrent modulations in double junctions by other groups, we investigated

the connections and differences between the two systems that are reported in chapter four. We conclude, in chapter five, with the experiment on the device discussed in the first section of this introduction, that is nicknamed the Heisenberg transistor.

Several chapters, or parts of chapters, have been published elsewhere. The most relevant references are listed below.

Chapter 2: H. S. J. van der Zant, F. C. Fritschy, W. J. Elion and J. E. Mooij,
Phys. Rev. Lett. **69**, 2971 (1992).
Chapter 3: W. J. Elion, J. J. Wachters, L. L. Sohn and J. E. Mooij,
Phys. Rev. Lett. **71**, 2311 (1993).
Physica B **203**, 497 (1995).
Chapter 4: W. J. Elion, P. Hadley, and J. E. Mooij,
To appear in Proceedings of the ICTP-NATO workshop 'Quantum dynamics of Submicron structures', eds. H. Cerdeira, B. Kramer and G. Schön (Kluwer, 1995).
Chapter 5: W. J. Elion, M. Matters, U. Geigenmüller, and J. E. Mooij,
Nature **371**, 594 (1994).
Longer publications based on chapters 2 and 3 are in progress.

1.7   Appendix: Sample fabrication

The procedure for sample fabrication is pictured in figures 1.10, 1.11 and 1.12.

mask

E-beam resist
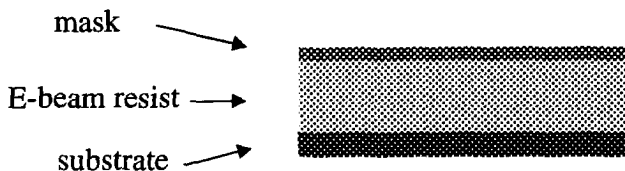
substrate

Figure 1.10: *Starting point is a silicium substrate with a 200 nm layer of electron-beam resist and a second layer of germanium or a harder type of E-beam resist. This top layer is used as a mask.*

a)

substrate   mask, partly resting on resist layer

b)

free-hanging 'bridge'
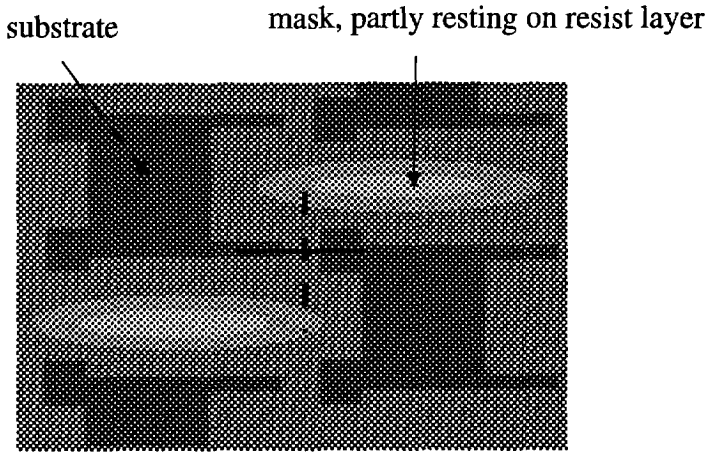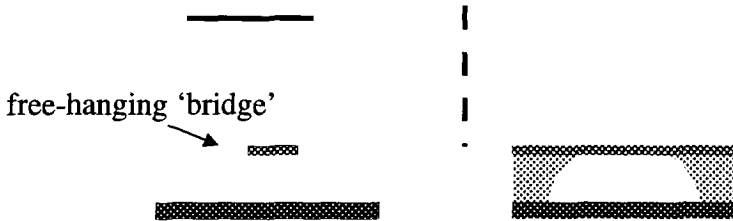
Figure 1.11: a: *Using nano-lithographic, and etching techniques a pattern is created as shown. The black figures are the places where both the resist layer and the mask layer have been etched away. Under the remaining part of the mask, the resist layer is partly etched away. The lighter elipses point out the area's where the mask rests on pilars of resist. b: Crosssections of the pattern corresponding to the solid and dashed lines in Fig. a. The underetching of the mask creates free-hanging bridges under which the junction is formed.*
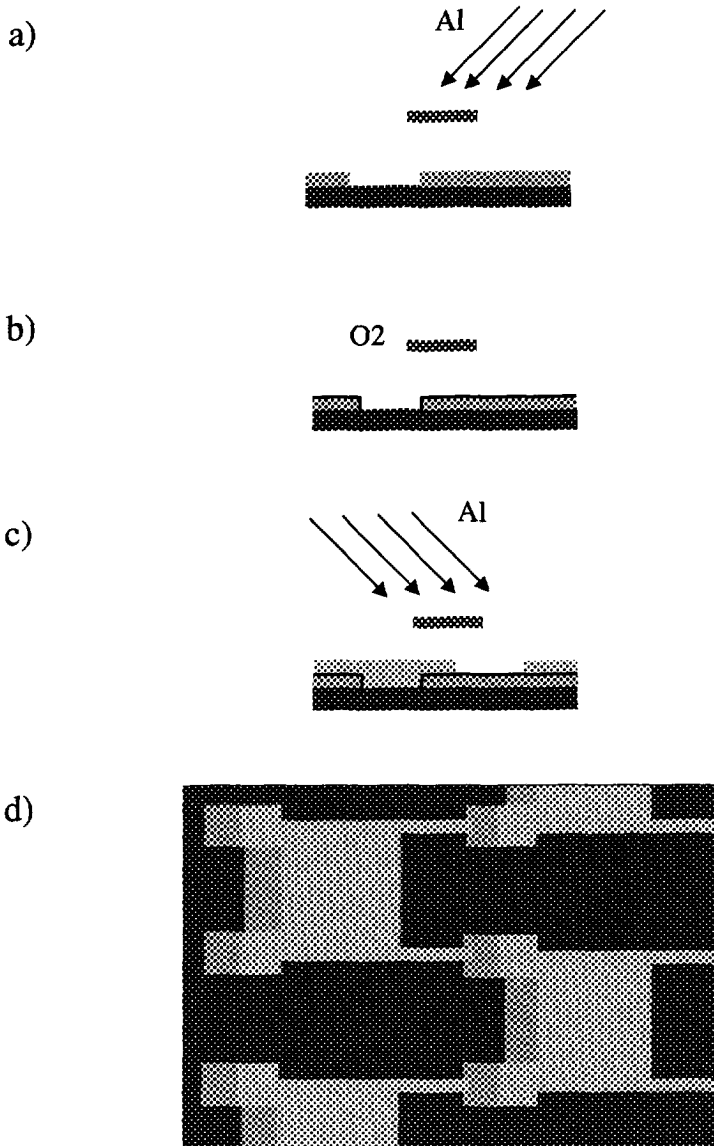
Figure 1.12: *The shadow evaporation process. a: The free hanging bridge in the mask casts its shadow on the silicium substrate when Aluminum is evaporated. b: The sample is subjected to a controlled oxygen pressure to form a barrier of the desired thickness. c: The second layer of aluminum is evaporated and the junction is formed. d: After lifting of the mask layer, an array of junctions results.*

References

[1] M. Tinkham, *Introduction to Superconductivity* (McGraw-Hill, New York, 1975).

[2] B. D. Josephson, Phys. Lett. **1**, 251 (1962).

[3] V. Ambegaokar and A. Baratoff, Phys. Rev. Lett. **10** 486 (1963).

[4] P. W. Anderson, in *Progress in Low Temperature physics* **5** ed. Gorter, C. J., 1 (North-Holland, Amsterdam, 1967).

[5] T. P. Orlando and K. A. Delin, *Foundations of Applied Superconductivity* (Addison-Wesley, New York, 1991).

[6] D. V. Averin and K. K. Likharev in *Mesoscopic Phenomena in Solids*, eds. B. L. Altshuler, P. A. Lee, and R. A. Webb, 173 (Elsevier, Amsterdam, 1991).

[7] M. Büttiker, Phys. Rev. B **36**, 3548 (1987).

[8] W. J. Elion, M. Matters, U. Geigenmüller, and J. E. Mooij, Nature **371**, 594 (1994).

[9] R. Fazio and G. Schön, Phys. Rev. B **43**, 5307 (1991).

[10] V. L. Berinskii, Zh. Eksp. Teor. Fiz. **59**, 907 (1970), J. M. Kosterlitz and D. J. Thouless, J. Phys. C **6**, 1181 (1973).

[11] P. Delsing in *Single Charge Tunneling*, eds. H. Grabert and M. H. Devoret, 249 (Plenum Press, New York 1992).

[12] H. S. J. van der Zant, F. C. Fritschy, W. J. Elion, L. J. Geerligs, and J. E. Mooij, Phys. Rev. Lett. **69**, 2971 (1992).

[13] M. P. A. Fisher, Phys. Rev. Lett. **65**, 923 (1990).

[14] C. Bruder, R. Fazio, A. Kampf, A. van Otterlo, and G. Schön, Phys. Rev. B **47**, 342 (1993) and A. van Otterlo, K,-H Wagenblast, R. Fazio and G. Schön, Phys. Rev. B **48**, 3316 (1993).

[15] U. Eckern and A. Schmid, Phys. Rev. B **39**, 6441 (1989).

[16] T. P. Orlando, J. E. Mooij, and H. S. J. van der Zant, Phys. Rev. B **43**, 10218 (1991).

[17] M. S. Rzchowski, S. P. Benz, M. Tinkham and C. J. Lobb, Phys. Rev. B **42**, 2041 (1990).

[18] H. S. J. van der Zant, F. C. Fritschy, T. P. Orlando, and J. E. Mooij, Phys. Rev. Lett. **66**, 2531 (1991).

[19] C. J. Lobb, D. W. Abraham, and M. Tinkham, Phys. Rev. B **36**, 150 (1983).

[20] H. S. J. van der Zant, unpublished results.

[21] H. S. J. van der Zant, F. C. Fritschy, T. P. Orlando, and J. E. Mooij, Phys. Rev. B **47**, 295 (1993).

[22] U. Eckern, private communication.

[23] U. Geigenmüller in *Macroscopic Quantum Phenomena*, eds. T. D. Clark et. al. (World Scientific, Singapore 1991) p 131.

[24] H. S. J. van der Zant, F. C. Fritschy, T. P. Orlando, and J. E. Mooij, Europhys. Lett. **18**, 343 (1992).

[25] P. A. Bobbert, Phys. Rev. B **45**, 7540 (1992).

[26] U. Geigenmüller, C. J. Lobb, C. B. Whan, Phys. Rev. B **47**, 348 (1993).

[27] U. Eckern and E. B. Sonin, Phys. Rev. B **47**, 505 (1993).

[28] Wenbin Yu, K. H. Lee and D. Stroud, Phys. Rev. B **47**, 5906 (1993).

[29] T. Hagenaars, P. H. E. Tiesinga, J. E. van Himbergen and J. V. Jose, Phys. Rev. B. **50**, 1143 (1994).

[30] Wenbin Yu and D. Stroud, Phys. Rev. B **49**, 6174 (1994).

[31] R. Fazio, A. van Otterlo and G. Schön, Europhys. Lett. **25** 435 (1994).

[32] E. Simanek, Solid State Comm. **48**, 1023 (1983).

[33] S. E. Korshunov, Physica B **152**, 261 (1988), A. I. Larkin, Yu. N. Ovchinikov, and A. Schmid, ibid. 266 (1989).

[34] R. Fazio, U. Geigenmüller, and G. Schön, in the Proc. of the Adriatico Research Conference on *Quantum Fluctuations in Mesoscopic and Macroscopic Systems*, (World Scientific, Singapore, 1991).

[35] B. J. van Wees, Phys. Rev. Lett. **65**, 255 (1990).

[36] B. J. van Wees, Phys. Rev. B **44**, 2264 (1991).

[37] R. Fazio, A. van Otterlo, G. Schön, H. S. J. van der Zant, and J. E. Mooij, Helvetica Physica Acta **65**, 228 (1991).

[38] Y. Aharonov and D. Bohm, Phys. Rev. **115**, 485 (1959).

[39] Y. Aharonov and A. Casher, Phys. Rev. Lett. **53**, 319 (1984).

[40] B. Reznik and Y. Aharonov, Phys. Rev. D **40**, 4178 (1989).

[41] M. H. Devoret and H. Grabert in *Single Charge Tunneling* ed. M. H. Devoret and H. Grabert, Plenum Press New York (1991)

[42] D. V. Averin, A. B. Zorin, and K. K. Likharev, Sov. Phys. JETP **61**, 407 (1985).

[43] E. Ben-Jacob, Y. Gefen, K. Mullen, and Z. Schuss, in *Proceedings of SQUID 1985*, (Walter de Gruyter and Co., Berlin, 1985).

[44] G. Schön and A. D. Zaikin, Physica B **152**, 203 (1988).

Chapter 2

Quantum phase transitions and vortex dynamics in Josephson-junction arrays

The data on 'square' arrays presented in this chapter are obtained by H.S.J. van der Zant and the data on 'triangular' arrays by W. J. Elion. A joint publication is in progress of which this chapter is an adapted version

Abstract: In Josephson-junction arrays where the Josephson coupling energy is of the same order of magnitude as the charging energy quantum phase transitions occur as a function of the ratio of these two energies and as a function of magnetic field. The dynamics of vortices in this regime shows interesting quantum-mechanical effects that we have experimentally studied in arrays with square and triangular cells.

2.1 Introduction

In superconducting two-dimensional (2D) systems like Josephson-junction arrays [1] and thin films [2], the enhancement of quantum-mechanical phase fluctuations and the corresponding localization of charge carriers induces superconductor-to-insulator phase transitions. In Josephson-junction arrays the charging effects that are responsible for localization of charge carriers are characterized by the

charging energy $E_C = e^2/2C$, where C is the junction capacitance. When the Josephson coupling energy E_J is much larger than the charging energy E_C, the number of Cooper pairs on the islands is undetermined. In this classical regime the phase of the superconducting wavefunction is a well-defined variable and any resistive behavior is due to motion of vortices. At low temperatures vortices are generally pinned in the intrinsic lattice potential so that arrays are in the super-conducting state. In the opposite limit $E_C \gg E_J$, the phase is undetermined and the Cooper pairs are localized on the superconducting islands by the Coulomb blockade. At low temperatures the arrays are insulating. This superconductor-to-insulator (S-I) transition [3, 4, 5] is shown in Fig. 2.1a, where current-voltage (I-V) curves are plotted of three different samples with increasing E_C/E_J ratio.

When E_C is of the same order as E_J, the competing dynamics between vortices and charges gives rise to new quantum effects and phase transitions. Evidence for quantum properties of vortices has been found in the observation of the in-terference of vortices [7] (the Aharonov-Casher effect) and of the field-induced superconductor-to-insulator transition triggered by a Bose-condensation of vor-tices [8, 9]. This magnetic-field-tuned transition is shown in Fig. 2.1b, where a field of 1 Gauss is used to drive the array from the superconducting state with a small critical current to the insulating state with a small Coulomb gap. This figure also clearly illustrates the duality between vortices and charges [6, 10, 11, 12]. At the superconducting side of the transition the vortices remain pinned until the bias current exceeds the so-called depinning current. At the insulating side, charges are localized by the Coulomb blockade until the bias voltage exceeds a certain threshold value.

Just as in the classical regime vortices can be induced by a magnetic field, in the insulating regime additional Cooper pairs can be brought on the islands by applying a voltage between the ground plane and the array. The resulting uniform charge distribution is known as charge frustration. The charge-vortex duality indicates the possibility of a charge-tuned S-I transition [13, 14]. Experimentally a uniform charge frustration is difficult to achieve because frozen-in offset charges are intrinsically present in fabricated arrays.

The physics of quantum vortex dynamics and phase transitions in artificially fabricated Josephson-junction arrays is closely related to work on thin granular and amorphous superconducting films. An overview on recent experiments is presented in ref. [2]. In granular films, superconducting grains are coupled by irregular Josephson junctions of different strength. The capacitance to ground of the islands is of the same order as the inter-grain capacitance whereas in
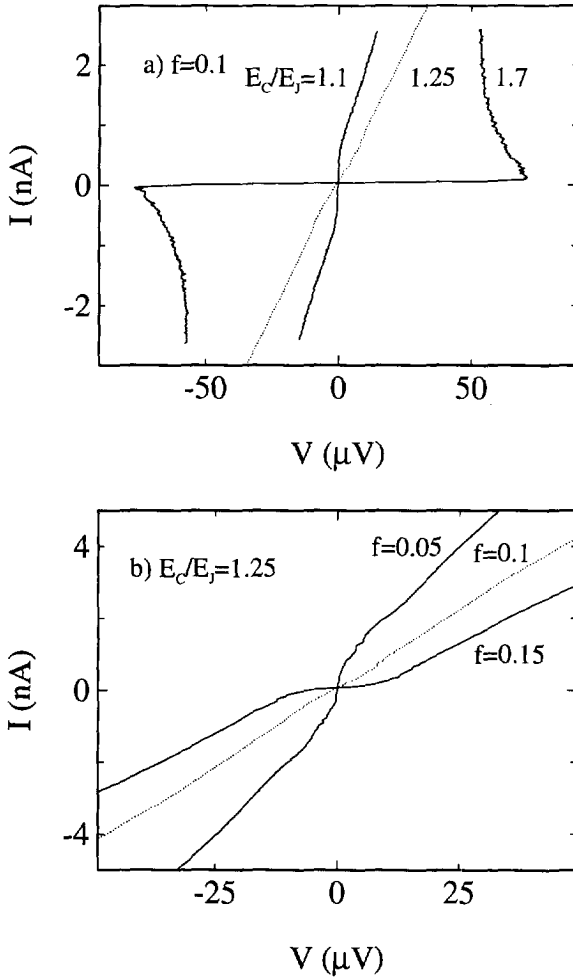
Figure 2.1: *Current-voltage characteristics measured at low temperatures as a function of a) the ratio E_C/E_J and b) the applied magnetic field, showing the crossover from superconducting-like to insulating-like behavior with a charging gap. The curve taken at $E_C/E_J = 1.7$ has been scaled with a factor of 8 in the y-axis.*

arrays the junction capacitance dominates. In amorphous films, the normal-
state resistance plays the role of the Josephson coupling and the localizing effect
of charges by random disorder can be compared to the charging effects in a
Josephson-junction array. Near the S-I transition the amplitude of the order
parameter is strongly suppressed [15], while in Josephson-junction arrays for the
fields and temperatures of interest only phase fluctuations of the order parameter
are important. Josephson junction arrays can be used as model systems for these
2D superconductors because parameters can be measured and to a large extent
varied independently. A disadvantage of fabricated arrays is that finite size effects
play a more important role than in films; typical arrays have sizes of 100 by 100
cells.

In a magnetic field the behavior of junction arrays is richer than that of films.
When in the classical limit $(E_C \ll E_J)$ a magnetic field is applied perpendicular
to the array vortices enter above some small critical field [16] and their density
increases with increasing magnetic field. Defining the frustration f as the number
of flux quanta per unit cell, about one vortex will be present per $1/f$ cells. At
fractional values of f the magnetic vortices form a lattice which is commensurate
to the underlying junction network. The stability of the vortex lattice against
a bias current leads to a decrease in the zero-bias resistance. In correspondence
with theoretical predictions [17, 18, 19] we observe dips, in order of their relative
strength, at $f = 1/2, 1/3, 1/4$ and $2/5$ in square arrays and at $f = 1/2, 1/4$
and $1/3$ in triangular arrays as is shown in Fig. 2.2. Recent work [20] shows
that in triangular arrays commensurate states occur at frustration values $f =
1/2 - 1/2N^{-1}$, where N is an integer number. In Fig. 2.2b we can clearly identify
these states for N=1 to 6. Near these fractional values of f, defects from the
ordered lattice (excess single vortices or domain walls) are believed to determine
the array dynamics. At commensurate fields with high stability such as $f = 1/2$
and $f = 1/4$ (square array) and $f = 1/3$ (triangular array) arrays qualitatively
behave in a similar way as near zero magnetic field. Because all properties of the
array are periodic in f with period $f = 1$ an increase of the applied frustration
beyond $f = 1/2$ does not lead to new physics.

Arrays in the regime where $E_C \ll E_J$ [21, 22, 23] and the regime where
$E_C \gg E_J$ [3, 24, 25] have been studied by other groups as well as ours. The
intermediate regime has not yet been investigated systematically. Here, we will
give an overview of the quantum-mechanical effects observed in these arrays and
compare them with existing theories. This chapter is organized as follows. In
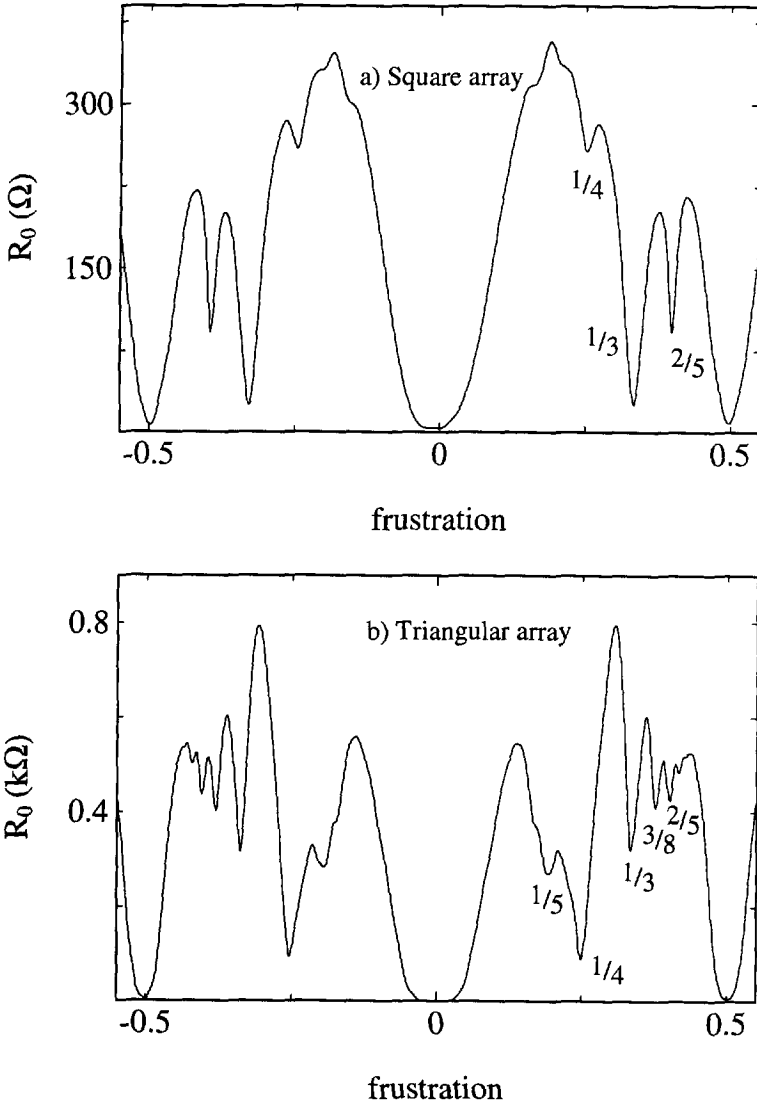the next section, we give the array characteristics and some of the experimental

Figure 2.2: *Typical plots of the zero-bias resistance versus magnetic frustration, for a) square array and b) triangular array. In addition to the commensurate states labeled in the figure, the triangular array also shows dips at $f = 5/12$ and $f = 3/7$.*

details. In section 3, we summarize results on the zero-field S-I transition as a function of the E_C/E_J ratio. In section 4 we will discuss in detail the arrays that are at the superconducting side of the zero-field phase diagram, but close to the transition. In the presence of a non-commensurate magnetic field, we observe a strong influence of the E_J/E_C ratio on the vortex dynamics. In section 5 we report on the S-I transition induced by magnetic field that is observed in the arrays closest to the transition and has been attributed to Bose-condensation of vortices. Finally we will present our conclusions and discuss the questions that remain on the vortex behavior in this regime.

2.2   Experimental details

Arrays in this study are fabricated of all-aluminum high-quality Josephson tunnel junctions with a shadow-evaporation technique [26]. The islands are coupled with small tunnel junctions to four neighbors (square cells) or to six neighbors (triangular cells). We will refer to these arrays as "square" or "triangular" respectively. The smallest junctions have an area of $0.01\,\mu m^2$. All arrays are 190 cells long (L=190) and 60 cells wide ($W = 60$). A unit cell of the array has an area (S) of $4\,\mu m^2$ and one island has an area of about $1\,\mu m^2$.

An independent estimate of the junction capacitance C is obtained from measuring the voltage offset (V_{offset}) at high bias currents at T=10 mK in a magnetic field of 2 T. Using the so-called local rule [27] and neglecting possible parasitic contributions (capacitance to ground and capacitances between islands further away) $V_{\text{offset}} = Le^2/(2C)$. We find C to be 1.1 fF for our smallest junctions leading to a charging energy ($E_C = e^2/(2C)$) of 0.84 K. The local rule is commonly used to determine the junction capacitance in small series arrays, in which the parasitic contribution is known. We find similar capacitance values in these systems when junctions are made with the same fabrication process.

We have measured C_0, the island capacitance to ground, in smaller arrays with high E_C/E_J ratio by applying a voltage between the array and the underlying ground plane. When sweeping the voltage one observes oscillations in the current just above the charging gap which, in the normal state, should have a period of e/C_0. From this experiment we find $C_0 = 12 \times 10^{-18}$ F so that for our arrays, C is at least two orders of magnitude larger than C_0.

The normal-state junction resistance R_n follows from the normal-state array resistance r_n measured at 4.2 K, $R_n = Wr_n/L$. The maximum junction critical current in the absence of charging effects and thermal fluctuations (I_c) is assumed

Sample	R_n (kΩ)	C (fF)	$\beta_c(0)$ $R_e = R_n$	E_J/k_B (K)	E_C/E_J	τ_V $(f = 0)$
S1	36	1.1	96	0.21	4.55	
S2	15.3	1.1	17.4	0.50	1.82	
S3	14.5	1.1	15.6	0.53	1.67	(0.28)
S4	11.5	1.1	12.4	0.66	1.25	0.4
S5	10.5	1.1	11.3	0.73	1.11	0.7
S6	5	1.1	5.4	1.5	0.56	0.83
S7	8	2	15.6	0.96	0.48	0.85
S8	6.8	1.7	11.3	1.1	0.45	0.88
S9	2.5	1.1	2.7	3.1	0.27	0.90
S10	3.3	3.5	11.3	2.3	0.14	
S11	1.14	1.1	1.2	6.7	0.13	0.95
T1	25.7	1.2	29	0.30	2.6	1.15
T2	23.8	1.7	39	0.32	1.7	1.6
T3	8.3	1.1	8.7	0.92	0.9	1.51
T4	4.7	1.1	7.2	1.6	0.35	1.85

Table 2.1: *Sample parameters*

to be given by the Ambegaokar-Baratoff value [28] with a measured critical temperature of 1.35 K. At low temperatures, I_cR_n=322 μV. The Josephson coupling energy of a junction E_J $(=\Phi_0 I_c/(2\pi))$ is inversely proportional to R_n. In this paper, we present data on arrays with R_n-values ranging from 1 kΩ to 36 kΩ, while junctions capacitances remain between 1-3.5 fF.

To compare the influence of the ratio of E_C/E_J on the properties of square and triangular arrays, we have to take into account that the different geometries will influence the freedom of the phases or localization of the charge carriers on the islands. In square arrays each island is coupled to four junctions while in triangular arrays each island is coupled to six junctions. The energy required to store an additional Cooper pair on an island in a triangular lattice is 2/3 times that in a square lattice with the same junction capacitances. Also we expect the freedom of the phase on the island to be determined by the Josephson coupling energy of all junctions connected to it. To account for these effects we have defined an effective ratio x as $x = E_C/E_J$ for square arrays and $x = 4E_C/9E_J$

for the triangular arrays.

In small series arrays it is known that all islands carry random offset charges that are presumably caused by charged defects in the junctions or substrate. Free charges will partly compensate these offset charges so that their value lies between $-e$ and $+e$. These charges can be nulled out by the use of a gate for each island. In a 2D array similar offset charges are expected. Here in practice they cannot be compensated because too many gate electrodes would be required, with complicated fabrication, and tuning, procedures. Some degree of intrinsic disorder is therefore present as random offset charges cause the strength of the charging energy to vary from site to site.

The degree of damping in junctions is commonly defined through the Mc-Cumber parameter $\beta_c(T) = 2\pi I_c(T)CR_e^2/\Phi_0$, where R_e is the effective damping resistance per junction. The junctions of all our arrays are underdamped ($\beta_c > 1$) even when we take $R_e = R_n$. At low temperatures and as long as the voltage across the junction is significantly lower than the gap voltage, we expect that the dissipation in the junctions is determined by the quasi-particle resistance which is orders of magnitudes larger than R_n.

At low temperatures, the flux penetration depth $\lambda_\perp(T) = \Phi_0/(2\pi\mu_0 I_c(T))$ is much larger than the array sizes so that the magnetic field is essentially uniform over the whole array. Self-induced magnetic fields can therefore be neglected in our arrays. A similar conclusion can be drawn by considering the ratio of the cell inductance (we estimate the geometrical inductance to be of the order of 1 pH) to the Josephson inductance (> 1 nA). In table I, we summarize the characteristics of the arrays that have been measured.

We measure the arrays in a dilution refrigerator inside μ-metal and lead magnetic shields at temperatures down to 10 mK. Electrical leads are filtered with rfi feedthrough filters at the entrance of the cryostat and at low temperatures by means of RC and microwave filters. Small perpendicular magnetic fields can be applied by two coils of superconducting wire, placed in a Helmholtz configuration.

2.3   S-I transitions in zero field

The S-I transitions as a function of the E_C/E_J ratio have been theoretically studied in infinite, square arrays in zero field and without disorder. Fazio and Schön [10] have calculated the phase diagram and from the vortex-charge duality estimated the critical value x_{cr} separating superconducting and insulating behavior at $T = 0$. In the absence of damping the result is $x_{cr} = \pi^2/(2a)$. The factor a

arises from the symmetry breaking term, which is the spin-wave contribution to the charge correlation function and is larger but of order one. Dissipation due to quasi-particle tunneling increases x_{cr} by a factor $(1 - \alpha_t^2)^{-1}$, where $\alpha_t = R_q/R_e$ [1].

It has been argued that the zero-temperature resistance R_{c0} at the critical point is finite so that the array acts like a normal metal right at the S-I transition [6]. From the vortex-charge duality one expects the resistance to be the quantum resistance of pairs, $R_q = h/4e^2 = 6.45$ kΩ. This value of the resistance can be thought of as the simultaneous passing of one Cooper pair and one vortex through the system. More detailed calculations on interacting bosons on a 2D lattice (Bose-Hubbard model) have shown that in the absence of disorder and dissipation R_{c0} has a universal value of $8R_q/\pi$ [29, 30]. When resistive shunting of the junctions is included, R_{c0} is expected to be of the order of $R_q/0.12$ [14].

Figure 2.3 shows the resistive transitions of six different square arrays in zero magnetic field. The array resistance per junction (R_0) is measured with a very small transport current $(< 10^{-3}I_c)$ in the linear part of the current-voltage characteristic. Three arrays become superconducting, two arrays insulating and one array close to the S-I transition shows a doubly reentrant dependence. The horizontal dashed line in Fig. 2.3 is the zero-temperature universal resistance value of $8R_q/\pi$.

The three samples that become superconducting at low temperatures, undergo a Kosterlitz-Thouless-Berezinskii (KTB) phase transition [31] with unbinding of vortex and antivortex pairs. The linear resistance above the KTB transition follows a square-root cusp dependence [32] on temperature. For classical square arrays the KTB-transition temperature is $T_V = \pi E_J/(2\epsilon_V k_B)$ with $\epsilon_V = 1.7$. When approaching the S-I transition we find that T_V decreases. At low resistance levels $(R_0 < 10^{-3}R_n)$, deviations from the square-root cusp dependence are found and the resistance decreases exponentially, indicating thermally activated behavior. We have shown that this is connected to single-vortex crossings over the finite width of the sample [16].

Two arrays become insulating, showing a continuous increase of R_0 as T is lowered. Like other groups [24, 25] we don't find evidence for an KTB transition of Cooper pairs excitations [10, 33, 34] which is possibly due to the small effective screening length [33, 35] or the presence of random offset charges [36]. Instead the measurements show an exponential decay of the conductance which is discussed in detail in ref. [24].

The resistance of sample S3 has a very remarkable dependence on temper-
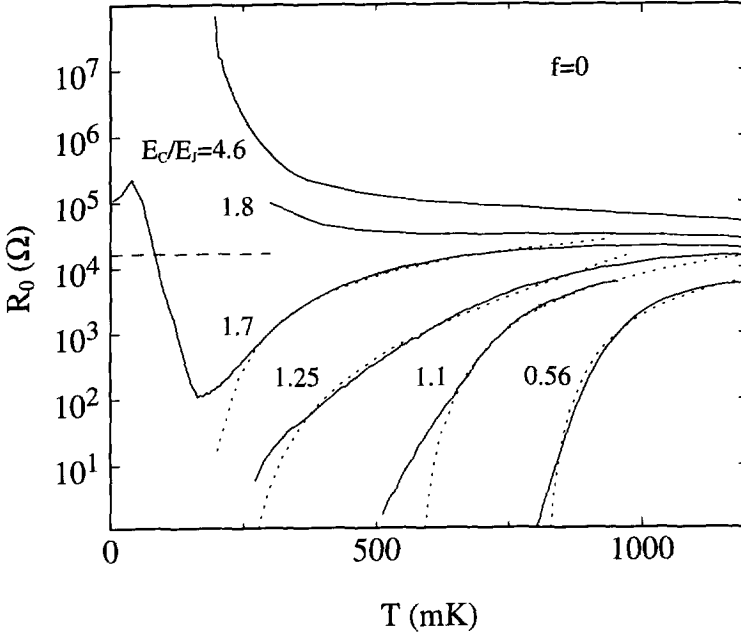
Figure 2.3: *The zero-field linear resistance per junction measured as a function of temperature for six different arrays. Curved dashed lines are fits to the vortex-KTB square-root cusp formula. The dashed horizontal line shows the zero-temperature universal resistance of the S-I transition at $f = 0$.*

ature. Starting at high temperatures, R_0 first decreases when the temperature is lowered. Over two orders of magnitude it follows the square-root cusp expression. Below T=150 mK, however, R_0 increases by more than three orders of magnitude, and at 40 mK it starts to decrease again. Singly reentrant behavior in the quantum regime is also observed in thin films [37]. It can be attributed to the influence of damping [38, 39], the combination of damping and finite size effects [40] or the presence of random offset charges on the islands [14]. For the second reentrant behavior at 40 mK we have no explanation. We have observed a clear second reentrant transition also in sample S4 at the commensurate field of 1/3 and in sample T1 at a frustration of f=0.03. It seems to be a general feature of arrays close to the transition.

Summarizing the zero-field results we have constructed the phase diagram shown in Fig. 2.4. The square and triangular markers represent data obtained on
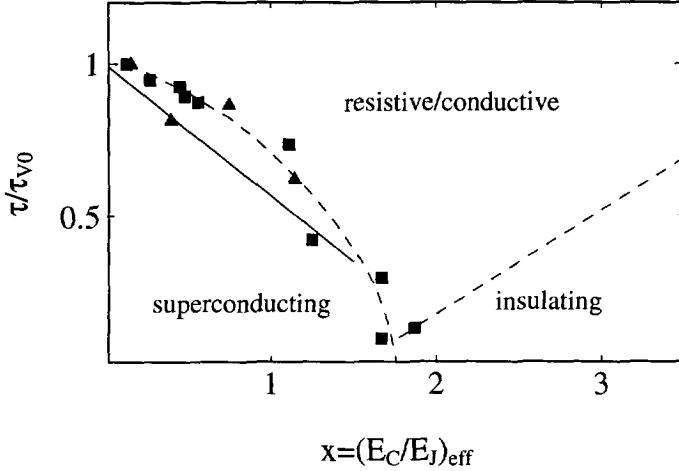
Figure 2.4: *Measured phase diagram of our arrays in zero magnetic field, showing the superconductor-to-insulator transition at $x = 1.7$. Squares represent data obtained on arrays with square cells, and triangles represent data of arrays with triangular cells. The scaling factor τ_{v0} is 1.45 for the square arrays and 1.7 for the triangular arrays. Dashed lines are guides to the eye. The solid line corresponds to theoretical results of José et. al. .The transition temperature of sample S1 at $x = 4.55$ and $\tau/\tau_{v0} = 1$ is not shown in the figure but falls on the line that separates the insulating from the conductive regime.*

square and triangular arrays respectively. The superconducting-to-normal phase boundary is the vortex-KTB phase transition. Temperature on the vertical axis in this figure is given in units of $\tau = k_B T/E_J$ and scaled to the experimentally determined KTB transition temperature τ_{V0} of the samples closest to the classical limit. For square arrays τ_{V0} is 0.95, which is close to the value of 0.9 that has been calculated [41, 42]. For the triangular arrays we find τ_{V0} is 1.7 which should be compared to the calculated value of 1.45 [19]. As a function of x a clear, systematic decrease of the KTB transition temperatures is observed, both for square and triangular arrays.

As discussed above no phase transition was observed for the insulating arrays. The data points represent the crossover from a region where $R_0 > 10^3 R_n$ to a region where $10^{-3} < R_0/R_n < 10^{+3}$. In the insulating regime, we find good quantitative agreement (within 15 %) with 'phase boundaries' from the Harvard [24]

and Chalmers [25] data when taking the same definition and specific capacitances. For the square arrays we find that $x_{cr}(f = 0) \approx 1.7$. If we neglect quasiparticle tunneling $a \approx 3$ in agreement with the predictions from Fazio and Schön [10].

The solid line in Fig. 2.4 is the result of a recent study in which corrections to the classical KTB-transition temperature are calculated using an analytic WKB renormalization group approach supported by non-perturbative Quantum Monte Carlo simulations [43]. These calculations indicate universal behavior when parameters are normalized as in Fig. 2.4. The dashed line is the Quantum Monte Carlo result which fits our data well especially in view of the absence of fitting parameters.

2.4   Vortex dynamics

In the classical regime where $E_C \ll E_J$, the dynamics of vortices is often explained in terms of non-interacting vortices obeying an equation of motion analogous to the equation for the phase difference across a single junction [44, 45, 46]. Vortices with mass M_V move in the intrinsic periodic potential of the lattice. Damping is taken into account by a phenomenological viscosity term. The cell-to-cell energy barrier E_b for a single vortex has been calculated numerically in a quasi-static approach [32] to be $E_b = \gamma E_J$, where $\gamma = 0.2$ for a large square array and 0.043 for a large triangular array. Depinning of vortices is expected at $(\gamma/2)(W + 1)I_c$.

In a continuum approach the vortex mass M_v is found to be $M_v = \Phi_0^2 C/2p^2$ for a square [44] and $\Phi_0^2 C/3p^2$ for a triangular lattice [47], where p is the distance between vortex positions in nearest neighboring cells. More recent calculations show that the dynamic band mass might be an order of magnitude larger [48].

The influence of a finite resistance shunting the junction can be translated into a vortex McCumber parameter that is $\beta_{c,v} = \gamma \beta_c$ in a square lattice and $\beta_{c,v} = 3\gamma\beta_c/2$ in a triangular lattice. In recent numerical calculations it has been shown that in an underdamped array an additional dissipation mechanism arises because the moving vortices induce oscillatory modes, called spin waves. These spin waves can lead to an effective damping that is higher than R_n [49, 50, 51, 52, 53].

For the experimental situation the single vortex model is clearly an oversimplification. Typical measurements are performed in a field of $f = 0.1$, where the distance between vortices is as small as three cells and vortex-vortex interaction may not be negligible. At the edges of the array, field dependent barriers may be present that are also not accounted for. Still several experimental results can well be explained within this model.

The temperature dependence of the zero-bias resistance (vortex creep) has been measured in square arrays. It shows exponential behavior and values for the corresponding energy barriers lie between 0.3 and 0.7 E_J [45, 54]. The depinning current at low temperatures for $\beta_c = 1$ approaches the calculated values in both square and triangular samples [23]. Lower values are found for higher values of β_c. Above the depinning current, there is a flux-flow branch where the resistance increases linearly with f for $f < 0.2$ and like in single junctions, hysteresis in the I-V curves indicates the presence of a mass term [21]. In the flux flow regime the effective damping resistance can be measured and is found to be of the order of R_n for β_c between about 1 and 50, and lower than R_n for higher values of β_c [23].

Here we will focus on the differences that we find in the vortex dynamics of arrays when approaching the S-I transition. For low vortex densities (low f and not too close to the S-I transition), we will discuss our results within the single vortex model. Theoretically it has been shown that the influence of phase fluctuations on the vortex dynamics can be modelled as a lowering of the cell-to-cell barrier, the depinning current and the vortex mass [55]. The trends that we observe in our experiments are in agreement with these predictions. Quantitatively, there are deviations indicating that the vortex dynamics near the transition are still not completely understood.

In Fig. 2.5, the resistance of sample S11 measured with a small current is shown as a function of $1/\tau$. For this array $1/\tau = 10$ corresponds to a temperature of about 650 mK. One clearly sees the exponential behavior, which extends over more than three orders of magnitude in R_0. All arrays on the superconducting side of the S-I transition show a region with exponential decay and we have fitted our data in this regime to a standard Arrhenius form with a frustration dependent energy barrier

$$R_0(\tau) = c_1 R_n e^{(-\gamma(f)/\tau)}. \tag{2.1}$$

In table II, we summarize the results of our samples giving the values of $\gamma(f)$ and c_1 for $f = 0.1$ of all samples and some f-values for one square and triangular array in particular.

The values of the energy barriers for our triangular and square arrays are plotted in Fig. 2.6a. Just as in the zero-field phase diagram we have plotted the effective ratio x on the x-axis of Fig. 2.6a and for the square arrays we have added some values obtained on arrays in the classical regime.

For square arrays the energy barriers initially increase as x increases with about a factor of four. Around $x = 1/2$, there is a sharp decrease of almost
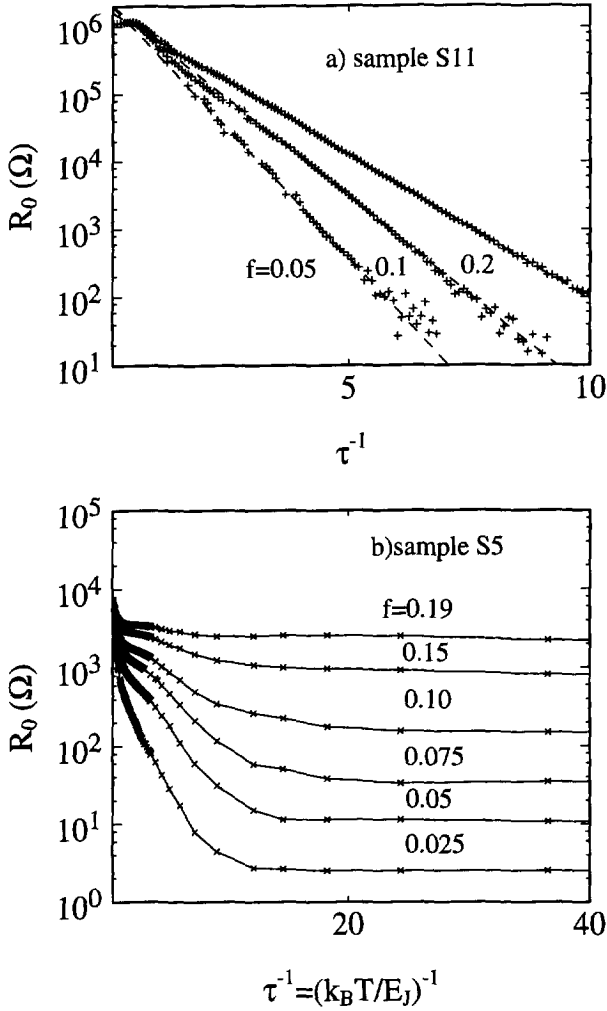
Figure 2.5: *The linear resistance per junction of array S11 (a), and array S5 (b) measured as a function of inverse renormalized temperature* $\tau^{-1} = (k_B T/E_J)^{-1}$ *for various values of the magnetic field.*
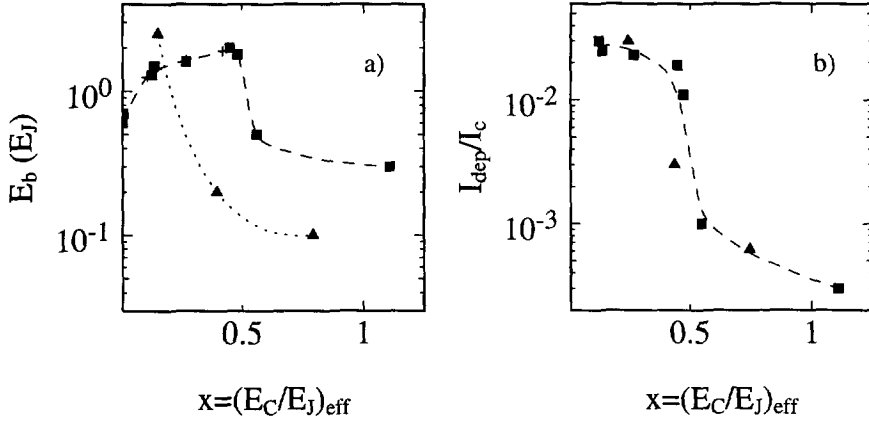
Figure 2.6: a: Energy barriers, E_b, determined from the thermally activated behavior of the zero bias resistance at $f = 0.1$, for different samples versus x. b: The array depinning current normalized to the array critical current of different samples as a function of x for f=0.1 at a temperature of 10 mK. The connecting lines are only a guide to the eye.

$2E_J$ and from that point on the energy barriers decrease. At the S-I transition, $E_b \approx 0$. Similar behavior is found for other values of the frustration. The three datapoints on triangular arrays indicate a similar sharp decrease at a slightly lower value of x, $0.15 < x < 0.4$. For the higher x values the energy barriers of the triangular arrays are about a factor of 3 smaller than those for square arrays.

Quantum fluctuations are expected to reduce the effective barrier height for vortex motion. At this point we don't have an explanation for the fact that the energy barriers initially increase as we approach the transition. When plotting the data as function of the plasma frequency of the single junctions $\omega_p = \sqrt{8E_J E_C}$ in the array, the increase of the barrier is found to be close to $\hbar\omega_p$. The sharp decrease both for square and triangular arrays occurs at the point where $\hbar\omega_p = E_J$.

In the classical regime the energy barriers are roughly proportional to the depinning current. In the case of finite zero bias resistance the depinning current is defined as the current where the voltage deviates 2 μV from the linear zero-bias, or supercurrent branch. We have determined these depinning currents as a function of x from the I-V curves at the temperature of 10 mK. In going from the classical to the quantum regime, we find that the hysteresis disappears and

Sample	f	$\gamma(f)$	c_1	R_{00} (Ω)	s_{meas}	s_{sv}	s_{meas}/s_{sv}
S4	0.1	-	-	2200	-	-	-
S5	0.025	0.7	0.1	2.6	10.2	2.6	3.9
	0.05	0.5	0.3	11	9.4	2.3	4.0
	0.075	0.4	0.5	35	8.6	2.2	4.0
	0.1	0.3	0.4	150	7.4	2.0	3.8
	0.15	0.1	0.4	850	6.0	1.4	4.3
	0.19	0.05	0.3	2300	5.1	1.2	4.4
S6	0.1	0.5	0.7	22	9.4	3.7	2.6
S7	0.1	1.8	0.1	0.02	16.7	5.7	2.9
S8	0.1	2.0	0.5	-	-	-	-
S9	0.1	1.6	0.4	-	-	-	-
S10	0.1	1.5	0.8	-	-	-	-
S11	0.1	1.3	2.0	-	-	-	-
T2	0.1	0.1	0.4	5067	3.5	0.7	5.1
T3	0.03	1.0	0.2	6.8	9.4	2.7	3.5
	0.05	0.5	0.2	74.6	7.4	2.1	3.6
	0.075	0.3	0.3	392	6.0	1.7	3.5
	0.1	0.2	0.4	746	5.7	1.5	3.8
	0.125	0.2	0.5	1057	5.5	1.5	3.6
T4	0.1	2.5	1.7	-	-	-	-

Table 2.2: *Resistive behavior*

that the critical current is largely suppressed. In Fig. 2.6b, the depinning current at $f = 0.1$ is shown as determined from the *I-V* curves. At low x the depinning current of square arrays is suppressed by about a factor of 3 and surprisingly the same for square and triangular arrays. The depinning current is clearly not proportional to the barrier height. Already in the classical regime it has been observed that the depinning current is sensitive to the amount of damping. In the quantum regime depinning will probably be triggered by quantum fluctuations. The depinning current will then not be so sensitive to the barrier height but mainly depend on the damping present.

For the samples with lowest x, those in the regime where the energy barriers decrease, we observe metallic behavior at the lowest temperatures; below a certain

critical temperature between 100 and 200 mK the resistance becomes temperature independent and remains finite down to the base temperature of 10 mK of our dilution refrigerator. In Table II we have also listed the values of the finite resistance per junction (R_{00}). We do not expect the metallic behavior to be due to an effective noise temperature of 100 mK in our heavily filtered set-up, because several samples do show a changing resistance below this temperature. For example in Fig. 2.3 we see that the resistance still changes considerably for $T < 100$ mK. We checked that varying the measuring current made no difference in $R_0(T)$ and self-heating effects can therefore also be excluded.

While at higher temperatures vortices are expected to be mobile due to thermal fluctuations, classically one would expect them to be pinned in the vortex lattice at 10 mK. The fact that we find a finite resistance at those temperatures signifies that there exist a quantum transport mechanism for vortices analogous to quantum tunneling of the phase in single junctions [56]. The exponential behavior at higher temperatures and the flattening off of the resistance at low temperatures fits well with the description of a single quantum-mechanical particle in a potential well. Assuming particles to be vortices with mass M_V tunneling through barriers of $E_b = \gamma(f)E_J$, one can estimate R_{00} from the analogy with single junctions [57] (moderate damping regime) :

$$R_{00} \approx 7.2 R_q f \sqrt{120\pi s} \ e^{-s}, \tag{2.2}$$

where s is given by

$$s = \frac{7.2}{\hbar} \sqrt{2E_b M_v} \ (1 + \frac{0.87}{\sqrt{\beta_{c,v}}}). \tag{2.3}$$

and $\beta_{c,v}$ is the vortex McCumber parameter. We have fitted our data to Eq. 2.2 and in Table II, we have listed the measured values of s as s_{meas}.

From the discussion on the measured values of the barrier height it is clear that significant modifications of the single vortex model are neccessary in this regime. However, to get a feeling for the magnitude of the measured quantum tunnel rates, we list the values that are calculated from equation 2.3 using the quasi-statically calculated, classical mass for a vortex [44], the measured barrier height and an effective damping of the normal state resistance. The measured values are about a factor of four higher than the ones calculated in the simple approximation but differences between samples and between values of frustration are small. The influence of the frustration and ratio E_C/E_J mainly manifests itself in the value of the barrier height. We could simply conclude that the results are consistent with the single vortex model using a mass that is an order of magnitude

higher than the one calculated in the static approximation. However as long as the dependence of the barrier height is not understood we do not want to stress this conclusion.

Another possible model for quantum tunneling of vortices that includes collective effects but also disorder, is variable range hopping as discussed by Fisher e.a. [58]. In this model the vortex hopping length increases with decreasing temperature. As the hopping length becomes larger than the distance between vortices the temperature dependence changes from the classical Arrhenius behavior to a power law of the form $\exp -(T_0/T)^r$, where T_0 is a function of the barrier height and r is a constant between 2/3 and 4/5. In this model a temperature independent resistance arises at low temperatures when the vortex hopping length equals the width of the finite sample. In the 60 cells wide arrays that we measured this seems not unreasonable. We have fitted the resistance in the temperature dependent regime to the predicted Arrhenius behavior at high temperatures, and the predicted power law at lower temperatures. For most arrays this does not improve the agreement. In view of the large number of fitting parameters involved we do not want to draw definite conclusions about the validity of this model.

2.5   Field-tuned transitions

In arrays with x near its critical value, where the strongest quantum fluctuations are expected there exists a critical field above which vortices Bose condense. As a Bose-condensate of vortices leads to insulating behavior this manifests itself as a magnetic-field-induced S-I transition. This field-tuned transition has been considered theoretically by Fisher [59] in disordered systems and has first been observed [60] in disordered InO_x films. In Fisher's description, at low magnetic fields vortices are pinned in a vortex glass. For higher fields, the vortex density increases and at some critical density, the vortices Bose-condense. The resultant vortex superfluid leads to an infinite resistance. Because charges and vortices are dual near the S-I transition, this transition can also be thought of as Bose condensation of charges that happens with decreasing magnetic field. In Josephson-junction arrays we don't expect vortices to form a disordered glass. Because of the disorder due to the random offset charges discussed before, the description is however adequate also for our system.

The general characteristic of this S-I transition is that when f is increased from zero, the temperature dependence of the resistance changes sign at critical values $\pm f_c$. This is visible in the $R_0(T)$ plots of Fig. 2.7. Below a critical value
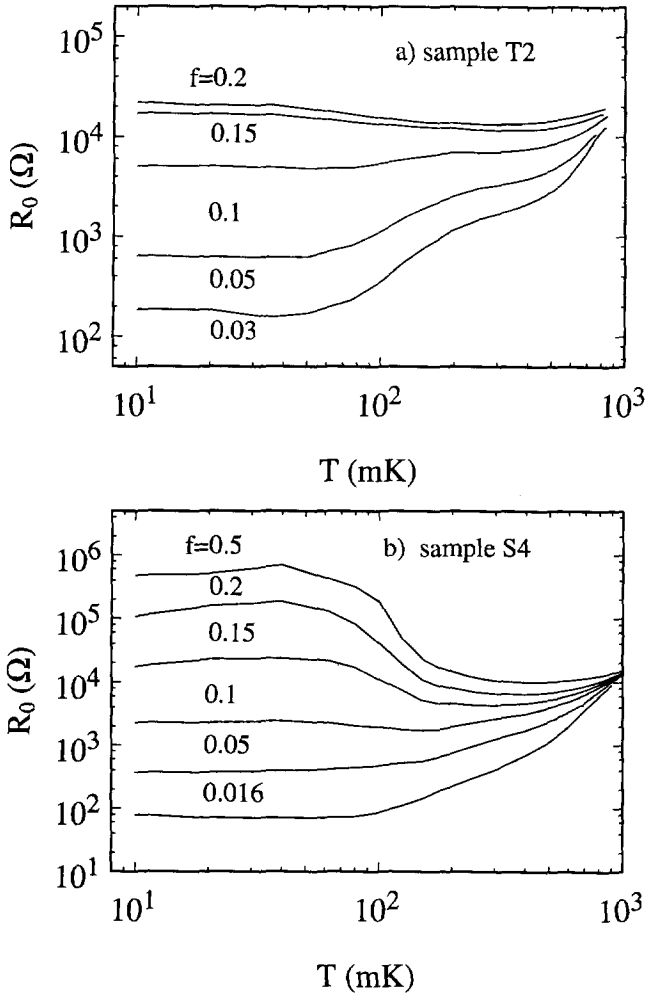
Figure 2.7: *The linear resistance of sample T2 (a) and sample S4 (b) as a function of temperature for different values of the magnetic field.*

f_c, the resistance has a tendency to decrease upon cooling down. The resistance versus temperature looks similar to the samples discussed in the previous section, including the metallic behavior at low temperatures. Above f_c the resistance has a tendency to increase and for low temperatures reaches a value that might be orders of magnitudes higher than the normal-state resistance. This sign change in the temperature dependence corresponds to the change in the *I-V* characteristic

frustration
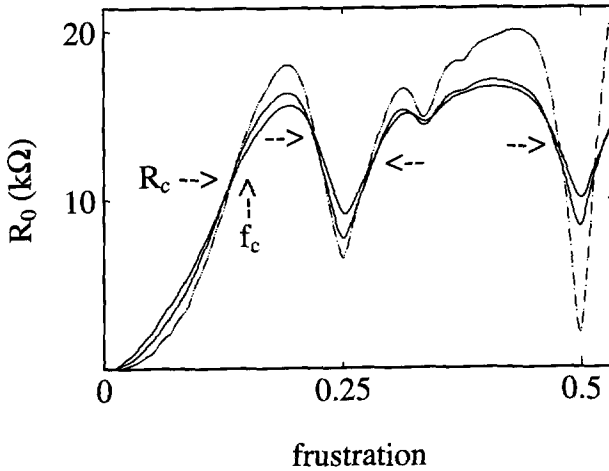
Figure 2.8: *The linear resistance per junction of array T2 measured as a function of the magnetic field for $T = 50$ mK (dotted line), 100 mK and 155 mK. Below the critical field f_c, the resistance decreases when T is lowered; above f_c in the range $f_c < f < 0.25$ the resistance increases.*

shown in Fig. 2.1b.

A detailed way of observing the field-tuned S-I transition is by measuring the resistance versus magnetic field for different temperatures. For sample T2 the result is shown in Fig. 2.8. In the range $0 < f < 1/3$, the $R(f)$ curves look very similar to the ones measured in thin films. Below the critical field $f_c=0.18$ the resistance becomes smaller when the temperature is lowered and above f_c the resistance increases. In the upper part of tabel III we give the values of f_c and R_c for the two square and the two triangular samples that showed similar field-tuned transitions.

According to Fisher [59], the slopes of the $R(f)$ curves at f_c should follow a power-law dependence on T with power $-1/(z_B \nu_B)$. The exponents z_B and ν_B characterize the scaling behavior of the field-tuned S-I transition. When on a double logarithmic plot the slopes of the $R(f)$ curves at f_c are plotted versus $1/T$, we find a straight line in the temperature range $50 < T < 500$ mK, as shown in Fig. 2.9 for sample T2 and S5. The reciprocal of this straight line equals the product $z_B \nu_B$. We find values between 1.2 and 2 in the different samples which are also listed in table III. These values are consistent with the values found in
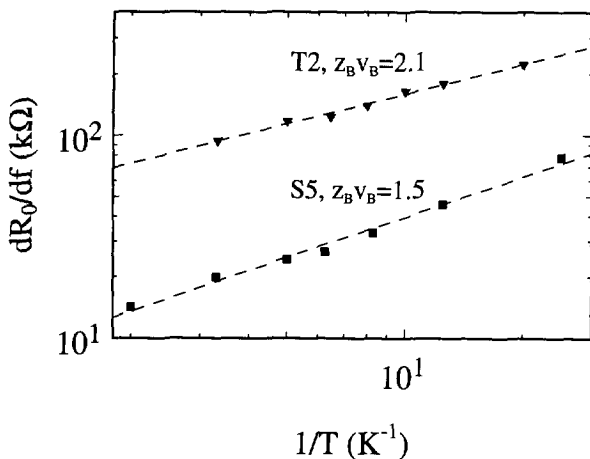
Figure 2.9: *The slopes of the $R(f)$ curves of samples T2 and S5 at f_c plotted as a function of the inverse temperature. The slope of the dashed lines determines the product of the critical exponents $z_B \nu_B$.*

other junction arrays [9], InO_x-films [60] and high-T_c films [61, 62] as well as with the theoretical expectations ($z_B = 1$ and $\nu_B \geq 1$). Right at the transition a universal resistance of the order of the quantum resistance is predicted [59]. We find resistances R_c between 2.5 and 11.5 kΩ.

A new feature introduced by Josephson-junction arrays is the existence of field-tuned transitions near commensurate values of the applied field, f_{comm} [8, 9]. Studying the $R(f)$ curves of sample T2 in more detail, we see critical behavior not only around $f = 0$, but also around $f = 1/4$, $f = 1/2$ and, slightly less pronounced, at $f = 1/3$ and $f = 2/3$. In this sample in total 10 critical points are present when going from $f = 0$ to 1. For sample S5 we see similar transitions at $f = 1/3$ and $f = 1/2$. For each of these values, except $f = 1/3$ in sample T2, $z_B \nu_B$ has been determined as described above. In the lower part of tabel III we list the results for sample T2 and S5, where we have defined $f_c = \pm f_{comm} \pm \delta$. For T2, we find values of $z_B \nu_B$ around 1 and critical resistance values of 11 kΩ. For the square array S5, the values of $z_B \nu_B$ are about the same, but the critical resistance is a factor 3 smaller. These transitions have not been studied theoretically. For samples close to the S-I transition the commensurate states generally become less pronounced which explains why in samples T1 and S4 we only observe a transition around f=0.

Sample	f_{comm}	δ	$R_c(k\Omega)$	$z_B\nu_B$
S4	0	0.1	2.5	1.2
S5	0	0.22	4	1.5
T1	0	0.02	4.5	(4.4)
T2	0	0.14	11.5	2.1
S5	1/2	0.05	3.4	1.2
	1/3	0.015	4.6	0.6
T2	1/2	0.025	11	0.7
	1/4	0.025	12	0.8
	1/3	0.01	14.5	-

Table 2.3: *Critical exponents of field-tuned transitions*

The changing nature of the *I-V* characteristic at the S-I transition is shown in Fig. 2.10 in more detail and once more illustrates the competing dynamics of vortices and charges.   Below f_c the *I-V* shows a supercurrent branch with a non-zero slope arising from quantum tunneling of vortices as discussed in the previous section. When the field is increased above f_c a small charging gap opens up in the supercurrent branch, but at larger scale the curve resembles an *I-V* characteristic on the superconducting side of the transition. As in studies on granular Al films [63], these characteristics can be interpreted as an electric-field tuned S-I transition where a dc bias voltage is used to overcome the Coulomb barrier and at least partly recover Josephson tunneling. In a single junction a negative resistance like we observe in our 2D arrays (see inset) is known as the 'Bloch nose' [3, 64]. For low currents, the *I-V* follows a high resistance branch, but at higher currents coherent Cooper pair tunneling processes (Bloch oscillations) become important and decrease the averaged voltage across the junction.

Studying the width of the gap as a function of frustration we find that it increases linearly with f as shown in Fig. 2.11. Theoretical studies on the Bose-Hubbard model have considered the width of this charging gap [14]. They expect the gap at $T = 0$ to be proportional to $\sqrt{f}$, and predict a linear dependence, as we observe in experiment, at $T \neq 0$ and/or in the presence of offset charges. The absolute value of the gap is much smaller than the one calculated without the presence of offset charges. Although detailed calculations for our case of arrays with small capacitances to ground are not available it is expected that the
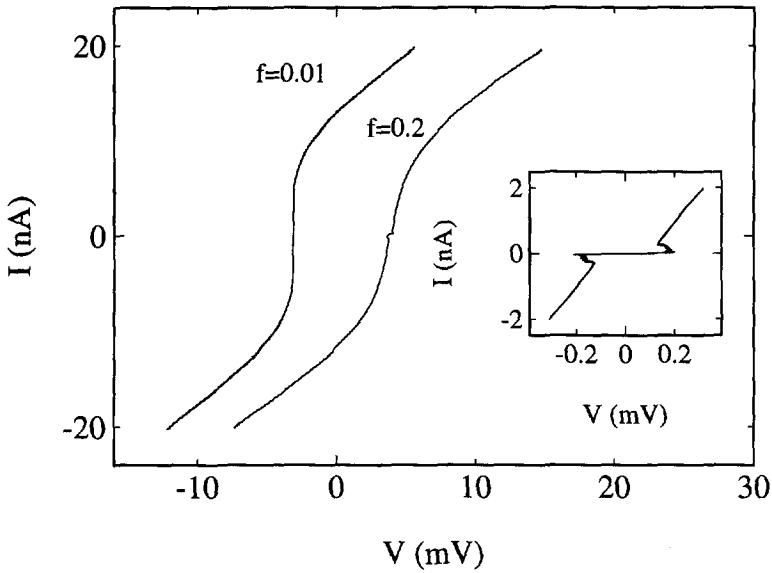
Figure 2.10: *Current-voltage characteristic of sample T1 at several values of the magnetic field. I-V characteristics are offset in the x-direction for clarity. Note the larger scale than that of Fig. 1. The inset shows the I-V characteristic at f=0.2 on an expanded scale.*
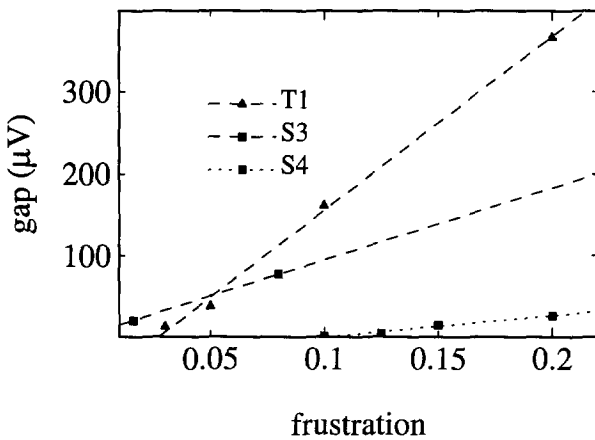

Figure 2.11: *The width of the gap of samples T1, S3 and S4 measured as a function of the frustration f.*

disorder will greatly reduce the effective threshold voltage [65].

2.6   Discussion and conclusion

In the zero-field phase diagram discussed in section 2.3 we used the effective ratio
of the Josephson coupling energy and the charging energy x. The guide to the
eye in fig 2.4 suggests that in terms of this effective ratio the transition for the
triangular arrays is at $x_{cr} = 1.7$, the same value as that of square arrays. We
have checked whether this leads to a consistent picture for the critical exponents
that are predicted for S-I transitions as a function of E_C/E_J in zero and non-zero
magnetic field [59]. In order to compare the theoretical results for films with our
results, we replace the amount of disorder Δ and the critical amount of disorder
Δ_c by the effective ratio x and x_{cr} respectively. The KTB transition temperature
τ_V and the critical field f_c should then scale like:

$$\tau_V \approx (x_{cr} - x)^{zv} \tag{2.4}$$

and

$$f_c \approx (x_{cr} - x)^{2v} \tag{2.5}$$

For the square arrays, using $x_{cr} = 1.7$, we find that $zv = 0.5$ and $v = 1.5$. Using
again $x_{cr} = 1.7$ for triangular arrays we find the same critical exponent $v = 1.5$.

In fitting our square and triangular data points to equation 2.5 we find that
the proportionality constant is a factor of 5 smaller for triangular arrays than
for square arrays. This indicates that the magnetic field suppresses the effective
E_J much stronger in a triangular array than in a square array but we don't
know of any exact calculation on the influence of the geometry on the field-tuned
transition. We note that results on vortex dynamics in the classical regime also
indicate a stronger influence of the magnetic field in triangular arrays.

Both for the zero-field S-I transition and at the field-induced transition it has
been argued that the zero-temperature resistance right at the transition should
be universal. For the transition in zero field we find at the transition a doubly
reentrant dependence of the resistance on temperature. The resistance at 10 mK
is close to the predicted value in absence of damping of 16 kΩ [29], but we cannot
be certain about its value at zero temperature. At the field-induced transitions at
higher magnetic fields the resistance is temperature independent below about 100
mK. The resistance right at the transitions is again of the order of the quantum
resistance but varies from 2.5 to 11.5 kΩ in between different samples. For the

triangular arrays we should probably look at the resistance per square, which is 0.5 times the junction resistance. In that case the resistances vary between 2 and 6 kΩ.

The phase transitions described above generally fit well with the observations on thin films. A new feature of these arrays are the phase transitions at commensurate values of the magnetic field that will be described elsewhere in more detail [66]. In arrays the dynamics of vortices are of special interest. The observations discussed in this chapter show that the decreasing ratio of E_C/E_J, or the enhancement of phase fluctuations, has a profound influence on the dynamics of vortices. With decreasing ratio of E_C/E_J we observe a decrease of the depinning current and surprisingly an increase of the barrier for thermally activated behavior. Closer to the transition both the barrier and the depinning current decrease and a finite zero-bias resistance appears that indicates some mechanism of quantum transport. In samples closest to the zero-field transition a magnetic field induces Bose-condensation of vortices.

Although we don't have an explanation for the anomalous behavior of the barrier height, the data do suggest a systematic dependence on the junction plasma frequency that should be investigated in more detail. We note that close to the transition the influence of random offset charge becomes important and might decrease vortex coherence. The exponential decrease of the resistance and the flattening off at low temperatures qualitatively fits well to the single-vortex model. The fact that the junction parameters are so well known, calls for a quantitative study of these quantum dynamics. When the random offset charges and possibly edge effects can be included in theoretical models it should be possible to decide on the general nature and the properties of the vortex in this quantum regime.

References

[1] J.E. Mooij and G. Schön in *Single Charge Tunneling*, eds. H. Grabert and M.H. Devoret (Plenum, New York 1992), Chapter 8 and references therein.

[2] Y. Liu and A.M. Goldman, Mod. Phys. Lett. B **8**, 277 (1993) and references therein.

[3] L.J. Geerligs, M. Peters, L.E.M. de Groot, A. Verbruggen, and J.E. Mooij, Phys. Rev. Lett. **63**, 326 (1989).

[4] H.S.J. van der Zant, L.J. Geerligs, and J.E. Mooij, Europhysics Lett. **19**, 541 (1992).

[5] C.D. Chen, P. Delsing, D.B. Haviland, and T. Claeson, Physica Scripta **T 42**, 182 (1992).

[6] M.P.A. Fisher, G. Grinstein and S.M. Girvin, Phys. Rev. Lett. **64**, 587 (1990).

[7] W.J. Elion, J.J. Wachters, L.L. Sohn, and J.E. Mooij, Phys. Rev. Lett. **71**, 2311 (1993).

[8] H.S.J. van der Zant, F.C. Fritschy, W.J. Elion, L.J. Geerligs, and J.E. Mooij, Phys. Rev. Lett. **69**, 2971 (1992).

[9] C.D. Chen, P. Delsing, D.B. Haviland, Y. Harada and T. Claeson, submitted to Phys. Rev. B

[10] R. Fazio and G. Schön, Phys. Rev. B **43**, 5307 (1991).

[11] B.J. van Wees, Phys. Rev. B **44**, 2264 (1991).

[12] R. Fazio, A. van Otterlo, G. Schön, H.S.J. van der Zant, and J.E. Mooij, Helv. Phys. Acta **65**, 228 (1992).

[13] C. Bruder, R. Fazio, A. Kampf, A van Otterlo, and G. Schön, Phys. Rev. B **47**, 342 (1993).

[14] A. van Otterlo, K.-H. Wagenblast, R. Fazio, and G. Schön, Phys. Rev. B **48**, 3316 (1993).

[15] J.M. Valles (Jr.), R.C. Dynes, and J.P. Garno, Phys. Rev. Lett. **69**, 3567 (1992).

[16] H.S.J. van der Zant, H.A. Rijken, and J.E. Mooij, J. Low Temp. Phys. **79**, 289 (1990).

[17] S. Teitel and C. Jayaprakash, Phys. Rev. Lett. **51**, 1991 (1983).

[18] T.C. Halsey, J. Phys. C **18**, 2437 (1985).

[19] W.Y. Shih and D. Stroud, Phys. Rev. B **30**, 6774 (1984).

[20] R. Théron, S. E. Korshunov, J. B. Simond, Ch. Leemann and P. Martinoli, Phys. Rev. Lett. **72**, 562 (1994).

[21] H.S.J. van der Zant, F.C. Fritschy, T.P. Orlando, and J.E. Mooij, Phys. Rev. Lett. **66**, 2531 (1991).

[22] T.S. Tighe, A.T. Johnson, and M. Tinkham, Phys. Rev. B **44**, 10286 (1991).

[23] H.S.J. van der Zant, F.C. Fritschy, T.P. Orlando, and J.E. Mooij, Phys. Rev. B **47**, 295 (1993).

[24] T. S. Tighe, A. T. Johnson, and M. Tinkham, Phys. Rev. B **47**, 1145 (1993).

[25] P. Delsing, C.D. Chen, D.B. Haviland, Y. Harada and T. Claeson, Phys. Rev. B **50**, 3959 (1994).

[26] L.J. Geerligs, Ph. D. thesis (Delft, 1990) (unpublished).

[27] U. Geigenmüller and G. Schön, Europhys Lett. **10**, 675 (1989).

[28] V. Ambegaokar and A. Baratoff, Phys. Rev. Lett. **10**, 846 (1963). P. Delsing, and T. Claeson, Phys. Rev. Lett. **67**, 1161 (1991). T. Claeson, Phys. Rev. Lett. **63**, 1180 (1989).

[29] M. Cha, M.P.A. Fischer, S.M. Girvin, M. Wallin, and A.P. Young, Phys. Rev. B **44**, 6883 (1991).

[30] E. Granato and J.M. Kosterlitz, Phys. Rev. Lett. **65**, 1267 (1990).

[31] V.L. Berezinskii, Zh. Eksp. Teor. Fiz. **59**, 907 (1970) [Sov. Phys. JETP **32**, 493 (1971)];
J.M. Kosterlitz and D.J. Thouless, J. Phys. C **6**, 1181 (1973).

[32] C.J. Lobb, D.W. Abraham, and M. Tinkham, Phys. Rev. B **36**, 150 (1983).

[33] J.E. Mooij, B.J. van Wees, L.J. Geerligs, M. Peters, R. Fazio, and G. Schön, Phys. Rev. Lett. **65**, 645 (1990).

[34] M. Sugahara, Jpn. J. Appl. Phys. **24**, 674, (1985).

[35] H.S.J. van der Zant and J.R. Phillips, (unpublished work).

[36] P. Bobbert, R. Fazio, U. Geigenmüller, and G. Schön, in *Macroscopic Quantum Phenomena*, eds. T.D. Clark et al. (World Scientific, Singapore, 1991), p 119.

[37] B.G. Orr, H.M. Jaeger, A.M. Goldman, and C.G. Kuper, Phys. Rev. Lett. **56**, 378 (1985).

[38] M. P. A. Fisher, Phys. Rev. Lett. **57**, 885 (1986).

[39] M. V. Simkin, Phys. Rev. B **44**, 7074 (1991).

[40] A.D. Zaikin, in *Quantum Fluctuations in Mesoscopic and Macroscopic Systems*, eds. H.A. Cerdeira et al., World Scientific, (1991), p 255.

[41] S. Teitel and C. Jayaprakash, Phys. Rev. B **27**, 598 (1983).

[42] R. Gupta, J. Delapp, G.G. Batrouni, G.C. Fox, C.F. Baillic, and J. Aposto-
     lakis, Phys. Rev. Lett. **61**, 1996 (1988).

[43] J. V. José and C. Rojas, Physica B **203**, 481-489 (1994). North Holland
     (1994).

[44] U. Eckern and A. Schmid, Phys. Rev. B. **39**, 6441 (1989).

[45] M. S. Rzchowsky, S. P. Benz, M. Tinkham, and C. J. Lobb, Phys. Rev. B
     42, 2041 (1990).

[46] T. P. Orlando, J. E. Mooij, and H. S. J. van der Zant, Phys. Rev. B **43**,
     10218 (1991).

[47] U. Eckern, private communication.

[48] U. Geigenmüller, in *Macroscopic Quantum Phenomena*, eds. T.D. Clark et
     al. (World Scientific, Singapore, 1991), p 131.

[49] P. A. Bobbert, Phys. Rev. B **45**, 7540 (1992).

[50] U. Geigenmüller, C.B. Whan and C.J. Lobb, Phys. Rev. B **47**, 348 (1993).

[51] U. Eckern and E. Sonin, Phys. Rev. B **47**, 505 (1993).

[52] Wenbin Yu, K. H. Lee and D. Stroud, Phys. Rev. B **47**, 5906 (1993), Wenbin
     Yu and D. Stroud, Phys. Rev. B **49**, 6174 (1994).

[53] T. Hagenaars, P. H. E. Tiesenga, J. E. van Himbergen, and J. V. José, Phys.
     Rev. B **50**, 1143 (1994).

[54] H. S. J. van der Zant, unpublished results.

[55] R. Fazio, A. van Otterlo and G. Schön, Europhys. Lett. **25**, 453 (1994).

[56] J.M. Martinis, M.H. Devoret, and J. Clarke, Phys. Rev. B **35**, 4682 (1987).

[57] H. Grabert, P. Olschowski and U. Weiss, Phys. Rev. B **36**, 1931 (1987).

[58] M.P.A. Fisher, T.A. Tokayasu, and A.P. Young, Phys. Rev. Lett. **66**, 2931
     (1991).

[59] M.P.A. Fisher, Phys. Rev. Lett. **65**, 923 (1990).

[60] A.F. Hebard and M.A. Paalanen, Phys. Rev. Lett. **65**, 927 (1990).

[61] G.T. Seidler, T.F. Rosenbaum, and B.W. Veal, Phys. Rev. B **45**, 10162
     (1992).

[62] S. Tanda, S. Ohzeki, and T. Nakayama, Phys. Rev. Lett. **69**, 530 (1992).

[63] W.W. Wu and P.W. Adams, Phys. Rev. B **50**, 13065 (1994).

[64] D.V. Averin, A.B. Zorin, and K.K. Likharev, Zh. Eks. Teor. Fiz **88**, 692 (1985) (Sov. Phys. JETP **61**, 407 (1985));
U. Geigenmüller and G. Schön, Physica B **152** , 186 (1988);
A.D. Zaikin and I.N. Kosarev, Phys. Lett. A **131**, 125 (1988).

[65] A. Alan Middleton and Ned S. Wingreen, Phys. Rev. Lett. **71**, 3198 (1993).

[66] H. S. J. van der Zant, W. J. Elion, L. J. Geerligs and J. E. Mooij, to be published.

Chapter 3

The Aharonov-Casher effect for vortices in Josephson-junction arrays

W. J. Elion, J. J. Wachters, L. L. Sohn, and J. E. Mooij

Department of Applied Physics, Delft University of Technology and Delft Institute for Micro-Electronics and Submicron technology (DIMES), P. O. Box 5046, 2600 GA Delft, The Netherlands

Abstract: We report on an experiment where we observe quantum-mechanical interference of vortices around an induced charge. In a specially designed sample, vortices move along a doubly connected path. On the superconducting island enclosed by the path a charge can be induced by capacitive coupling to a gate. In the resistance that arises from the moving vortices we find clear oscillations as a function of gate voltage. The period of the oscillations corresponds to the single electron charge e, due to the presence of a small but finite number of quasiparticles. The oscillations are due to quantum interference of vortices which is a manifestation of the generalized Aharonov-Casher effect.
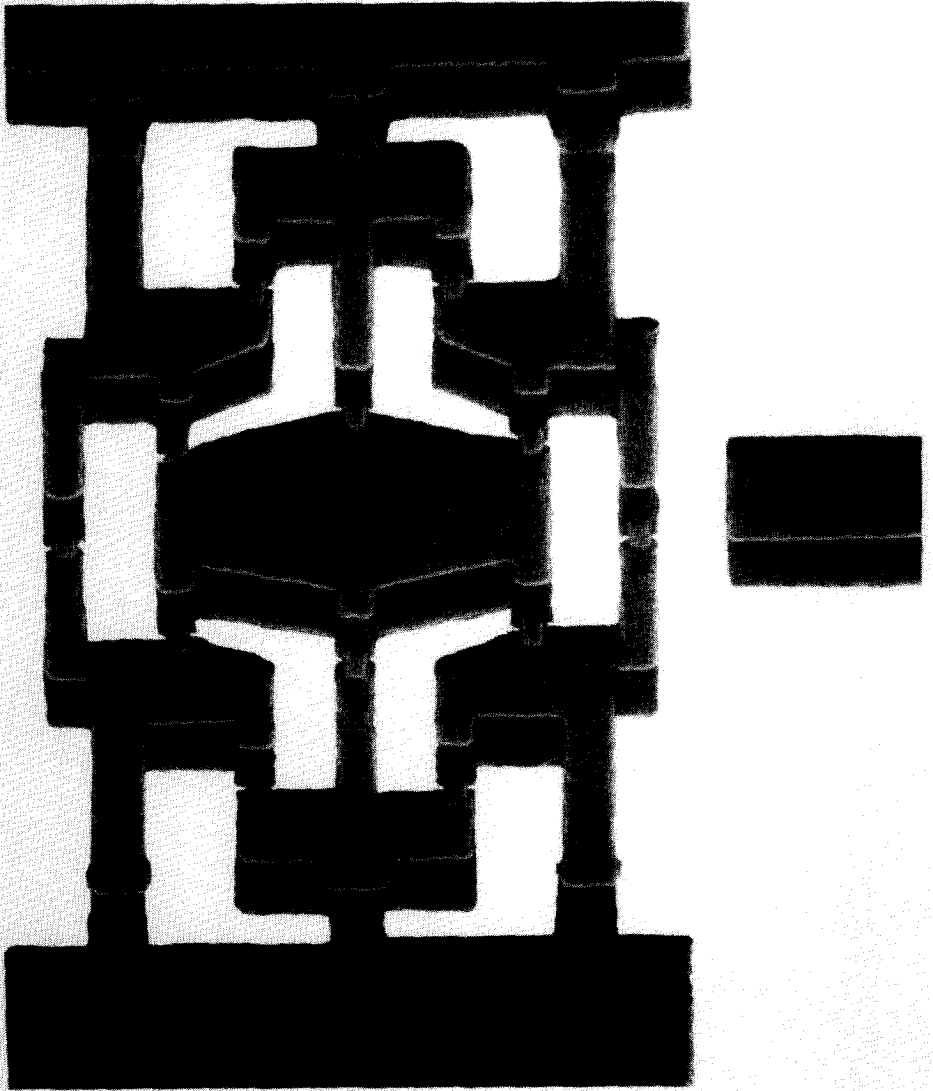
Figure 3.1: Scanning-electron-microscope photograph of the device used to measure the Aharonov-Casher effect for vortices.

3.1 Introduction

In a two-dimensional array of underdamped Josephson junctions it is possible to magnetically induce vortices, with associated supercurrents flowing through the junctions, and simultaneously induce a polarization charge on the superconducting islands. This idea has attracted ample theoretical interest, especially on the nature of the possible interaction between vortices and the polarized charge. As a consequence of the fact that vortices behave as macroscopic quantum particles [1, 2, 3, 4] it has been shown that a vortex moving around a polarized charge Q_g experiences a phase shift in its wavefunction [4, 5, 6]. This phase shift can lead to a persistent current of vortices or, when a vortex moves along a doubly connected path, to interference effects. Here we report on the first experiment that demonstrates this [7]. We measure the transport of vortices in a specially designed array shown in Fig 3.1 and Fig. 3.2. As a function of the charge induced on the island that is enclosed by the two possible vortex paths we observe clear periodic oscillations. This is due to quantum interference of vortices, which, as we will discuss later, is a manifestation of the Aharonov-Casher effect [8].

In a two-dimensional array of underdamped Josephson junctions, vortices in the classical regime are described as particles with a mass [9, 10]. This mass relates to the fact that a moving vortex will charge the junction capacitances (C). The corresponding electrostatic energy is proportional to the square of the vortex velocity, and can be viewed as the kinetic energy of the vortex. It has been proposed [1, 2, 3, 4] that a vortex can also be considered a macroscopic quantum particle. In fabricated arrays where the charging energy, $E_C = e^2/2C$, is only slightly smaller than the Josephson coupling energy, E_J, quantum-mechanical behavior of vortices has indeed been observed experimentally [11]. Arrays in this regime show a finite zero-bias resistance at 10 mK which is attributed to quantum tunneling of vortices. For E_J/E_C values of order one, a quantum phase transition can be induced by a magnetic field, as a result of Bose condensation of vortices [11].

The interaction between vortices and an induced charge was first described by Van Wees [5]. He considers a ring-shaped array of Josephson junctions that is bounded by superconducting banks. A charge Q_g can be induced on the inner bank by means of a small capacitor that is connected to a voltage source. A vortex in this array is restricted to a circular path. When a current I flows from the inner to the outer bank, the vortex experiences a tangential force $F = \Phi_0 I/L$, where Φ_0 is the flux quantum $h/2e$ and L is the circumference of the loop. After a vortex

has moved around the circular path once its position is the same as at the start. Therefore the force F cannot be expressed as the gradient of a scalar potential. Instead a charge vector potential A_Q, defined as $\oint A_Q dl = Q_g$, is introduced so that the force on the vortex equals $F = \Phi_0 dA_Q/dt$. The resulting generalized vortex momentum is thus $p + \Phi_0 A_Q$ and the corresponding Hamiltonian of the system is

$$H = \frac{(p + \Phi_0 A_Q)^2}{m_v} + E_p(x) \tag{3.1}$$

Here $E_p(x)$ is a small periodic potential term that is proportional to the Josephson coupling energy and arises from the discreteness of the lattice. m_v is the vortex mass that equals $\Phi_0^2 C/2S$ in a square lattice with cell area S. A vortex that moves around the loop once will acquire a phase shift of $\frac{2\pi}{2e} \oint A_Q dl = 2\pi \frac{Q_g}{2e}$. The charge on the inner ring induces a persistent vortex current that results in a persistent voltage. When the loop is open, so that vortices can enter at one point and exit at another, the same relative phase difference, $2\pi \frac{Q_g}{2e}$, is imposed on the two vortex paths between the points.

The dynamics of quantum vortices in a charged junction array have been addressed by several other authors. Orlando et. al. [6] have arrived at similar conclusions as Van Wees by applying the Bohr Sommerfeld criterion to the canonical momentum of vortices in a superconducting ring. Fazio [4] et. al. have calculated the energy levels of a small ring-shaped array in the presence of a vortex. They find that these levels are sensitive to the charge induced on the center island.

The interference of vortices around an induced charge can be visualized as the dual of the interference of Cooper pairs moving in a loop that encloses magnetic flux. In the same way that the latter is related to the Aharonov Bohm effect [12], the interference of vortices is a form of the Aharonov-Casher effect. In the original work Aharonov and Casher discussed the interference of a magnetic particle moving around an infinite line charge. This effect has been observed for neutron beams [13]. Reznik and Aharonov [14] pointed out that magnetic vortices in a superconductor should also experience the AC effect. In the Josephson-junction arrays considered here, the Josephson penetration depth is comparable to the size of the array and the magnetic flux is divided over all cells. Still, a moving vortex is connected with a moving flux quantum and the vortex interference around an induced charge is a manifestation of the generalized Aharonov-Casher effect.

In the remaining sections we will present our experimental results on the interference of vortices. The specially-shaped array that we use is smaller than
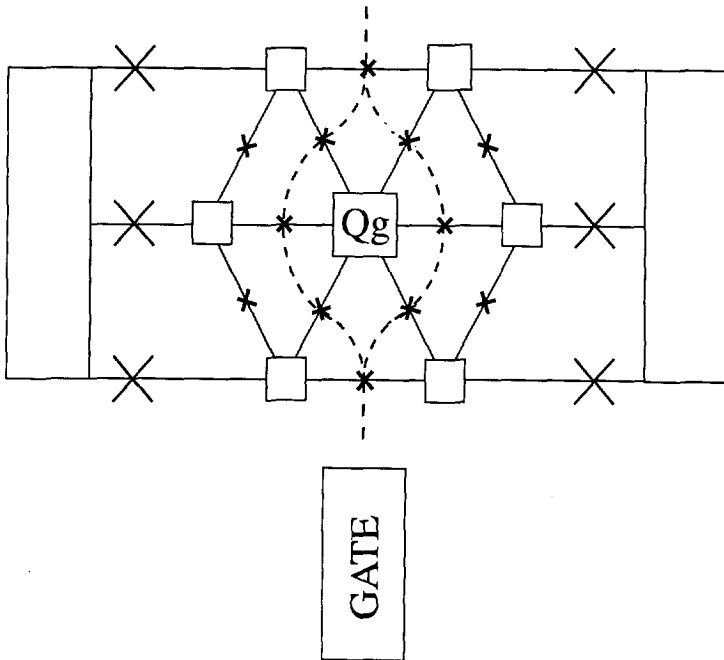
Figure 3.2: *Schematic layout of the sample. Rectangles are superconducting aluminum islands and crosses denote Josephson junctions. The junctions in the hexagon have a smaller junction area than the junctions that couple the array to superconducting current and voltage contacts. The dashed lines show the possible vortex paths.*

arrays that we have previously studied for other purposes. We have therefore investigated the classical properties of the array in some detail using numerical simulations. First we will describe the experimental details of our samples. We will discuss the measured I-V characteristics for different magnetic fields and compare them with the results of simulations performed in the classical limit. We will then discuss the influence of the applied gate voltage on the I-V characteristic. The periodic oscillations that we observe in the flux-flow resistance are due to the Aharonov-Casher effect. The last section contains a discussion of the presented results and conclusions.

3.2   Sample layout and parameters

In Fig. 3.2 we show the layout of the device that we designed to measure quantum interference of vortices. Main part of the device is a hexagon-shaped array consisting of six triangular cells of small Josephson junctions. A vortex can move across the hexagon along two possible paths that are drawn with a dashed line in Fig. 3.2. On the superconducting island enclosed by the two paths, a charge can be induced by a gate that is fabricated near and in the same plane as the array.

Quantum effects in arrays generally become more pronounced as the charging energy is increased with respect to the Josephson coupling energy. However, if the charging energy is larger than the Josephson coupling energy a superconductor-to-insulator (S-I) phase transition occurs. We therefore choose the junction parameters such that the ratio E_J/E_C of the junctions in the hexagon is between 1 and 1.5.

The hexagon-shaped array is coupled to superconducting busbars via junctions that have a larger critical current. The corresponding larger Josephson coupling energy ensures that the barrier for a vortex to cross these junctions is higher and thus confines the vortex to the two paths in the hexagon. When the coupling energy is too large we expect that the freedom of the phases on the outer islands will be restrained and the hexagon, no longer resembles a 2D array. Contacts are connected to the busbars to current bias the array and measure the voltage. Because the gate is evaporated in the same plane as the junctions it will capacitively couple to all islands in the array. As long as the vortex is confined to the hexagon only the center island is enclosed by the vortex path. The relative phase difference between the vortex paths should then solely be determined by the charge induced on this center island.

Junctions are underdamped $Al - Al_2O_3 - Al$ junctions that are fabricated with a standard shadow-evaporation technique [15]. The larger critical current of the side junctions is obtained by using a larger junction area. Consequently, the capacitance of these junctions is larger by the same factor, that we refer to as α. We have measured several samples with different junction parameters and different values of α. Here we will report on samples A, B and C that have values of α of 3, 2 and 1.5 respectively. The normal state resistance of the junctions in the hexagon is 5.5 kΩ for sample A, 7.7 kΩ for sample B and 8.2 kΩ for sample C. The capacitance of these junctions is about 1fF in all samples and the ratio of E_J over E_C is calculated to be 1.5, 1.1 and 1.0 for samples A, B, and C. These parameters are summarized in Table I.

Sample	α	R_n (kΩ)	C (fF)	E_J/E_C	T_{ac} (mK)
A	3	5.5	1	1.5	450
B	2	7.7	1	1.1	500
C	1.5	8.2	1	1.0	650

Table 3.1: *Sample parameters*

Measurements were performed in a dilution refrigerator at temperatures down to 10 mK. Leads were extensively filtered both at room temperature with rfi feedthrough filters and at mixing chamber temperature with RC and microwave filtering. Magnetic shielding was provided by μ-metal and lead shields. With a small magnet, magnetic fields up to 1 mT could be applied perpendicular to the array.

3.3 Current-voltage characteristics

The conductive properties that we measure in samples A, B, and C are very similar. As we will show later, a value of $\alpha = 3$ is most ideal to observe the Aharonov-Casher oscillations. We will therefore discuss the properties of sample A in detail and where neccessary comment on differences with samples B and C.

In Fig. 3.3 we show the measured critical current of array A as a function of magnetic field. This critical current is defined as the bias current where the voltage exceeds 2 μV. For specific values of the magnetic field, such as 0.8, 1.2, 1.7 and 2.2 Gauss, the critical current exhibits sharply pronounced minima. In a large array one finds broad minima in the critical current due to the matching of the vortex lattice and the junction lattice [16]. The sharp dips that we find resemble more those found in a long Josephson junction or an array of junctions in parallel. In these systems each dip in the critical current marks the transition between a number of N and $N + 1$ flux quanta in the array. In the classical simulations that will be discussed in the next section, we find that in our small array the dips also correspond to transitions between different vortex configurations. In general all properties of a Josephson-junction array are periodic in the applied flux, with a period of one flux quantum per cell. Because of the different cell sizes in our sample, full periodicity does not occur within the range of 1 mT of our small magnet. The critical current of samples B and C shows similar behavior. The
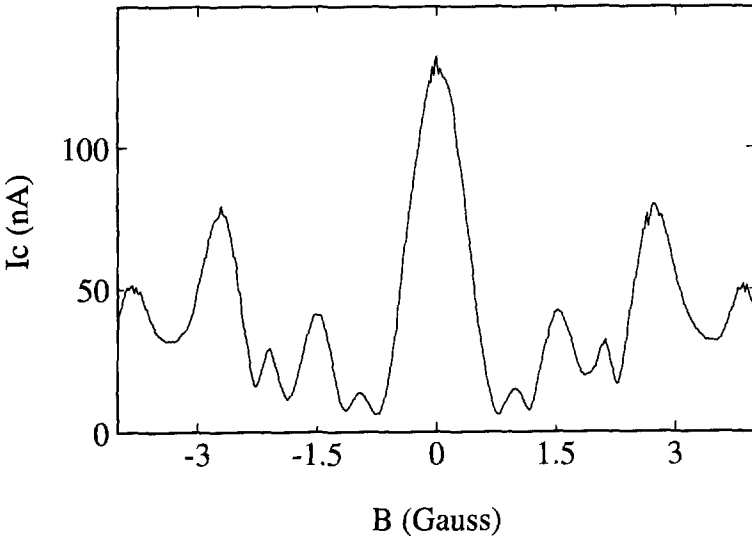
Figure 3.3: *The critical current of sample A as a function of magnetic field applied perpendicular to the array.*

dips occur within 15 % of the same field values as in sample A, while the relative height of the dips varies for the different samples.

We can distinguish three different types of current-voltage (*I-V*) characteristics for different values of the magnetic field. In zero field, as shown for sample A in Fig. 3.4a, the voltage jumps to the BCS gap voltage as soon as the current exceeds the critical current. A similar *I-V* characteristic is found for all values of the magnetic field where the critical current is higher than about 20 nA. When the bias current is increased further as shown in Fig. 3.4b, the voltage jumps to two, three and four times the gap voltage in a manner that resembles the row-switching feature in large arrays. The two rows in the hexagon can not switch independently, which results in a smearing of the fourth jump.

For magnetic fields where the critical current is suppressed to below 20 nA, we find the *I-V* characteristic shown in Fig. 3.5a. Below the gap a resistive regime is visible that we will refer to as the flux-flow branch. The resistance of this branch is of the order of the normal state resistance of the junctions. Hysteretic features are present around the critical current. Looking more closely at the return branch in the hysteretic part of the *I-V* characteristic we find that it consists of two parts that have a different resistance. Similar features are more pronounced at higher
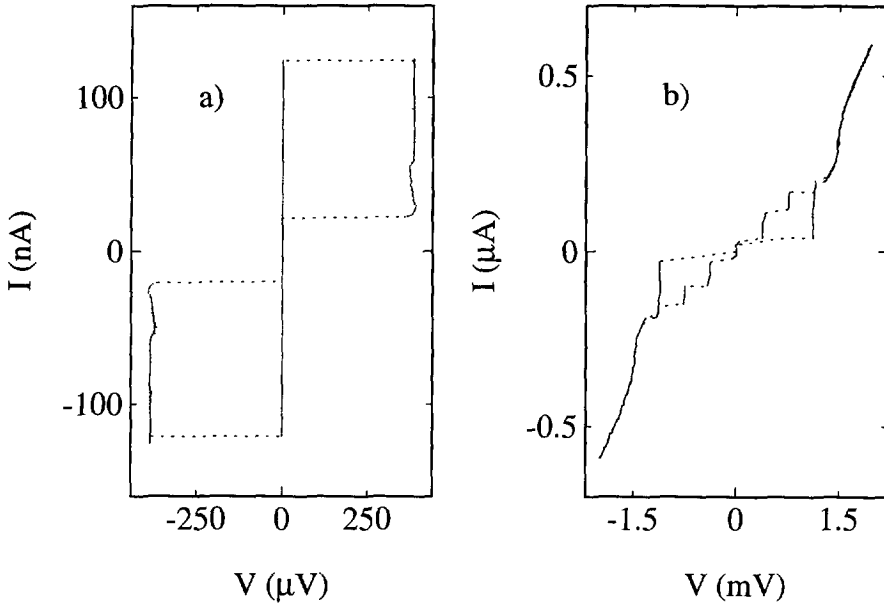
Figure 3.4: *a: The current-voltage characteristic of sample A in zero field. b: I-V characteristic on larger scale, in a field of 1.2 Gauss. The row switching feature is visible for all magnetic fields.*

field values that we will not discuss further in this paper. We attribute these effects to the small size and the different junction parameters in our array.

In Fig. 3.5b, we show the *I-V* characteristic for a magnetic field of 1.2 Gauss, which corresponds to a dip in the critical current. Hysteretic features are no longer visible and detailed analysis shows that the differential resistance below the apparent critical current remains finite. For this particular magnetic field we measure a zero-bias resistance of 80 Ω. A similar zero-bias resistance has been observed in large arrays with this E_J/E_C ratio [11]. We associate this branch with quantum tunneling of vortices through the array. We have also measured this zero-bias resistance directly using a lock-in technique. The measuring current is 1 nA which is significantly lower than the measured depinning current and we have checked that the voltage depends linearly on this current. As a function of magnetic field we observe sharp peaks at the field values where the critical current is most suppressed. For samples B and C the zero-bias resistance is generally higher but of the same order of magnitude as in sample A.
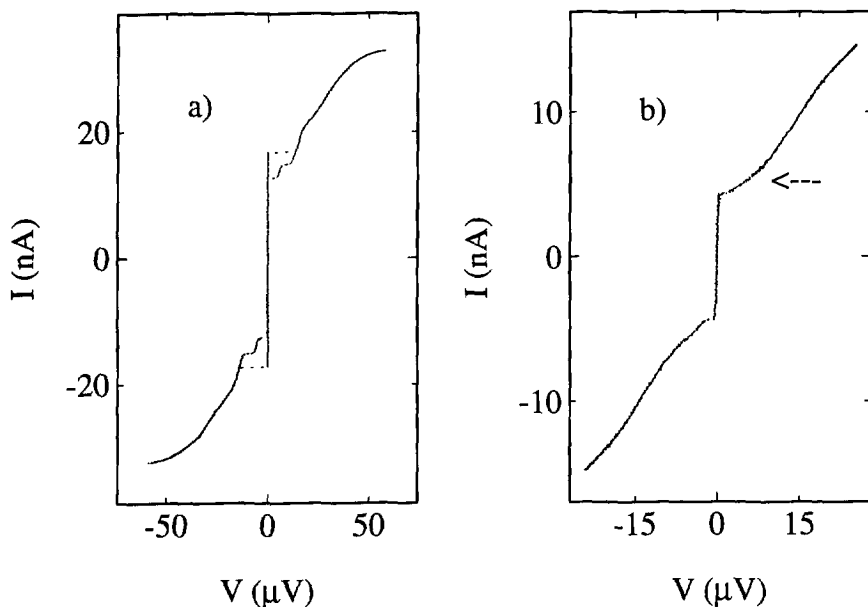
Figure 3.5: a: *Current-voltage characteristic of sample A in a magnetic field of 0.65 Gauss. The flux-flow branch appears for all magnetic fields where the critical current is suppressed below about 20 nA. b: I-V characteristic in a magnetic field of 1.2 Gauss which corresponds to a pronounced dip in the critical current. The arrow points at the bias current at which the differential resistance shown in Fig. 3.9 was measured.*

The fact that a magnetic field can tune the *I-V* characteristic to show either semiclassical or quantum-mechanical features is typical for these small arrays. In larger arrays a change in the nature of the *I-V* characteristic with applied magnetic field is only observed for an E_J/E_C ratio in between 0.9 and 0.7. In this regime the magnetic field induces a superconductor-to-insulator phase transition. Our small arrays have a somewhat higher E_J/E_C ratio and do not show such a phase transition.

3.4   Simulations

The geometry of the sample that we use is different from the usual arrays that we measure, in that it is very small and that it has different cell sizes. Although the
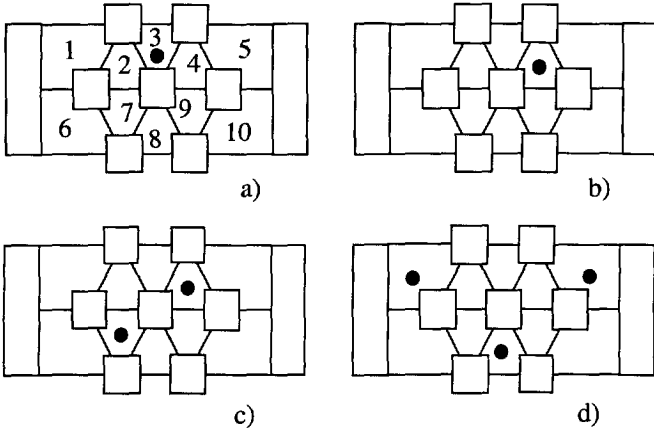
Figure 3.6: *The equilibrium vortex positions for a)* 0.08 ≤ *f* ≤ 0.095, *b)* 0.1 ≤ *f* ≤ 0.12, *c)* 0.125 ≤ *f* ≤ 0.205 *and d)* 0.21 ≤ *f* ≤ 0.235. *For f < 0.08 there are no vortices present. All configurations can be mirrored around the symmetry axes of the array.*

measured *I-V* characteristics show a depinning current and a flux-flow regime just like those of large arrays, we found it essential to check whether these phenomena can indeed be associated with the depinning and flow of vortices. We therefore investigate the classical properties of the array, (i.e. neglecting charging effects) using static and dynamic numerical simulations [17].

The geometry used corresponds to that of the fabricated sample. The cell areas have been estimated from the sample layout, assuming that flux penetrating a superconducting island can be added to the flux through the nearest cell. The area of the outer cells numbered 1, 5, 6 and 10 (see Fig. 3.6), is twice as large as the cell area of the middle cells in the hexagon, 2,4,7 and 9. The area of cells 3 and 8 is smaller than that of cell 2 by a factor of 4/5. The magnetic field is given in units of frustration *f* which is defined as the flux through cell 2 divided by the flux quantum.

Static Properties

In the classical limit the Hamiltonian of the array is:

$$H = \Sigma_{<i,j>} E_{J,ij}[1 - cos(\phi_i - \phi_j - \Psi_{ij})] - \frac{\hbar}{2e} I \vartheta \tag{3.2}$$

where the sum is over the nearest neigbours, ϕ_i is the phase of the ith island, $\Psi_{ij} = (2\pi/\Phi_0) \int_i^j \mathbf{A} dl$, with $\mathbf{A} = Hx\hat{y}$ the magnetic vector potential and ϑ is

the phase difference across the busbars. Starting from an initial random phase configuration, we solve the equation $(\partial H/\partial \phi_i) = 0$ iteratively to find the local minimum of energy [18]. To identify the vortex positions we sum the phase differences in each of the cells. A vortex corresponds to a sum of the phase differences of an integer number times 2π. Repeating this procedure several times the minimum phase and vortex configurations have been calculated as a function of magnetic field. Our results are shown in Fig. 3.6. For a magnetic field higher than 0.075 the energy of the system is lowered by introducing a vortex in cell 3 or 8. For fields higher than 0.095 the vortex is preferably present in cell 2, 4, 7 or 9. When the frustration exceeds $f = 0.12$ a second vortex enters the array and for $f = 0.21$ the third. The repulsion between vortices at this point is so strong that vortices will also be present in the outer cells.

We have calculated the barrier that a vortex has to overcome to move through the array by fixing the phase difference ϑ across the busbars and calculating the ground state energy as a function of ϑ. The result is shown in Fig. 3.7.

For zero field the energy of a vortex in the array is higher than outside. As the field increases this potential barrier changes to a potential well in which a vortex is trapped. For this small array the field dependent edge barriers are clearly more important than the cell to cell barriers that have been calculated in large arrays [18]. The energy plots correspond to a vortex moving quasi-statically through the hexagon. We can estimate the energy barrier for a vortex to cross the outer larger junctions by setting the phase difference across the junction between cells 1 and 6 to π. The corresponding energy at f=0.08 is 4.5 E_J higher than the energy for a vortex in the hexagon. If we repeat this calculation for the case where $\alpha = 1.5$ the energy difference is only E_J. We conclude that the possibility to find a vortex in the outer cells is significantly higher if $\alpha = 1.5$ than if $\alpha = 3$.

Dynamic Properties

We have calculated the dynamic properties of our array modelling each junction with the RCSJ (resistively and capacitively shunted junction) model. The resulting coupled second order differential equations are of the form:

$$\beta_c \frac{d^2\gamma_{ij}}{dt^2} + G_N \frac{d\gamma_{ij}}{dt} + \sin\gamma_{ij} = \frac{I}{I_c} \tag{3.3}$$

where β_c is the McCumber parameter $2ei_cCR_n^2/\hbar$ and γ_{ij} is the gauge-invariant phase difference, $\phi_i - \phi_j - \Psi_{ij}$. To account for the large quasiparticle resistance in our underdamped junctions we use a voltage-dependent shunt-resistance. This
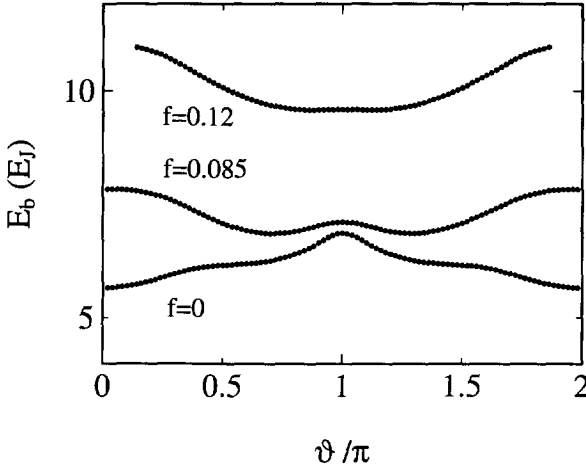
Figure 3.7: *Quasi-statically calculated energy barriers for a vortex to cross the Aharonov-Casher sample, for the case where* $\alpha = 3$

shunt resistance is the normal state resistance, R_n, for voltages above the gap, and $100R_n$ for lower voltages. As the geometrical inductance of the cells is estimated to be 10 pH we have neglected self inductance in our simulations.

Using a fourth order Runge-Kutta method the coupled differential equations are solved. The resulting *I-V* characteristics are compared to the experimental data, and analysed in terms of the individual phase differences. The calculated critical current versus magnetic field is shown in Fig. 3.8a. The structure is very similar to that found experimentally (Fig. 3.3). Comparing the critical current with the calculated vortex configurations in Fig. 3.6, we find that the dip at f=0.08 corresponds to a transition from zero to one vortex in the array. The dip at f=1.2 corresponds to the transition from one to two vortices and the dip at 2.0 corresponds to a transition from two to three vortices. At a frustration of 1.6, where a dip is also visible, the difference between having vortices in cells 2 and 9 and having vortices in cells 2 and 4 is minimal. The absolute value of the calculated critical current is larger than the measured result. We expect the critical current to be reduced by quantum fluctuations. As the junctions in the hexagon are more sensitive to quantum fluctuations than the larger junctions this effect will also change the relative depth of the different dips.
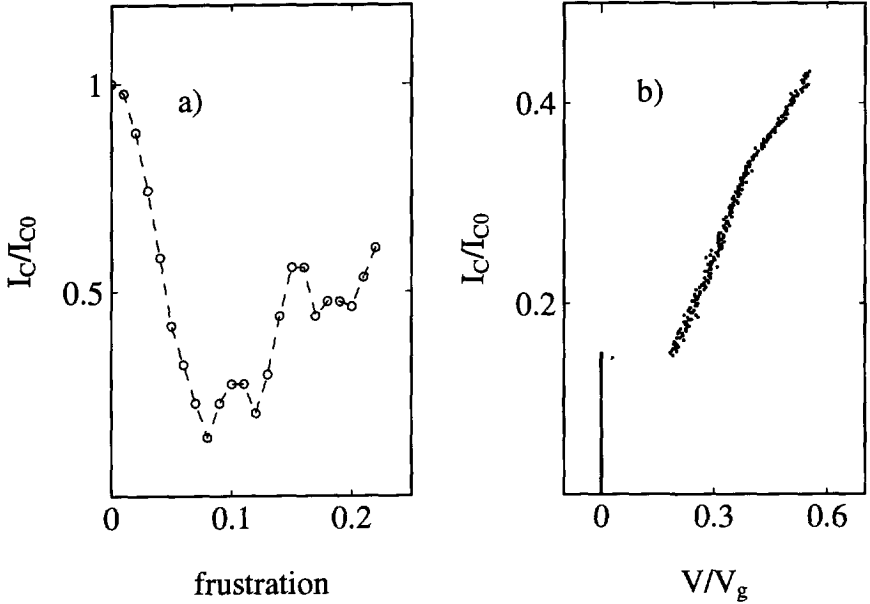
Figure 3.8: *a:* *Critical current versus magnetic field, calculated by solving the set of classical RCSJ equations for all junctions in the array. Current is normalized to its zero field value. b: Calculated current-voltage characteristic for $f = 0.08$. Current is normalized to the zero field critical current and voltage to the BCS gap voltage. The resistive branch corresponds to vortices moving across the array over one of the possible paths in the hexagon.*

The calculated *I-V* characteristic for the magnetic field that corresponds to the first dip in the critical current is shown in Fig. 3.8b. As in the experiment we observe a critical current, a resistive branch below the gap and a jump to the superconducting gap voltage at higher currents. We do not find a zero-bias resistance in these classical simulations. We have evaluated the time dependence of the phase differences of the individual junctions for a fixed bias current. In the flux-flow branch we find that vortices move through the hexagon along one of the expected paths.

In larger underdamped arrays it is well known that motion of vortices can induce oscillatory modes that are called spin waves. In our small system, we do find that phases oscillate after the vortex has left the array, but we do not find any systematic behavior.

Although the voltage in the flux-flow branch is much lower than the BCS gap voltage, the shape of the *I-V* characteristic is to a large extent determined by the normal state resistance. The subgap resistance can also be chosen 10.000 times the normal state resistance without a significantly different result. From the phase differences across the individual junctions we find that the voltage across specific junctions does exceed the gap on time scales of the order of the junction plasma frequency. In order to obtain a solution which corresponds to flux-flow, we have to use a normal state resistance of 1 kΩ instead of the actual value of 5.5 kΩ of sample A. The fact that we have to assume a somewhat lower value for the normal state resistance signifies that in the experiment there is an additional source of dissipation that is not included in the simulations. As a possible mechanism we think of high frequency damping due to the low impedance of the leads to the current source.

3.5 Influence of the gate-voltage, Aharonov-Casher oscillations

All measurements discussed thus far were performed with the gate connected to ground to ensure a constant induced charge on the center island. In this section we will discuss the changes occurring in the *I-V* characteristic when the gate voltage is swept. To detect changes accurately we use a standard lock-in technique and measure the differential resistance for different values of the current bias. At a field of 1.2 Gauss, corresponding to the second and deepest dip in the critical current we current-bias the sample at 5 nA. This is just above the critical current which is pointed out by the arrow in the *I-V* characteristic at this field, shown in Fig. 3.5b. In Fig. 3.9 the differential resistance of sample A is shown as a function of gate voltage. Clearly a periodic modulation is visible. We choose a large enough bias current to not include the tiny remaining hysteresis in the modulation which would result in anomalously large oscillations. Still the modulation amplitude is largest just above the depinning current and decreases for higher bias currents. Similar oscillations were found at other values of the magnetic fields. At magnetic fields where the depinning current is smallest we generally find the largest modulation amplitudes.

The depinning current itself also shows some modulation with gate voltage especially when its absolute value is strongly suppressed. For the field of 1.2 Gauss this modulation is shown in Fig. 3.10. The relative amplitude of these

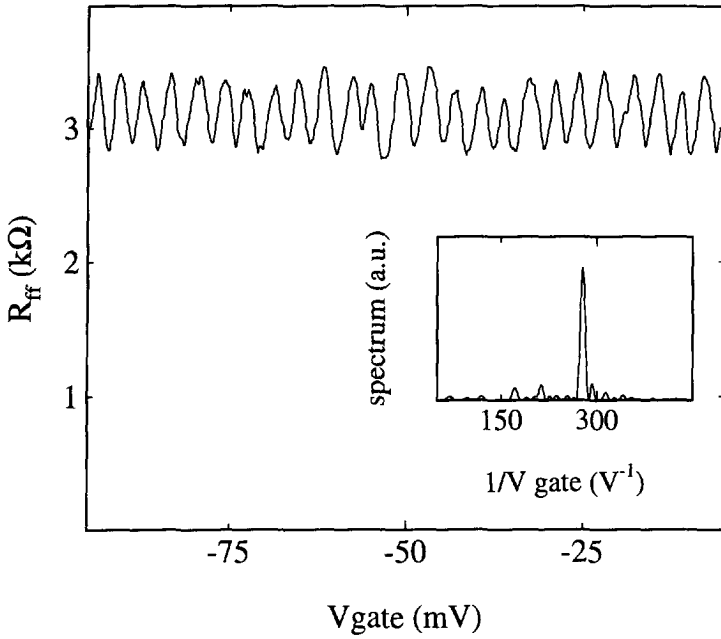Figure 3.9: *Differential resistance of sample A as a function of gate voltage in a field of 1.2 Gauss, which corresponds to the current-voltage characteristic of Fig. 3.5b. The bias current is 5 nA with 0.25 nA modulation amplitude. inset: Fourier transformation of the signal.*
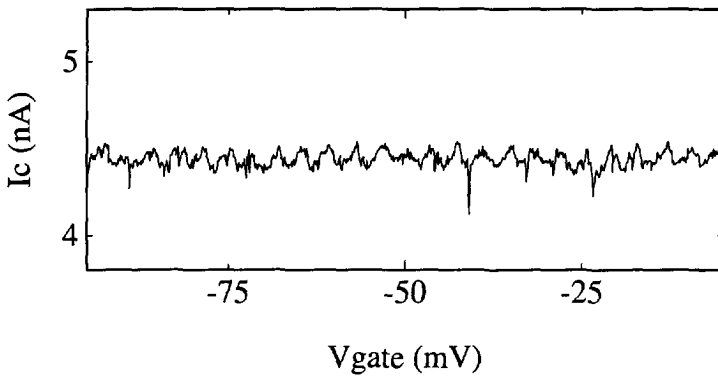

Figure 3.10: *Critical current of sample A versus gate voltage in a field of 1.2 Gauss, which corresponds to the I-V characteristic of Fig. 3.5b.*
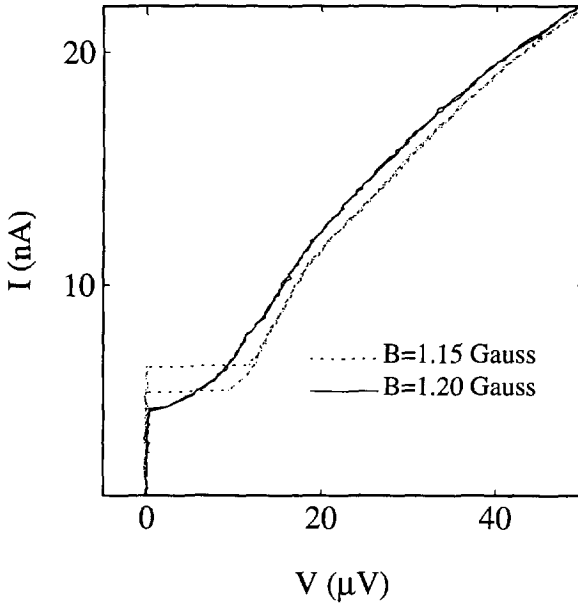
Figure 3.11: *Current-voltage characteristics of sample A in a magnetic field of 1.2 Gauss (solid line) and 1.15 Gauss (dashed line).*

oscillations does not exceed a few percent. We did not find any influence on the critical current in zero field, nor at any magnetic field where no flux-flow branch is present in the *I-V* characteristic. We did not measure the full *I-V* characteristic at different gate voltages. We do however want to compare the measured oscillations due to the gate voltage with the changes that occur in the *I-V* characteristic as a function of magnetic field, shown in Fig. 3.11. Measuring the magnetically induced change with the lock-in technique described above would yield larger but qualitatively similar oscillations as those observed as a function of gate voltage.

To determine the period of the oscillations we measured the capacitance of the gate to the center island. We fabricated a different sample using essentially the same layout as in Fig. 3.2. All large junctions were shorted and six small junctions were left out, so that the center island was only connected to the superconducting banks via two junctions. We measured several samples with a junction resistance higher than 50 kΩ and applied a 2 T magnetic field to completely suppress superconductivity. The measured *I-V* characteristic shows the

Coulomb gap that is typical for a high-resistance double junction. The current just above the threshold voltage is known to show an e-periodic dependence on gate voltage. From the period of these oscillations we find that the capacitance of the gate to the center island is 40 aF.

The oscillations in the *I-V* characteristic are shown to be e-periodically dependent on the charge on the center island. These oscillations are only measurable when a flux-flow branch is present in the *I-V* characteristic and the voltage across the array can be attributed to the crossing of vortices. We therefore conclude that the transport of vortices depends e-periodically on the charge enclosed by the two most favorable vortex paths. The Aharonov-Casher effect for vortices in Josephson-junction arrays has a fundamental period of 2e. However, as mentioned in ref. [5], this full periodicity is only measurable when typical quasiparticle tunneling times are long on the time scale on which the gate voltage is varied. Although one might not expect quasiparticles to be present at a temperature of 10 mK, it is experimentally well known that it is difficult to completely eliminate them [19, 20, 21, 22]. In our simulations we find that quasiparticles can also be generated in the array when vortices are moving through. The tunnel rates for quasiparticles are so small that no significant contribution to the current is expected. Still, on the typical five minute time scale on which the gate voltage is varied, tunneling of quasiparticles is not negligible. Whenever the gate-induced charge exceeds the value of e/2, a quasiparticle will tunnel onto the island and reset the charge to -e/2. In this manner the induced charge will remain between the limits of [-e/2,e/2] and e-periodic behavior will be observed.

For the magnetic field of 2.2 Gauss, we find the oscillation shown in Fig. 3.12, that consists of more than one Fourier component. From the simulations that we discussed in the previous section, we know that at this particular magnetic field vortices will also be present in the outer cells. When the motion of the vortices is no longer confined to the hexagon, the charge on other islands than the center island of the array will influence the relative phase difference between the two vortex paths.

The importance of confining the vortices to the hexagon is illustrated by the results of the measurements on samples B and C. Both samples show similar oscillations as sample A in the flux-flow resistance, and smaller oscillations in the critical current. The zero-bias resistance is higher than in sample A and oscillations can also be detected in the zero-bias resistance. For the lowest magnetic field where the critical current is at a minimum the oscillations are similar to the ones observed in sample A at this field. The Fourier transform shows a clear peak,
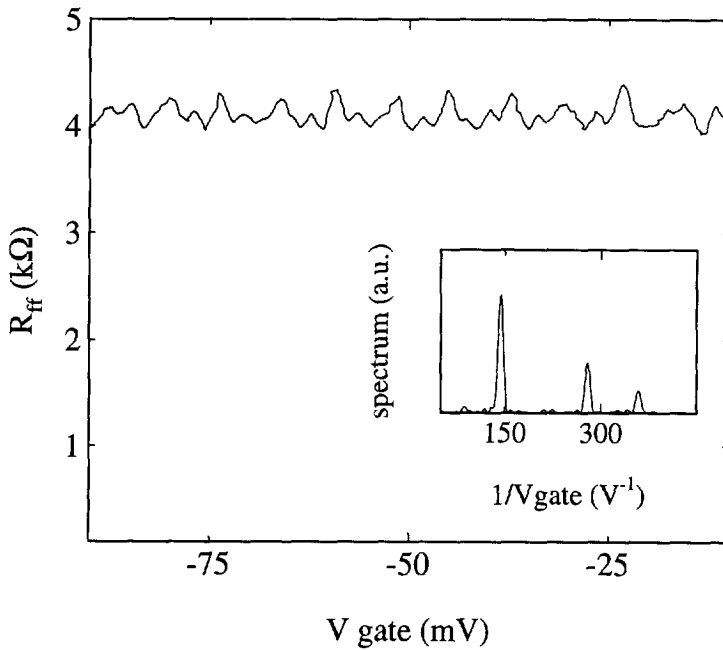
Figure 3.12: *Differential resistance of sample A in the flux-flow branch as a function of gate voltage in a field of 2.2 Gauss. inset: Fourier transformation of the signal.*

shown in Fig. 3.13 for sample C, at a frequency of $265V^{-1}$, which corresponds to an e-periodic oscillation around the middle island. In sample B some beating of the oscillation is visible. At the second dip of the magnetic field the oscillations in both samples become complex. The Fourier transform of sample C shown in Fig. 3.13, shows three different periods, each similar to the ones we observed in sample A at a field of 2.2 Gauss. These different periods may well result from the vortices being no longer well confined to the hexagon. In these samples we expect the confinement to be less effective because the outer junctions are only larger by a factor of 1.5 or 1.

Measurements on other samples confirmed the importance of α. We did not measure on samples with α larger than three as the junction barriers, that are only a few atomic layers thick, then easily short. Most likely, when the size of the outer junctions is increased, a too large part of the current will flow through the outer junctions in the hexagon. As expected, also the value of E_J/E_C is
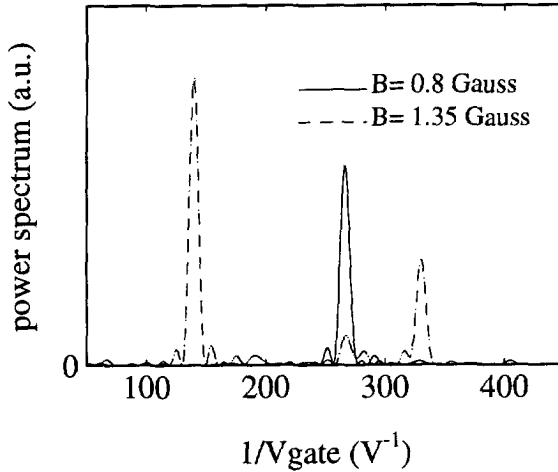
Figure 3.13: *Fourier transformation of the oscillations in the flux-flow regime in Sample C, at a field of 0.8 Gauss (solid line) and 1.35 Gauss (dashed line). These field values correspond to the first and the second dip in the critical current respectively.*

important. Small ratios seem to lead to larger oscillation amplitudes, but when E_J/E_C is smaller than 1 the dips in the critical current become less pronounced and mainly complex oscillations are observed. We expect the vortices to become less localized as E_J/E_C decreases and therefore confinement might no longer be effective at too small values.

We have looked at the behavior of all three samples in the normal state by applying a magnetic field of 2 T. The *I-V* characteristic shows the remnants of a charging gap. The resistance at zero-bias is less than twice the normal-state resistance in all samples. We did not find any influence of the gate voltage on the *I-V* characteristic in samples A and B. Sample C does however show a complex periodic modulation of the current at a fixed bias voltage. A Fourier transformation of this modulation shows the same three frequencies as we observed in this sample in the Aharonov-Casher oscillations at higher magnetic fields. From these measurements we conclude that the influence of the gate on the *I-V* characteristic is generally smaller in the normal state than in the superconducting state. The oscillations in sample C indicate that the different periods observed in some oscillations in samples in the superconducting state are indeed due to

charge induced on other islands than the central one.

To study the temperature dependence of the oscillation amplitude, and thus of the vortex interference, we have measured the oscillations in samples A, B, and C at different temperatures. When raising the temperature the relative oscillation amplitude had decreased by a factor of 10 at a temperature of 450 mK for sample A, 500 mK for sample B and 650 for sample C. Because the oscillation amplitude is very sensitive to the value of the current bias and because the shape of the I-V characteristic changes with temperature, we do not want to be specific about the precise shape of the decrease.

The effect of finite temperature has been discussed for a closed ring geometry [5]. For a free vortex in a loop with a circumference L the separation between levels is estimated to be $8E_C/L^2$. In our small array we expect the vortex mass to be higher and the level separation to be lower than 100 mK. In experiments on Aharonov-Bohm interference in normal metal rings the phase shift σ not only depends on the enclosed magnetic flux Φ but also on the difference in length between the left and right path ΔL. The total phase shift thus becomes $\sigma = 2\pi\Phi/\Phi_0 + 2\pi\Delta L/\lambda$, where λ is the wavevector of the participating electrons [23]. When thermal fluctuations become larger than the distance between energy levels the distribution of the wavevectors will equal ΔL and the interference averages out. In our Aharonov-Casher sample we can roughly estimate the vortex wavelength assuming that one vortex moves through the triangular lattice of the hexagon at constant velocity. A typical voltage of 10 μV corresponds to a vortex wavelength that is larger than array size. On this scale we expect the left and the right vortex path to be symmetric and it is not so clear how the separation between energy levels will determine the temperature dependence.

The interference does depend on the ratio between the charging energy of the center island and the temperature. In particular we expect the amplitude of the interference to decrease when quasiparticles are no longer localized by the Coulomb energy. The tunneling of Cooper pairs on and off the center island does not influence the acquired phase difference of the vortices, because the interference is a 2e periodic effect. Tunneling of a quasiparticle however, changes the phase difference by π. As long as the tunneling times are longer than the typical vortex passing time of 200 ps we expect to see a gradual decrease as a function of temperature. In our experiment the quasiparticles will not be in thermal equilibrium and exact calculation is impossible. The measured values, listed in Table 1 as T_{ac}, are in the right temperature range.

3.6   Discussion and conclusion

To find a flux-flow solution in the I-V characteristic there must be damping present in the system. In our classical simulations the dissipation in the flux-flow regime is mainly determined by the normal state resistance, which is a consequence of the voltage across specific junctions momentarily exceeding the gap voltage. This occurs when a vortex crosses a junction, but also due to the complex oscillations of the phases that a vortex excites in its wake. In our simulations we have to assume a smaller normal-state resistance than we actually had in our experiment in order to find a branch in which vortices move at a more or less controlled speed. This signifies that an additional damping mechanism is present in our experimental system. We expect that in our small array the high-frequency components of the motion of the phases on the busbars will be damped by the low impedance of the electromagnetic environment. As the plasma frequency of the junctions is of the same order of magnitude as the Josephson coupling energy, quantum fluctuations can certainly not be neglected. These quantum fluctuations will change the interaction between the vortices and the spinwave-type oscillations but no quantitative predictions are available for our small system. It would be interesting to study the dissipation theoretically in more detail and possibly translate results into an effective inelastic scattering length for vortices.

The fact that we find an e-periodic dependence on the gate voltage in our superconducting system is a phenomenon that has often been observed in, for instance, double junction systems [19, 20, 21, 22]. It is clear that the presence of quasiparticles will reduce the expected period. That quasiparticles are present at these low temperatures has been attributed to thermal fluctuations in the measurement leads and to the breaking up of Cooper pairs on the island by incident photons. In our array quasiparticles might also be created by the moving vortices.

There are similarities between a double junction system and our Aharonov-Casher experiment. In a double junction, a supercurrent is observed when the Josephson coupling energy is of the same order of magnitude as the charging energy. This current arises because charge eigenstates are coupled by the Josephson coupling [24]. By applying a gate voltage to the island in between the junctions, the energy required to have an additional Cooper pair on the island can be lowered, which increases the supercurrent. It would be interesting to compare both systems by calculating the quantum mechanical tunneling rates for Cooper pairs through the Aharonov-Casher sample. Including the influence of the environ-

ment through the $P(E)$ function, as discussed in for instance ref. [25], one could probably also analyze the dissipation mechanism discussed in the last section. However, the complex geometry and the fact that one also needs to consider finite voltage solutions make this a difficult task.

We have shown elsewhere [26] that the double junction can also be analyzed in terms of the phase differences across the junctions that are the conjugate variables to the charge. The tunneling of Cooper pairs is shown to be equivalent to the interference of the phase variable, which shows the close relation with the experiment that is reported on here. An important feature for the presently discussed experiment is that we analyse the interference in a flux-flow branch where vortices move at a controlled speed. We also find that in our geometry, where charges are induced on several islands, the path along which the vortices move is important.

The concept of a charge vector potential that is responsible for the Aharonov-Casher effect, has been used also to describe infinite arrays where equal amount of charge is induced on every island [4, 27]. This charge frustration plays the dual role to magnetic frustration. Theoretical results indicate [28] that when E_J and E_C are of the same order of magnitude both mechanisms have a similar influence on the array behavior but of opposite sign. In our experiment we do not know what gate voltage corresponds to zero induced charge because offset charges will be present on the island. The influence of the induced charge on the I-V characteristic is much smaller than the influence of the magnetic field, but shows similar features.

To conclude: We have observed that the transport of vortices through an array depends periodically on the induced charge enclosed by the possible vortex paths. These oscillations are due to the quantum mechanical interference of vortices and clearly demonstrate the Aharonov-Casher effect.

Acknowledgements

References

[1] E. Simanek, Solid State Comm. **48**, 1023 (1983).

[2] U. Eckern and A. Schmid, Phys. Rev. B **39**, 6441 (1989).

[3] S. E. Korshunov, Physica B **152**, 261 (1988), A. I. Larkin, Yu. N. Ovchinikov, and A. Schmid, ibid. 266 (1988).

[4] R. Fazio, U. Geigenmüller, and G. Schön, in *Proc. of the Adriatico Research Conference on Quantum Fluctuations in Mesoscopic and Macroscopic Systems, July 1990*, (World Scientific, Singapore, 1991) and R. Fazio, A. van Otterlo, G. Schön, H. S. J. van der Zant, and J. E. Mooij, Helvetica Physica Acta **65**, 228 (1991).

[5] B. J. van Wees, Phys. Rev. Lett. **65**, 255 (1990).

[6] T. P. Orlando and K. A. Delin, Phys. Rev. B **43**, 8717 (1991).

[7] W. J. Elion, J. J. Wachters, L. L. Sohn, and J. E. Mooij, Phys. Rev. Lett. **71**, 2311 (1993).

[8] Y. Aharonov and A. Casher, Phys. Rev. Lett. **53**, 319 (1984).

[9] H. S. J. van der Zant, F. C. Fritschy, T. P. Orlando, and J. E. Mooij, Phys. Rev. Lett. **66**, 2531 (1991).

[10] H. S. J. van der Zant, F. C. Fritschy, T. P. Orlando, and J. E. Mooij, Europhys. Lett. **18**, 343 (1992).

[11] H. S. J. van der Zant, F. C. Fritschy, W. J. Elion, L. J. Geerligs, and J. E. Mooij, Phys. Rev. Lett. **69**, 2971 (1992).

[12] Y. Aharonov and D. Bohm, Phys. Rev. **115**, 485 (1959).

[13] A. Cimmino, G. I. Opat, A. G. Klein, H. Kaiser, S. A. Werner, M. Arif, and R. Clothier, Phys. Rev. Lett. **63** , 380 (1989).

[14] B. Reznik and Y. Aharonov, Phys. Rev. D **40**, 4178 (1989).

[15] L. J. Geerligs, PhD thesis, Delft University of technology (1990).

[16] H. S. J. van der Zant, F. C. Fritschy, T. P. Orlando, and J. E. Mooij, Phys. Rev. B **47**, 295 (1993).

[17] L. L. Sohn, J. J. Wachters, U. Geigenmüller, W. J. Elion, and J. E. Mooij, Physica. B **194-196**, 1059 (1994).

[18] C. J. Lobb, D. W. Abraham, and M. Tinkham, Phys. Rev. B **27**, 150 (1983); M. S. Rzchowski et al., Phys. Rev. B **42**, 2041 (1990).

[19] L. J. Geerligs, V. F. Anderegg, J. Romijn, and J. E. Mooij, Phys. Rev. Lett. **65**, 377 (1990).

[20] M. T. Tuominen, J. M. Hergenrother, T. S. Tighe, and M. Tinkham, Phys. Rev. Lett. **69**, 1997 (1992).

[21] P. Joyez, P. Lafarge, A. Filipe, D. Esteve, and M. H. Devoret, Phys. Rev. Lett. **72**, 2458 (1994).

[22] T. M. Eiles, and J. M. Martinis, Phys. Rev. B **50** 627 (1994).

[23] A. Douglas Stone and Y. Imry, Phys. Rev. Lett. **56**, 189 (1986).

[24] D. V. Averin and K. K. Likharev, in *Mesoscopic phenomena in solids*, edited by B. L. Altshuler, P. A. Lee and R. A. Webb (Elsevier Science Publishers, North-Holland 1991).

[25] M. H. Devoret and H. Grabert in *Single Charge Tunneling* ed. M. H. Devoret and H. Grabert, Plenum Press New York (1991).

[26] W. J. Elion, P. Hadley and J. E. Mooij, To appear in *Proceedings of the ICTP Workshop on Quantum dynamics of submicron structures*, eds. H. Cerdeira, G. Schön and B. Kramer (Kluwer, 1995).

[27] B. J. van Wees, Phys. Rev. B **44**, 2264 (1991).

[28] C. Bruder, R. Fazio, A. Kampf, A. van Otterlo, and G. Schön, Phys. Rev. B **47**, 342 (1993) and A. van Otterlo, K.-H. Wagenblast, R. Fazio, and G. Schön, Phys. Rev. B **48**, 3316 (1993).

Chapter 4

Interaction between charges and flux quanta in small and large networks of Josephson junctions

W. J. Elion, P. Hadley and J. E. Mooij

Department of Applied Physics,Delft University of Technology and
Delft Institute for Micro-Electronics and Submicron Technology
PO Box 5046, 2600 GA Delft, The Netherlands

Abstract: In systems of Josephson junctions where the charging energy is of the same order of magnitude as the Josephson coupling energy, it is equally natural to describe the system in terms of the charge on the junction capacitors or in terms of the gauge-invariant phase difference across the junction. A changing gauge-invariant phase difference implies motion of flux quanta across the junction. By analyzing a double junction in terms of these moving flux quanta a parallel can be drawn with a 2D Josephson junction array through which vortices move. The influence of an induced charge can in both systems be attributed to quantum interference of flux quanta.

4.1   Introduction

The dynamics of classical Josephson junctions are usually described in terms of the gauge-invariant phase difference ϕ. The derivative of this phase with respect to time is proportional to the charge Q on the junction capacitor. When the junctions dynamics are treated quantum mechanically, charge and phase do not commute. This leads to an Heisenberg uncertainty relation $\Delta\phi\Delta Q \geq e$ [1]. The fluctuations depend on the ratio between the Josephson coupling energy E_J and the charging energy $E_C = \frac{e^2}{2C}$, where C is the junction capacitance. For large Josephson coupling energy phase fluctuations are small and it is convenient to describe the junction dynamics in terms of this phase. If the charging energy is largest, the charge on the junction capacitor is the most natural choice.

Instead of the gauge-invariant phase difference one can also use a variable that has the dimension of magnetic flux. A phase slip of 2π then corresponds to the motion of a flux quantum across the junction. If a junction is connected in a closed loop l, this is the simple consequence of Faradays law: $\oint \mathbf{E}.dl = -\frac{\partial}{\partial t}\Phi(l)$, where $\Phi(l)$ is the flux enclosed by the loop. The issue will be discussed in some more detail in the next section.

Several experiments on systems of junctions with comparable Josephson and charging energy show the interplay between Josephson and charging effects [2, 3, 4, 5, 6]. In this intermediate regime the physical mechanisms can be explained in terms of Cooper pair tunneling or phase motion and the choice for either conjugate variable depends on convenience or convention. An example is the system of two small Josephson junctions in series that is also known as the Bloch-transistor. At temperatures lower than E_C/k_B single Cooper pair tunneling events are energetically unfavorable. However, the Josephson coupling energy couples charge eigenstates [7] and when the coupling is strong enough a supercurrent is observed to flow through the system. The electrostatic energy of a Cooper pair on the island in between the two junctions can be changed by applying a voltage to a gate that is coupled to the island through a small capacitor. As a function of the charge induced on this gate capacitor a modulation of the supercurrent is observed that is 2e-periodic as long as the presence and creation of quasiparticles can be neglected [2, 3, 4, 5, 6, 8].

We will show that there is an equivalent description of this system in terms of interference of flux quanta. This concept follows from earlier work on single junctions that we will briefly recapitulate in the next section. The interesting aspect of this approach is that it gives more insight into the relation between a
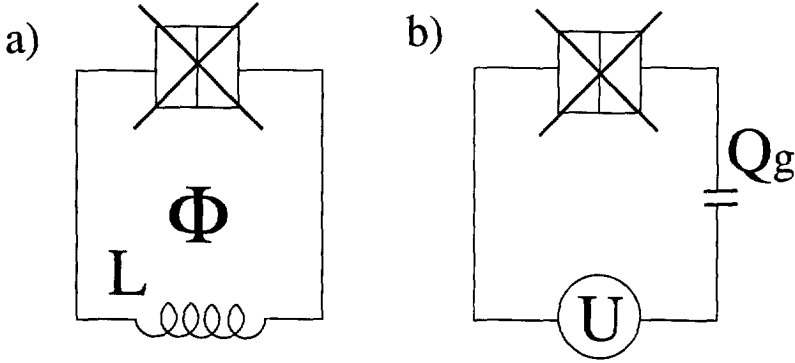
Figure 4.1: *Schematic drawing of a) the rf-SQUID and b) the Cooper pair box.*

double junction and a two-dimensional array through which vortices pass. We will compare the motion of vortices in arrays with the motion of flux quanta in smaller systems of junctions. In particular we compare the interference of flux quanta in a double junction with the quantum interference of vortices that has been predicted [9] and observed [10] in a Josephson junction array.

4.2 Persistent currents of Cooper pairs and flux quanta

A familiar system in which flux is clearly related to tunneling of the gauge-invariant phase difference is the rf-SQUID that is schematically drawn in Fig. 4.1a.

The Hamiltonian of the system reads:

$$H = \frac{Q^2}{2C} + \frac{(\Phi - \Phi_{ext})^2}{2L} - E_J \cos(2\pi \frac{\Phi}{\Phi_0}) \tag{4.1}$$

Here L is the loop inductance, Φ is the flux in the loop and Φ_{ext} is the externally applied flux. The gauge-invariant phase difference across the junction is given by $2\pi \frac{\Phi}{\Phi_0}$. If the inductance is large the Hamiltonian is periodic in Φ with a period of one flux quantum $\Phi_0 = h/2e$. The energy eigenstates can be classified according to the Bloch theorem [11, 12]. Each value of the applied flux corresponds to a persistent current of Cooper pairs in the ring. There are interesting predictions for macroscopic coherence of two quantum states at $\Phi = \Phi_0/2$ [13] but these have so far not been observed experimentally.

The dual circuit to the rf-SQUID is the Cooper pair box that is shown in Fig. 4.1b [14]. A single Josephson junction is connected to a voltage source via a capacitor. If the capacitor is very small compared to the junction capacitance the induced charge Q_g can be treated as a control parameter and the Hamiltonian of the system is

$$H = (Q - Q_g)^2/2C - E_J \cos \phi \qquad (4.2)$$

For $E_C \gg E_J$ the gate voltage charges the gate capacitor and effectively changes the voltage across the junction. The charge Q can be interpreted as the momentum operator in the phase representation. For every gate voltage there is a persistent motion of the phase difference across the junction and consequently a persistent current of flux quanta. When the gate-voltage is increased and the charge on the gate-capacitor exceeds e, a Cooper pair will tunnel across the junction to keep the system in its lowest energy band.

The rf-SQUID and the Cooper pair box are dual systems, where the roles of phase and charge are reversed [14]. The induced charge Q_g plays the role of the flux in the example of the rf SQUID.

A subtle difference between the variables of flux and phase is that the phase is periodic, while the flux is an extended variable. This issue has been extensively discussed in literature [15, 16, 17]. It is argued that for a junction that is coupled to the electromagnetic environment there is a finite change in energy connected with the changing of the phase difference and the situation before and after a 2π phase slip are therefore not indistinguishable. In the example of the rf-squid the loop inductance makes it in principle possible to count the number of flux quanta present in the ring. In this case the charge on the junction capacitor is a continuous variable. For a junction that is decoupled from the environment as in the Cooper pair box, the change in energy connected with a 2π phase slip is zero. The Hamiltonian is periodic in either flux or phase difference and the conjugate variable, the charge on the island, is discrete.

4.3   Interference of flux quanta in a double junction

The Cooper pair box discussed above shows persistent currents of phase-difference or flux. We can extend the picture by looking at the "open" geometry where a doubly connected path leads to interference. The approach we will take is
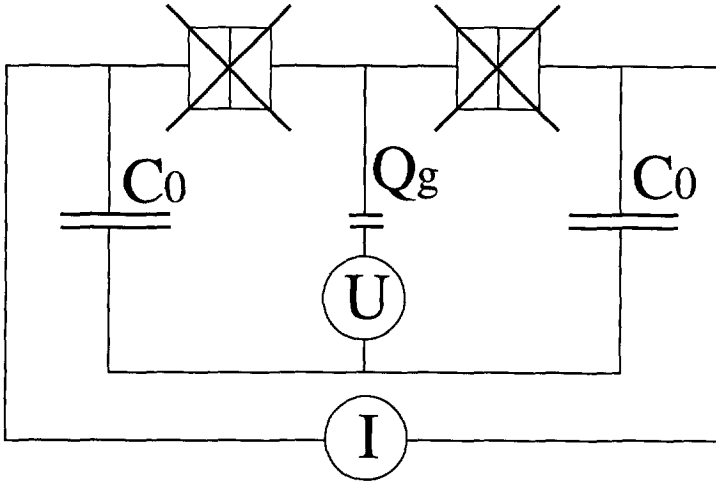
Figure 4.2: *Schematic drawing of the double junction discussed. Two large ca-pacitors are connected in parallel with the current source, which closely resembles the situation in the experiment.*

analogous to the picture of the washboard potential that is commonly used for a single junction in the classical limit. We connect the junction through a perfect current source, which is equivalent to making the inductance in Fig. 4.1a go to infinity. The phase difference ϕ across the junction obeys the following equation of motion:

$$\frac{\Phi_0}{2\pi} C\ddot{\phi} + I_c \sin\phi = I \tag{4.3}$$

This equation resembles the equation of motion of a particle in a washboard potential. Because damping is not included in this model dynamic calculations are not possible. Still the washboard model is valid to calculate the critical current of the system, which is the current above which the equation has no stable solution. The position of the particle in ϕ-space has a one to one correspondence to the position of a flux quantum moving in real space. Although we cannot tell the position of the flux quantum exactly, we know that when the phase difference across the junction changes by 2π, a flux quantum moves across.

We use the same approach in a more complicated system consisting of two junctions in series, the Bloch-transistor. The island in between the two junctions is coupled to a gate with a small capacitor C_g so that a charge Q_g can be induced. The system is connected to a current source in parallel with two large capacitors C_0. This connection, shown in Fig. 4.2, closely resembles the experimental set-up,

where all the measurement leads have a large capacitance to ground.

The Hamiltonian is:

$$H = \frac{(Q_- - Q_g)^2}{2C + C_g} + \frac{Q_+^2}{2C + 2C_0} - 2\frac{\Phi_0}{2\pi} I_c \cos\frac{\phi_+}{2} \cos\frac{\phi_-}{2} - 2I\frac{\Phi_0}{2\pi}\phi_+ \qquad (4.4)$$

The variables are $\frac{\Phi_0}{2\pi}\phi_+$ and $\frac{\Phi_0}{2\pi}\phi_-$ where ϕ_+ is the sum of the phase differences of both junctions and ϕ_- is the difference between them. The conjugated variables are the charge on the external capacitors ,Q_+, and the charge on the island Q_- respectively.

An outline of the derivation of this Hamiltonian is given in the Appendix to this chapter. The Hamiltonian corresponds to the classical equations of motion:

$$\dot{Q}_+ + 2I_c \sin\frac{\phi_+}{2} \cos\frac{\phi_-}{2} = 2I \qquad (4.5)$$

$$\dot{Q}_- + 2I_c \cos\frac{\phi_+}{2} \sin\frac{\phi_-}{2} = 0 \qquad (4.6)$$

These equations resemble those of a particle in a two-dimensional potential landscape. Because of the different capacitances in the problem, the particle has a different (band) mass in the two directions. In general the capacitance of the leads to ground C_0 will be much larger than the capacitance to the gate C_g and ϕ_+ is a classical variable. The applied current tilts the potential in the ϕ_+ direction and the critical current is determined by the onset of motion of this external phase. In Fig. 4.3a we draw the minimum energy of the system as a function of the external phase difference ϕ_+.

When the external phase difference approaches the value of π the internal phase difference switches from 0 to 2π or to -2π. These possibilities correspond to a phase slip occurring, or the flux quantum crossing, over the left or over the right junction. By measuring the flux through the loop with the current source it is in principle possible to tell that the external phase difference has changed with 2π. The internal phase difference is a periodic variable and the value of -2π and 2π are indistinguishable from the initial value of 0. Reducing the internal phase difference to values between $[-\pi, \pi]$ we find a doubly connected path in ϕ-space that is shown in Fig. 4.3b. This path is equivalent to a doubly connected path of a flux quantum in real space.

Until now we have followed a completely classical approach. It is known that when the charging energy becomes of the order of the Josephson coupling energy, the internal phase difference becomes a quantum mechanical variable. We then
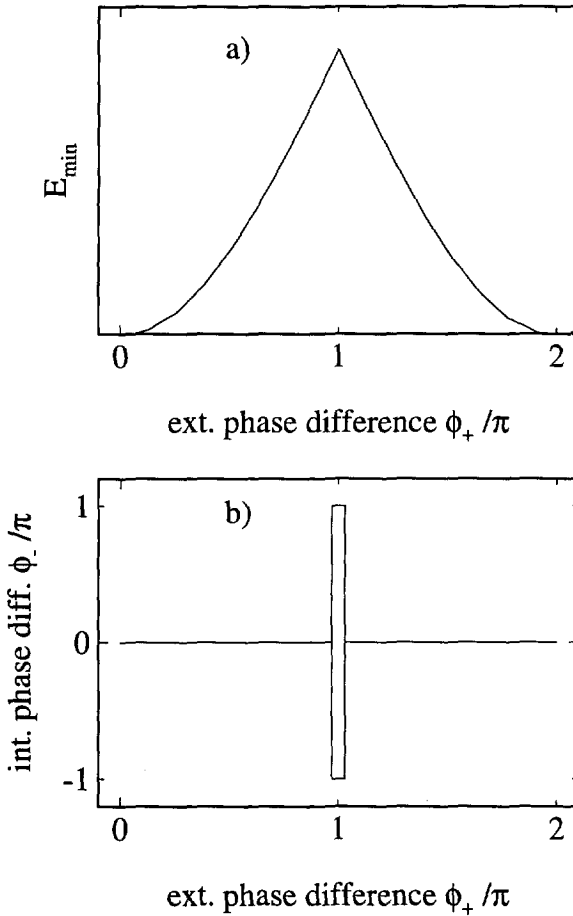
Figure 4.3: a: *Minimum energy as a function of the external phase difference ϕ_+* b: *Corresponding doubly connected path in ϕ-space.*

expect quantum interference to occur between the two paths shown in Fig. 4.3b. The induced charge Q_g gives rise to a phase difference between both paths just as in the dual system ,a DC squid, the phase difference between the interfering Cooper pairs depends on the applied flux. Like in ref.[9] we could also define a charge-vector potential in the periodic ϕ_- direction as $Q_g = - \oint d\phi_- A_q$ to show that there will be a phase shift between both paths that is equal to $2\pi \frac{Q_g}{2e}$. This interference will influence the onset of phase motion, and thereby the critical current of the system.

As discussed in the introduction to this chapter, the critical current has experimentally been observed to depend on gate voltage. The usual description in terms of tunneling of Cooper pairs is equivalent, and dual to, the interference of flux quanta discussed above.

4.4   Vortices in 2D arrays

It is interesting to compare the motion of flux quanta across a junction with the motion of vortices in a two-dimensional Josephson junction array. An array of $N \times N$ junctions can be described with N^2 coupled equations of motion. In the presence of a magnetic field, the energy of the array is lowered by introducing a number of vortices. These vortices correspond to a special pattern in the configuration of the phases. The complexity of the description can be largely reduced by using an equation of motion for the vortices, instead of for the junctions. For a vortex moving along the x-direction in the array this equation takes the form:

$$M_v \ddot{x} + \eta \dot{x} - \gamma E_J \sin(2\pi x) = \frac{I}{I_c} \qquad (4.7)$$

$M_v = \frac{\Phi_0^2 C}{2}$ is the vortex mass, x is the position of the vortex in units of the lattice constant and γ depends on the lattice geometry. η is the effective damping. It has been shown experimentally that vortices act like particles with a mass that move in the periodic potential of the junction lattice [18, 19].

The additional degrees of freedom are attributed to spin waves, fluctuations of the phases around the equilibrium value. Although dissipation in an array is not yet completely understood, it is clear that in a large array these spin waves provide an effective damping mechanism for the moving vortex, even if the junctions themselves are underdamped [21]. The damping present ensures that a vortex can move through the array at a controlled speed, which manifests itself as a branch of finite resistance below the gap that is called the flux flow resistance.

In a double junction there is no flux flow regime. The voltage switches to the superconducting gap as soon as the current exceeds the critical current. When the system is measured using a voltage bias it has been found that Cooper pairs cannot only tunnel at zero voltage but also, to a lesser extent, at specific voltages that match dissipative modes of the electromagnetic environment. In very small arrays with a special layout we have observed the *I-V* characteristic shown in Fig. 4.4.   The behavior resembles that of a double junction but the additional degrees of freedom enhance and broaden the resonances. There seems to be a
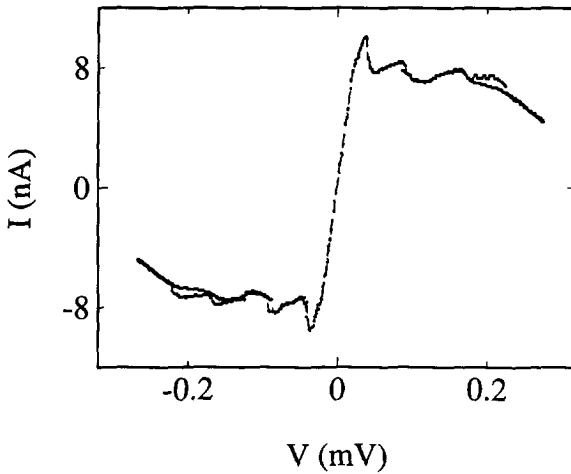
Figure 4.4: *Example of a current-voltage characteristic of a small 2D structure which resembles both the double junction and a larger array. The sample consists of a pentagon-shaped array that is connected with two large junctions on each side to the superconducting busbars. Just as for the Y-sample shown in Fig. 5.1, an extra voltage probe is present. The lead resistance in this two point measurement has not been substracted.*

smooth transition between the double junction, with frequency dependent damping provided mainly by the environment, and a large array where the damping is determined by the junctions in the array.

The number of vortices in an infinitely large array is equal to the number of flux quanta applied. In a typical fabricated array with small $Al - Al_2O_3 - Al$ junctions, the Josephson penetration depth is so large that the magnetic flux is not confined to the center of the vortex but almost uniform across the array. Still a moving vortex carries a flux quantum. To inject current into an array experimentally, superconducting busbars are often connected to the two sides. The phase difference between the busbars can be viewed as the analogue of the external phase difference in a double junction. Each vortex that moves across the array will give rise to a 2π phase slip across the busbars. For low magnetic fields where it is not favorable to have a vortex in the array the complete array resembles a single junction with an effective Josephson coupling energy that depends on the magnetic field.
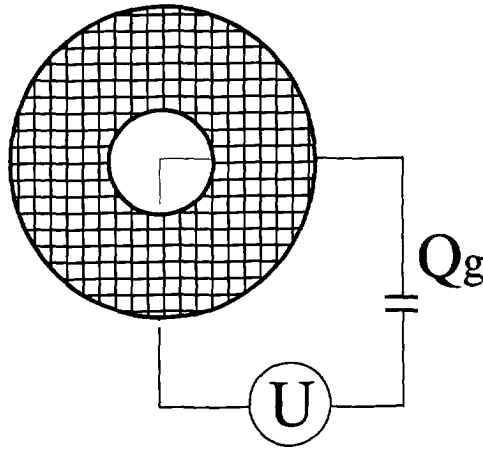
Figure 4.5: *The proposed geometry to measure persistent current of vortices.*

4.5   Interference of vortices

In arrays with small junctions vortices have been shown to exhibit quantum mechanical properties [22]. Van Wees [9] has studied quantum states of vortices in a ring shaped array, bounded by superconducting banks as shown in Fig. 4.5.

A charge Q_g can be induced to the superconducting inner ring, by means of a small gate capacitance. If the Josephson coupling energy is larger but of the same order as the charging energy of the junctions, a voltage is induced between the inner and outer bank that corresponds to a persistent current of vortices in the array. This persistent current is analogous to the persistent current of flux quanta moving across the junction in the Cooper pair box. A charge vector potential is defined as A_q through the relation $Q_g = - \oint A_q dl$. The generalized vortex momentum becomes $P_v + \Phi_0 A_q$ and the appropriate vortex Hamiltonian is:

$$H = \frac{(P_v + \Phi_0 A_q)^2}{2M_v} + E_p(x) \tag{4.8}$$

where P_v is the canonical vortex momentum and E_p is the periodic potential of the lattice that is assumed to be small. In an array where vortices can cross along a doubly connected path, quantum vortices interfere as a function of the induced charge. This prediction has been tested in a recent experiment [10] using a specially-shaped array. As a result of vortex crossings, a resistive branch is observed in the *I-V* characteristic. The slope of this branch shows a periodic

modulation with the charge induced on an island enclosed by the two possible vortex paths. This effect is due to interference of vortices.

4.6 Hall-effect for vortices

The notion of a charge vector potential can also be used for an infinitely large array in which the same non-zero charge q_g is induced on every island. In analogy to the well know magnetic frustration, the induced charge in this case is known as charge frustration. A vortex moving in this array is predicted to experience a force $F = q_g . \Phi_0 (\vec{v} \times \hat{n})$. Here $\vec{v}$ is the vortex velocity and $\hat{n}$ is the unit vector perpendicular to the array. This force is sometimes referred to as the Magnus force because its direction is perpendicular to the vortex velocity and gives rise to an Hall angle. Contrary to the Aharonov-Casher effect, the Hall effect is a classical phenomenon arising from the gate capacitor charging the islands. A handwaving argument for the existence of this force is the following. When a vortex moves across a junction connecting islands A and B, a potential difference is induced that is proportional to the vortex velocity. The energy on the capacitance to the gate of islands A and B changes by an amount $(V_g^2 - (V_g - V_{A(B)})^2)/2C_g$, where $V_A = -V_B$ are the potentials of island A and B. For $V_g = 0$ the energy that the vortex requires to change the phase of island A and B will be the same. If V_g is not zero it will be different. The fact that the phase on one island can change with less energy cost than the other leads to a bending of the vortex path. The actual path depends on the energy of all islands and also on the dissipation present. The force can however conveniently be described by the expression given above, acting on a point-like vortex particle.

There is one fundamental question to this description. If the vortex is viewed as a point particle it will never be located on the superconducting islands in the array. On the other hand, the induced charge and the corresponding charge-field is only present on the islands. In this sense the vortex in the charge-frustrated array is equivalent to an electron moving through a two dimensional space in which a lattice of screened (AB) fluxes is present. Aharonov e.a. [23] have shown that in this case also a Hall effect exists that is periodic in the flux with period Φ_0.

We have also defined a charge vector potential for the double junction system in section 3 of this chapter. When biasing the system with a non-floating and finite voltage bias it is possible to induce an asymmetry in the voltages across both junctions. This will be discussed in the next chapter in more detail. We do

not propose to call this asymmetry a Hall effect. A similar asymmetry is present in the dual system which is the DC squid. Here the current flowing through both junctions is no longer equal when a magnetic field is applied.

4.7   Conclusion

We have shown how a vortex crossing an array bears close resemblance to a flux quantum that crosses a junction when the phase difference changes by 2π. Both in an array and in a double junction the I-V characteristic can be influenced by an induced charge. In the case of an array this can clearly be attributed to interference of vortices along a doubly connected path. In a less intuitive manner, a double junction can also be described in terms of interfering flux quanta. This description is the dual of the usual description in terms of tunneling of Cooper pairs. In an array the same vector potential that determines the phase shift for interfering vortex paths, leads to a Hall angle when all islands in the array are charged uniformly.

The interference of flux quanta discussed above relies on the concept of charge quantisation just as interference of Cooper pairs is the result of flux quantisation. The interference of Cooper pairs in an rf-SQUID is also related to persistent currents in normal metal rings. Apart from the absence of macroscopic coherence in the normal state, the physical mechanism of a quantum mechanical phase shift induced by the magnetic field is the same. In the normal state the dual to the Aharonov-Bohm effect [24] is the Aharonov-Casher effect [25] where flux quanta move around an infinite line charge. The interference of flux quanta in systems of Josephson junctions is a generalized form of the Aharonov-Casher effect.

Acknowledgements

4.8 Appendix: Interference-description of the Bloch transistor

In the circuit of Fig. 3 current conservation in every node means:

$$\begin{cases} I_c \sin \phi_1 + \frac{\Phi_0}{2\pi} C\ddot{\phi}_1 - I - C_0 \dot{V}_1 = 0 \\ I_c \sin \phi_2 + \frac{\Phi_0}{2\pi} C\ddot{\phi}_2 - I - C_0 \dot{V}_2 = 0 \\ I_c \sin \phi_1 + \frac{\Phi_0}{2\pi} C\ddot{\phi}_1 - I_c \sin \phi_2 - \frac{\Phi_0}{2\pi} C\ddot{\phi}_2 + C_g \dot{V}_g = 0 \end{cases} \tag{4.9}$$

where $\phi_{1(2)}$ are the gauge-invariant phase differences across junction 1(2), $V_{1(2)}$ are the voltages across the large capacitances C_0, and V_g is the voltage across the gate capacitance.

Also the sum of the voltages around every loop should be zero.

$$\begin{cases} V_1 + U - V_g + \frac{\Phi_0}{2\pi}\dot{\phi}_1 = 0 \\ V_2 - U + V_g + \frac{\Phi_0}{2\pi}\dot{\phi}_2 = 0 \end{cases} \tag{4.10}$$

where U is the voltage applied to the gate C_g.

It is useful to change to sum and difference variables, $\phi_+ = \phi_1 + \phi_2$ and $\phi_- = \phi_1 - \phi_2$. We find the following set of equations:

$$\begin{cases} \frac{\Phi_0}{2\pi} C\ddot{\phi}_+ - C_0(\dot{V}_1 + \dot{V}_2) + 2I_c \sin\frac{\phi_+}{2}\cos\frac{\phi_-}{2} = 2I \\ \frac{\Phi_0}{2\pi} C\ddot{\phi}_- + C_g \dot{V}_g + 2I_c \cos\frac{\phi_+}{2}\sin\frac{\phi_-}{2} = 0 \\ C_g \dot{V}_g = -C_0(\dot{V}_1 - \dot{V}_2) \\ \frac{\Phi_0}{2\pi}\dot{\phi}_+ = -(V_1 + V_2) \\ \frac{\Phi_0}{2\pi}\dot{\phi}_- = 2V_g - 2U - (V_1 - V_2) \end{cases} \tag{4.11}$$

We introduce two new variables: The charge on the island

$$Q_- = \frac{\Phi_0}{2\pi} C\dot{\phi}_- + C_g V_g \tag{4.12}$$

and the total charge on the other capacitors:

$$Q_+ = \frac{\Phi_0}{2\pi} C\dot{\phi}_+ - C_0(V_1 + V_2) \tag{4.13}$$

The equations can now be written as 4 equations of motion:

$$\begin{cases} \dot{Q}_+ + 2I_c \sin\frac{\phi_+}{2}\cos\frac{\phi_-}{2} = 2I \\ \dot{Q}_- + 2I_c \cos\frac{\phi_+}{2}\sin\frac{\phi_-}{2} = 0 \\ Q_+ = \frac{\Phi_0}{4\pi}(2C + 2C_0)\dot{\phi}_+ \\ Q_- = \frac{\Phi_0}{4\pi}(2C + C_g)\dot{\phi}_- + Cg(U + \frac{(V_1 - V_2)}{2}) \end{cases} \tag{4.14}$$

with the "boundary" condition:

$$C_g \dot{V}_g = -C_0(\dot{V}_1 - \dot{V}_2) \tag{4.15}$$

Defining $Q_0 = CgV$ and assuming $V_1 - V_2 \ll U$ the Lagrangian of the system becomes:

$$L = \frac{Q_-^2 - Q_0^2}{2C + C_g} + \frac{Q_+^2}{2C + 2C_0} + \frac{\Phi_0}{2\pi} 2I_c \cos\frac{\phi_+}{2} \cos\frac{\phi_-}{2} + 2I\frac{\Phi_0}{2\pi}\phi_+ \tag{4.16}$$

The conjugate variable of $\frac{\Phi_0}{2\pi}\phi_-$ is

$$\frac{2\pi}{\Phi_0}\frac{\delta L}{\delta\phi_-} = Q_- \tag{4.17}$$

and the conjugate variable of $\frac{\Phi_0}{2\pi}\phi_+$ is

$$\frac{2\pi}{\Phi_0}\frac{\delta L}{\delta\phi_+} = Q_+ \tag{4.18}$$

The Hamiltonian that follows from this Lagrangian then takes the familiar form:

$$H = \frac{(Q_- - Q_0)^2}{2C + C_g} + \frac{Q_+^2}{2C + 2C_0} - \frac{\Phi_0}{2\pi} 2I_c \cos\frac{\phi_+}{2} \cos\frac{\phi_-}{2} - 2I\frac{\Phi_0}{2\pi}\phi_+ \tag{4.19}$$

References

[1] P. W. Anderson in *Progress in Low Temperature physics* **5** ed. C. J. Gorter, (North-Holland, Amsterdam, 1967).

[2] L. J. Geerligs, V. F. Anderegg, J. Romijn, and J. E. Mooij, Phys. Rev. Lett. **65**, 377 (1990).

[3] M. T. Tuominen, J. M. Hergenrother, T. S. Tighe, and M. Tinkham, Phys. Rev. Lett. **69**, 1997 (1992).

[4] P. Lafarge, P. Joyez, D. Esteve, C. Urbina, M.H. Devoret, Phys. Rev. Lett. **70**, 994 (1993).

[5] T. M. Eiles, J. M. Martinis, Phys. Rev. B **50**, 627 (1994).

[6] D. B. Haviland, Y. Harada, P. Delsing, C. D. Chen and T. Claeson, Phys. Rev. Lett **73**, 1541 (1994).

[7] D. V. Averin and K. K. Likharev, in *Mesoscopic phenomena in solids* eds. B. L. Altshuler, P. A. Lee and R. A. Webb, (Elsevier Science Publishers, North-Holland, 1991).

[8] K. A. Matveev, M. Gisselfält, L. I. Glazman, M. Jonson, and R. I. Shekter, Phys. Rev. Lett. **70**, 2940 (1993).

[9] B. J. van Wees, Phys. Rev. Lett. **65**, 255 (1990).

[10] W. J. Elion, I. I. Wachters, L. L. Sohn and J. E. Mooij, Phys. Rev. Lett. **71**, 2311 (1993).

[11] F. Bloch, Phys. Rev. Lett. **21**, 1241 (1968).

[12] A. Widom, G. Megaloudis, T. D. Clark, H. Prance and R. J. Prance, J. Phys. A **15**, 3877 (1982).

[13] C. D. Tesche in *Proceedings of SQUID '85* eds. H. D. Hahlbohm and H. Lübbig, (De Gruyter, Berlin, 1985).

[14] M. Büttiker, Phys. Rev. B **36**, 3548 (1987).

[15] K. K. Likharev and A. B. Zorin, Journal of low temperature physics **59**, 347 (1985).

[16] E. Ben-Jacob, Y. Gefen, K. Mullen and Z. Schuss in *Proceedings of SQUID '85* eds. H. D. Hahlbohm and H. Lübbig, (De Gruyter, Berlin, 1985).

[17] G. Schön and A. D. Zaikin, Physica B **152** 203, 1988.

[18] H. S. J. van der Zant, F. C. Fritschy, T. P. Orlando, and J. E. Mooij, Phys. Rev. Lett. **66**, 2531 (1991).

[19] H. S. J. van der Zant, F. C. Fritschy, T. P. Orlando, and J. E. Mooij, Europhys. Lett. **18**, 343 (1992).

[20] U. Eckern and A. Schmid, Phys. Rev. B. **39**, 6441 (1989).

[21] U. Geigenmüller, C. J. Lobb and C. B. Whan, Phys. Rev. B **47**, 348 (1993), see also refs. 25-30 in chapter 1.

[22] H. S. J. van der Zant, F. C. Fritschy, W. J. Elion, L. J. Geerligs and J. E. Mooij, Phys. Rev. Lett. **69**, 2971 (1992).

[23] Y. Aharonov, H. Pendleton and A. Petersen, Int. Journal of Theoretical Physics **2**, 213 (1969).

[24] Y. Aharonov and D. Bohm, Phys. Rev. **115**, 485 (1959).

[25] Y. Aharonov and A. Casher, Phys. Rev. Lett. **53**, 319 (1984).
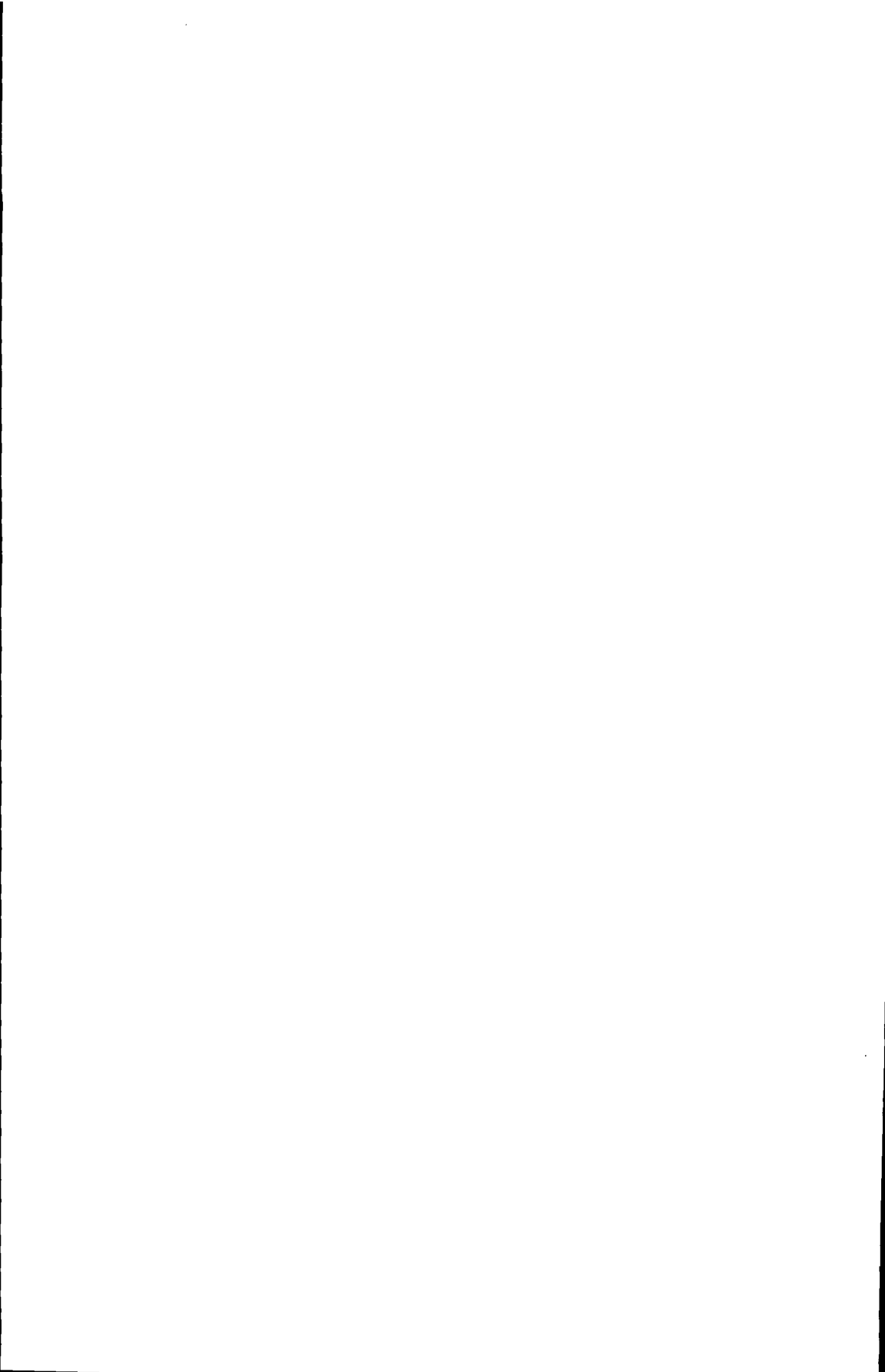
Chapter 5

Heisenberg's principle

5.1 Introduction

While pioneering research is inevitably unpredictable this aspect is usually not stressed when results are presented. A good example is the article on the demonstration of the Heisenberg principle in a superconductor that is reproduced in section three of this chapter. Originally we intended to measure the Hall effect for vortices in a small Josephson junction array. It has been predicted that moving vortices experience a force perpendicular to their velocity when charge is induced on the islands of an array [1, 2]. To measure this we thought of a Y shaped array, shown in Fig. 5.1, where vortices enter at one end and can choose two paths to leave the array. On the island where the vortex path splits a charge can be induced with a gate. The fraction of vortices going out through the left and right path should depend periodically on the induced charge.

When the finite size of the sample turned out to have a large influence, we decided to first study how the voltage is divided in a much smaller structure, two junctions in series with a gate capacitively coupled to the island in between the two junctions. As we will show in the next section one expects the voltage across both junctions to depend on the gate voltage and bias voltage. To study these effects we used a sample that had been fabricated for another purpose and that was slightly different from what we had in mind originally. Only after the first measurements were performed we realized that the sample was very suitable to demonstrate the fundamental Heisenberg uncertainty relation between phase and number of Cooper pairs in a superconductor. Sofar we have only performed detailed study of the latter phenomenon of which we will report in this chapter.

Possibly at the expense of clarity we will present the results in this chapter in chronological order. First we will discuss the expected voltage asymmetry that
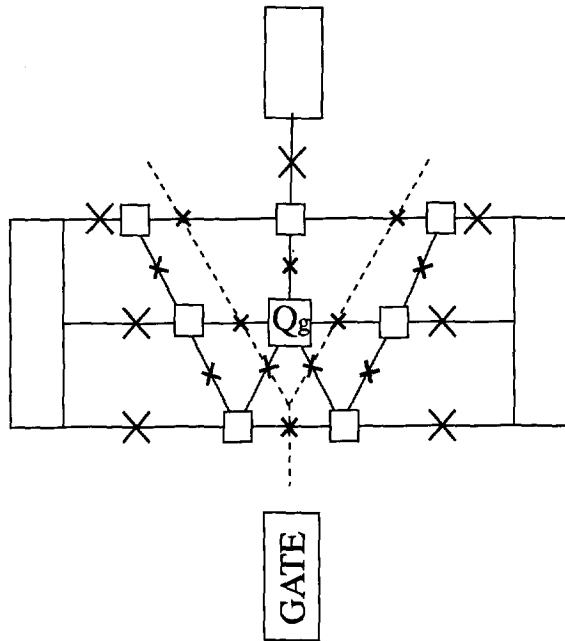
Figure 5.1: *Proposed geometry to measure Hall effect for vortices. The squares are superconducting islands and the crosses denote Josephson junctions. The dashed line shows the possible vortex paths.*

we wanted to study in the double junction system. Then we will report the results of the first measurements that showed interesting effects in the critical current of the device.

5.2   Voltage asymmetry in a double junction

The AC Josephson relation states that a voltage across a Josephson junction directly corresponds to motion of the phase difference across that junction. This relation also holds when the junction capacitance C is so small that the charging energy $E_c = e^2/2C$ of the junction is larger than the Josephson coupling energy. In geometries where the flow of Cooper pairs is blocked by the charging energy the phase difference will be subject to quantum fluctuations. Still the expectation value obeys the AC Josephson relation. Büttiker [3] has discussed the consequences for the case where a voltage is induced across a single junction through a small gate capacitor and a voltage source. Taking the Josephson cou-
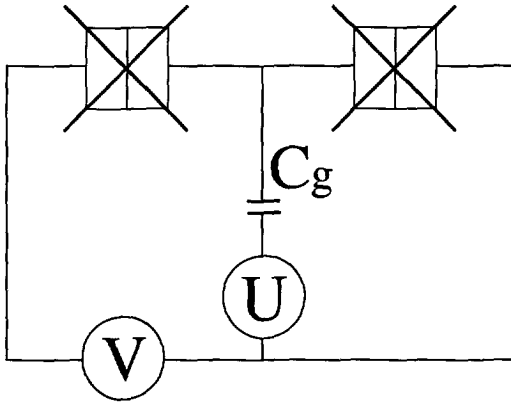
Figure 5.2: *Two superconducting tunnel junctions in series, connected to a voltage source V. The center island has a small capacitance C_g to a gate voltage source U.*

pling energy as a small perturbation in the Hamiltonian he has shown that the gate voltage induces a persistent motion of the gauge-invariant phase difference. For two junctions in series a similar phenomenon occurs. Consider, as shown in Fig. 5.2, a double junction biased with voltage V and with a gate voltage U applied to the center island through a small capacitor. When $V = 0$ this system is very similar to the single Cooper pair box. In the limit of small E_J the potential on the center island V_c shows the familiar saw-tooth dependence on the gate voltage that we show in Fig. 5.3. For low voltages the island potential is given by $V_c = UCg/(2C + C_g)$. When the gate voltage exceeds the value of e/Cg the energy of the system will be lowered by the tunneling of a Cooper pair onto the island. A non-zero potential of the island will cause a voltage difference of opposite sign across both junctions. The phase difference reacts correspondingly and a current of flux quanta moves across both junctions in different directions. For a symmetrically applied bias voltage V lower than e/C one expects voltages across the left and right junctions of $V_c - V/2$ and $V_c + V/2$.

If E_J is comparable to the charging energy the situation becomes more complex. The equation of motion for the difference ϕ_- of the phase across the left and the right junction is [4]:

$$(\frac{\Phi_0}{2\pi})^2 (C + \frac{C_g}{2})\ddot{\phi}_- + 2E_J \sin \frac{\phi_-}{2} = 0 \tag{5.1}$$
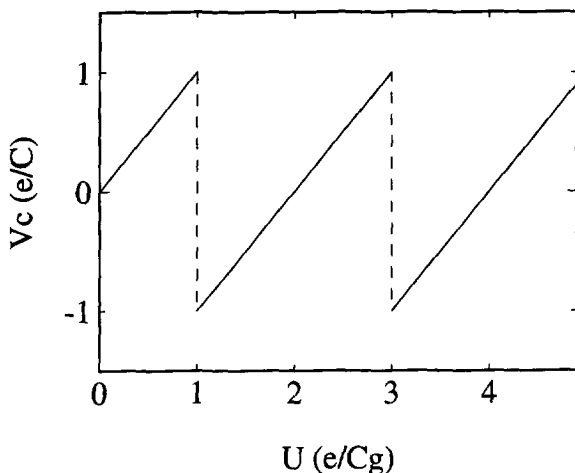
Figure 5.3: *The potential of the center island V_c as a function of the applied gatevoltage U, in the limit of small E_J.*

with at t=0

$$\frac{\Phi_0}{2\pi}\frac{2C + C_g}{C_g}\dot{\phi}_- = -2U \tag{5.2}$$

For $E_J = 0$ we recover the results given above, considering that $2V_c = \frac{\Phi_0}{2\pi}\dot{\phi}$. For finite E_J the equation resembles that of a particle with mass moving in a periodic potential. The gate voltage determines the velocity at t=0. We assume the particle to be at the bottom of the well at t=0, so that for large E_J it will just oscillate back and forth. The average velocity, and the average island potential, will be equal to zero. If the particle obeys classical mechanics its velocity becomes different from zero when the kinetic energy at the bottom of the potential is larger than the barrier height. This condition is satisfied if $\frac{C_g{}^2}{2C + C_g}U^2 \geq 2E_J$. Taking a maximum value $C_g U = e$ this becomes $\frac{e^2}{2C + C_g} \geq 2E_J$. When approaching this limit quantum fluctuations have to be taken into account that will smoothen the transition.

If the bias voltage is non-zero, the potential well becomes time dependent. Hadley [5] has numerically studied the classical voltage solutions for zero gate voltage, including a finite amount of damping. The results show that for the underdamped junctions case the voltage is generally not divided symmetrically over the two junctions. The results depend sensitively on bias voltage and for

some voltages show possibly chaotic behaviour.

We planned to experimentally study these asymmetry effects in a double junction with a third junction coupled to the island as a probe to measure the voltage. To reduce the chance of a phaseslip across this junction its critical current must be large compared to the measuring current of the voltage meter. On the other hand if this junction is too large we expect to destroy the charging effects on the central island and thereby the influence of the gate voltage. In the device that was used, the third junction was formed by two junctions in parallel, a DC squid, so that the effective Josephson coupling energy could be modulated by the magnetic field. Important aspect of this sample is that the contact pad to which this junction is connected is a large superconductor of which the phase is classical. The next section describes the results that we obtained measuring the supercurrent through the device while this pad was not yet connected to any measuring apparatus but just to macroscopic measuring leads.

5.3 Direct demonstration of Heisenberg's uncertainty principle in a superconductor

W. J. Elion, M. Matters, U. Geigenmüller, and J. E. Mooij

*Department of Applied Physics, Delft University of Technology
and Delft Institute for Micro-Electronics and Submicron technology (DIMES),
P. O. Box 5046, 2600 GA Delft, The Netherlands*

A Heisenberg uncertainty relation exists between any two non-commuting variables of a quantum-mechanical system. In a superconducting grain one has the number of Cooper pairs (n) and the phase of the superconducting wave function (φ). Suppressing fluctuations in either variable leads to enhanced fluctuations in the other [6, 7]. In a fabricated device we can suppress quantum-mechanical fluctuations in the phase with a SQUID that provides a variable coupling between the grain and a large superconducting reservoir. We measure the supercurrent that flows through two small-capacitance Josephson tunnel junctions that are connected to the grain. The total capacitance of the grain is so

**small that the number of Cooper pairs is well-defined and charge trans-
port through the grain is only possible through quantum-mechanical
fluctuations in n. Strong coupling of the phase to the reservoir leads
to enhanced fluctuations in n. As a result, we observe a large increase
in the supercurrent through the grain.**

In the superconducting state, Cooper pairs of electrons form a condensate that
can be described with one macroscopic wave function. As a general consequence
of this description, the number of Cooper pairs and the phase of the super-
conducting wave function are non-commuting variables [6]. The corresponding
Heisenberg uncertainty relation has the form $\Delta n \Delta \varphi \geq 1/2$. Due to the periodical
nature of φ, slight modifications are neccessary when $\Delta \varphi$ becomes of the order
of 2π [8]. Anderson [7] discussed the implications of this uncertainty relation
in connection with the Josephson effect[9]. For an isolated grain the number of
Cooper pairs is fixed and the phase is completely uncertain. If two macroscopic
superconductors are connected via a thin insulating barrier, the phase difference
between the two is well-determined. The number of Cooper pairs in each su-
perconductor fluctuates strongly. Depending on the phase difference charge will
flow through the barrier. With the present-day nanofabrication technology it is
possible to experimentally study the intermediate regime where the uncertainties
in n and φ are comparable. An example is the system of two small Josephson
junctions in series. The capacitance of the junctions can be made so small that
the electrostatic energy required to add one Cooper pair to the island in between
the junctions is much larger than the thermal energy $k_B T$. This charging energy
will tend to keep the number of Cooper pairs on the island fixed. The Josephson
coupling connects charge eigenstates differing by one Cooper pair. This coupling
induces quantum-mechanical fluctuations of the charge, which result in a super-
current through the device. The influence of the ratio of the charging energy and
the Josephson coupling energy on the maximum supercurrent of a double junction
has been studied both theoretically [10, 11] and experimentally [12, 13, 14, 15, 16].

We have proceeded from a different angle: we keep the junction parameters
of the double junction fixed and explicitly use the fact that, due to the Heisen-
berg relation, charge fluctuations increase when fluctuations in the phase are
suppressed. Suppression of the phase fluctuations can be achieved by coupling
the island with a third Josephson junction to a superconducting reservoir that
has a large capacitance to ground. Since the reservoir is otherwise unconnected
the average current through this junction must be zero and the classical phase
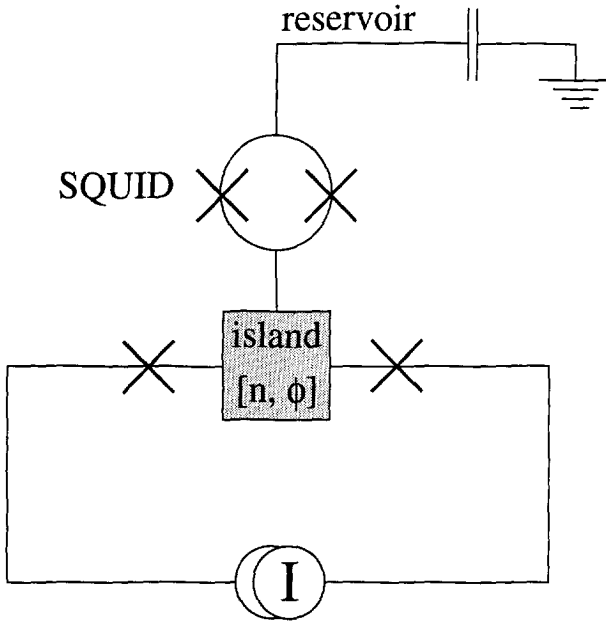
Figure 5.4: *Layout of our device. The crosses are $Al - Al_2O_3 - Al$ Josephson junctions that are connected with aluminium lines. The junction parameters are such that the quantum mechanical fluctuations of the number of Cooper pairs and the phase of the island are comparable. The large capacitor represents the capacitance to ground of a macroscopic lead that is not connected to any measuring apparatus. This reservoir has a superconducting phase that is constant in time. The SQUID, consisting of two junctions in parallel can be treated as a single junction with a flux-dependent Josephson coupling energy. The stronger the effective Josephson coupling between the island and the reservoir, the more the fluctuations in the phase of the island are suppressed. All leads are filtered with rfi feedthrough filters at room temperature and with RC and microwave filters at mixing chamber temperature. The resulting frequency-dependent response of the bias circuitry is responsible for a non-ideal behaviour of the current source.*

of the superconducting reservoir is equal to the average value of the phase φ of the island. Quantum fluctuations of φ will give rise to a time-dependent phase difference. As the Josephson energy of the junction is increased by such a phase difference, fluctuations in φ will be suppressed. Stronger effective Josephson coupling results in stronger suppression of the fluctuations. To be able to actually tune fluctuations in the phase, we have connected the island to a superconducting reservoir via two junctions in parallel, a SQUID (Fig. 5.4). We use this SQUID as a single junction of which the critical current, and thereby the effective Josephson coupling energy, can be changed by applying a small magnetic field perpendicular to the device [16, 17]. The effective Josephson coupling is largest when the number of magnetic flux quanta threading the loop is integral. For half-integral numbers the Josephson coupling will be close to zero so that the island is practically decoupled from the superconducting reservoir.

We have fabricated the device shown in Fig. 5.4, choosing junction parameters such that the Josephson coupling energy is of the same order of magnitude as the charging energy. In this regime both the phase of the island and the number of Cooper pairs are quantum mechanical variables that fluctuate around their equilibrium value. We have measured the current-voltage characteristics of the two junctions that are connected to the current source. We observe a supercurrent branch with a residual resistance that is lower than our measuring sensitivity of 10 Ω. We can clearly identify a switching current at which the voltage jumps to the superconducting gap. In Figure 5.5 we plot the measured switching current as a function of flux through the SQUID. We observe a large modulation that is periodic with a period of one flux quantum through the SQUID. For integral number of flux quanta phase fluctuations are most strongly suppressed and the resulting enhanced charge fluctuations lead to an increase in the supercurrent.

We have calculated the influence of the flux on the supercurrent through the device using the method described in ref. [10]. The ground state energy is calculated from the electrostatic hamiltonian which is the sum of the charging energy of the island and the Josephson coupling of all four junctions. The critical current of the device follows from the derivative of the ground state energy with respect to the phase difference of the measuring contacts. Thermal fluctuations of φ at our measuring temperature of 10 mK are negligible considering the energy difference of 2 K between the ground state and the first excited state. The influence of the flux through the SQUID on the critical current is the purely quantum mechanical consequence of tuning the phase fluctuations on the island and vanishes in the classical limit where the Josephson coupling energy is much
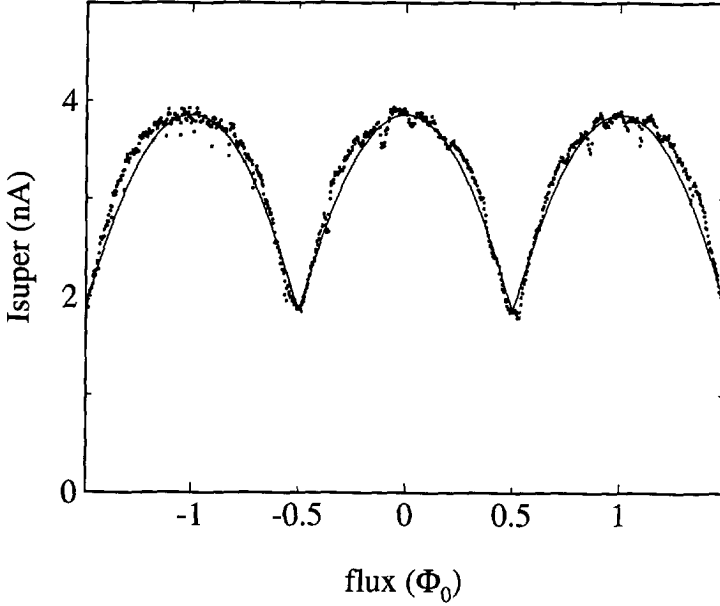
Figure 5.5: *Maximum supercurrent versus flux through the SQUID. The dots
represent the switching current measured through the junctions connected to
the current source. The solid line shows the calculated results, that are scaled
linearly to account for the small but finite classical noise in the leads and the
environmental impedance in the measurement. Flux is plotted in units of the
flux quantum $\Phi_0 = h/2e$. For zero flux in the SQUID the coupling between the
phase of the island ϕ and the reservoir is strongest and fluctuations in ϕ are
suppressed. As a consequence, fluctuations in the number of Cooper pairs are
enhanced which results in a large increase of the supercurrent. The magnetic
field, that we apply perpendicular to the device, is of the order of a few gauss
and does not influence the other junctions of the system. The measurements
are performed at a temperature of 10 mK. We have verified that there is no
non-integral offset charge present on the island at the time of the measurement.*

larger than the charging energy. The calculated critical current is generally found to be larger than the measured switching current because of small but finite classical noise present in the leads. [14, 15, 18] The exact relation depends on the details of the environmental impedance. In absence of a generally established theory we have scaled the critical current linearly. Fig. 5.5 shows good agreement of both relative amplitude and periodicity of the maximum supercurrent in theory and experiment.

We have experimentally shown that fluctuations in the phase of the superconducting island of a double-junction system can be modulated without changing the Josephson coupling energy of the junctions that carry the bias current. The resulting modulation of the supercurrent clearly illustrates the Heisenberg uncertainty principle for phase and number of Cooper pairs on a superconductor. Squeezing the fluctuations of one variable by the coupling to a reservoir, with the purpose of enhancing the transport connected with the other conjugate variable, may find wider application in quantum coherent circuits.

References

[1] B. J. van Wees, Phys. Rev. B **44**, 2264 (1991).

[2] R. Fazio, A. van Otterlo, G. Schön, H. S. J. van der Zant and J. E. Mooij, Helvetica Physica Acta **65**, 228 (1992).

[3] M. Büttiker, Phys. Rev. B **36**, 3548 (1987).

[4] See the appendix of chapter 4 of this thesis.

[5] P. Hadley, private communication.

[6] M. Tinkham, *Introduction to Superconductivity* (McGraw-Hill, New York, 1975).

[7] P. W. Anderson, in *Progress in Low Temperature physics* **5** (ed. Gorter, C. J.), 1-43 (North-Holland, Amsterdam, 1967).

[8] P. Carruthers, and M. M. Nieto, Rev. of Mod. Phys. **40** 411 (1963).

[9] B. D. Josephson, Phys. Lett. **1**, 251 (1962).

[10] D. V. Averin and K. K. Likharev in *Mesoscopic Phenomena in Solids*, ed. Altshuler, B. L., Lee, P. A., and Webb, R. A.), 173 (Elsevier, Amsterdam, 1991).

[11] K. A. Matveev, M. Gisselfält, L. I. Glazman, M. Jonson, and R. I. Shekter, Phys. Rev. Lett. **70**, 2940 (1993).

[12] L. J. Geerligs, V. F. Anderegg, J. Romijn and J. E. Mooij, Phys. Rev. Lett. **65**, 377 (1990).

[13] M. T. Tuominen, J. M. Hergenrother, T. S. Tighe, and M. Tinkham, M. Phys., Rev. Lett. **69**, 1997 (1992).

[14] P. Joyez, P. Lafarge, A. Filipe, D. Esteve, and M. H. Devoret, Phys. Rev. Lett. **72**, 2458 (1994).

[15] T. M. Eiles and J. M. Martinis, Phys. Rev. B **50**, 627 (1994).

[16] D. B. Haviland, Y. Harada, P. Delsing, C. D. Chen, and T. Claeson, Phys. Rev. Lett. **73**, 1541 (1994).

[17] T. A. Fulton, P. L. Gammel, D. J. Bishop and L. N. Dunkleberger, Phys. Rev. Lett. **63**, 1307 (1989).

[18] R. L. Kautz and J. M. Martinis, Phys. Rev. B **42**, 9903-9932 (1990).

Summary

In this thesis we report on measurements on different networks of Josephson junctions. The capacitance C and the critical current of the junctions are such that the Josephson coupling energy is of the same order of magnitude as the charging energy $e^2/2C$. The competing influence of both energy scales leads to several interesting quantum phenomena.

In two-dimensional arrays of Josephson junctions superconductor-to-insulator (S-I) phase transitions occur as a function of the ratio between the charging energy and the Josephson coupling energy, and as a function of magnetic field. We have measured these phase transitions using arrays with different junction parameters and with square and triangular cells. The experimental results are compared to theoretical work. Special attention is payed to the dynamics of magnetically induced vortices close to the S-I transition. In a magnetic field the zero-bias resistance of the array shows an exponential dependence on temperature. For the arrays closest to the S-I transition this resistance flattens off below a certain temperature between 200 and 100 mK. The fact that in these samples a finite zero-bias resistance persists down to 10 mK indicates the presence of a quantum transport mechanism for vortices. Qualitatively the results match predictions for the thermally activated and quantum tunneling of a single particle in a potential well. To explain results quantitatively several questions remain to be solved.

We have further studied properties of vortices in the quantum regime, in a specially shaped sample where magnetically induced vortices cross along a doubly connected path. On the superconducting island enclosed by the path a charge is induced by means of a gate. The resistance arising from the vortex crossings shows clear e-periodic dependence on the induced charge. These oscillations are due to quantum interference of vortices which is a generalized form of the Aharonov-Casher effect. The quantum interference of vortices in Josephson junction arrays is fundamentally 2e-periodic, but observation of the full periodicity in our experiment is hindered by the presence of a finite number of quasiparticles.

In systems of two junctions in series, with comparable charging energy and

Josephson coupling energy, the maximum supercurrent depends on the charge induced on the island in between the two junctions. There is a subtle relation between the Aharonov-Casher effect discussed above and the gate-induced oscillations in the supercurrent through a double junction. The supercurrent can be interpreted as the current at which the sum of the phase differences of both junctions is no longer stable, or equivalently as the current at which flux quanta start to move across the junction. The two possible ways for flux quanta to cross, over the left or the right junction, form a doubly connected path. In this description the influence of a gate voltage on the supercurrent can be attributed to interference of flux quanta that move along this path. Differences between the motion of vortices in an array and the dynamics of the phase difference in a double junction are discussed.

We have also measured the supercurrent through a double junction system using a special layout. In addition to the junctions connected to the current source, the center island was connected with two junctions in parallel, a DC SQUID, to a superconducting reservoir with a large capacitance to ground. The phase of the reservoir is classical and the Josephson coupling of the SQUID squeezes the quantum mechanical fluctuations of the phase on the island. When the effective Josephson coupling of the SQUID is reduced by applying a magnetic field we observe a strong suppression of the supercurrent through the double junction. The enhancement of phase fluctuations on the island corresponds to localization of Cooper pairs. This experiment clearly demonstrates the Heisenberg uncertainty relation between charge and phase, that is the central ingredient for the quantum phenomena discussed in this thesis.

Samenvatting: Quantum phenomena in netwerken van Josephsonjuncties

In dit proefschrift wordt experimenteel onderzoek beschreven aan netwerken van Josephsonjuncties, kleine contacten van twee stukken supergeleidend materiaal met daartussen een elektrisch isolerende barrière. In het supergeleidende materiaal wordt de stroom gedragen door Cooperparen, deeltjes die bestaan uit twee gekoppelde elektronen. Om het gedrag van een supergeleider quantummechanisch te kunnen beschrijven, gebruikt men één macroscopische golffunctie, een vergelijking van de vorm $\Psi = |\Psi|e^{i\varphi}$. De amplitude $|\Psi|^2$ van die golffunctie is een maat voor het aantal Cooper paren in de supergeleider. Een directe fysische interpretatie van de fase φ van de golffunctie, die een waarde tussen 0 en 2π kan aannemen, is niet zo eenvoudig. Het blijkt echter dat in een Josephsonjunctie, waar twee supergeleiders door een dunne barrière verbonden zijn, stroom door die barrière loopt die evenredig is met het verschil in de fases van beide supergeleiders. Dat de Cooperparen door de isolerende barrière heen kunnen tunnelen is een typisch gevolg van de quantummechanica, waar geen klassiek analogon voor bestaat. In welke mate ze door de barrière tunnelen hangt af van de zogenaamde Josephson-koppelingsenergie, die bepaald wordt door de eigenschappen van de junctie.

Tweedimensionale arrays van Josephsonjuncties bestaan uit een rooster van stukken supergeleidend materiaal, de supergeleidende eilanden, die zijn verbonden met Josephson juncties. In zo'n netwerk kunnen faseverschillen geïnduceerd worden met een magneetveld dat loodrecht op het netwerk wordt aangelegd. Als gevolg hiervan ontstaan wervelstromen die vortices genoemd worden. Het gedrag van vortices vertoont veel overeenkomst met dat van deeltjes, of balletjes. Het rooster van Josephson juncties vormt een potentiaallandschap dat voorgesteld kan worden als een eierdoos. Een stroom die door het array gestuurd wordt, oefent een kracht uit op de vortices. Als de stroom groot genoeg is kunnen deze wervelstromen als geheel door het array bewegen, zoals balletjes door een gekan-

109

telde eierdoos. Doordat een bewegende vortex een spanning veroorzaakt, kan de dynamica van deze wervelstromen experimenteel bestudeerd worden.

Voor de kleine juncties die met de huidige technieken zoals beschreven in de appendix van hoofdstuk 1 kunnen worden gemaakt, hangt de grootte van de superstroom door een junctie niet meer alleen af van het faseverschil. Een Josephsonjunctie bestaat uit twee (super)geleidende vlakken met een isolerend medium daartussen, en vormt een condensator waarvan de capaciteit in eerste benadering evenredig is met de oppervlakte van de junctie. Wanneer een Cooper-paar naar een supergeleidend eiland tunnelt, zullen de condensatoren gevormd door de juncties die aan het eiland zijn verbonden elektrisch geladen worden. De ladingsenergie die hiervoor nodig is, is $e^2/2C_\Sigma$, waarbij C_Σ de som van de capaciteiten is. Juncties met een oppervlak van 0.1 μm^2 hebben een capaciteit van slechts 1 fF en bij de temperaturen rond 10 mK waarbij gemeten wordt, is er niet altijd genoeg energie beschikbaar. De relatieve sterkte van de Josephson-koppelingsenergie en de ladingsenergie bepaalt of er een superstroom door de barrière loopt of dat de barrière isolerend is. In deze systemen wordt duidelijk dat er een Heisenberg onzekerheidsrelatie bestaat tussen de fase en de lading op een supergeleider. Als de ladingsenergie klein is, wordt de stroom door de barrière volledig bepaald door het faseverschil. Als gevolg van de stroom die door de juncties loopt, zal het aantal Cooperparen op de supergeleider sterk fluctueren. Als de ladingsenergie groot is, ligt het aantal Cooperparen op een eiland vast en er kan geen superstroom lopen. Het faseverschil fluctueert zo sterk dat het fysisch een onbepaalde parameter is. De 'Quantum Phenomena' uit de titel van dit proefschrift slaan op de effecten die optreden in het gebied tussen deze twee uitersten.

In tweedimensionale netwerken, arrays, van Josephsonjuncties treedt een super-geleider-isolator faseovergang op bij het variëren van de ratio tussen de Joseph-son-koppelingsenergie en de ladingsenergie. Wanneer het array isolerend is, is het model van vortices of wervelstromen die zich als balletjes gedragen niet meer een-voudig toe te passen. Aan de supergeleidende kant, maar vlakbij de faseovergang, is het gedrag van vortices bestudeerd. Het blijkt dat de vortices die opgebouwd zijn uit biljoenen quantummechanische deeltjes, zelf ook weer quantummecha-nische effecten vertonen. Zo kan een vortex als geheel door de hobbels van het potentiaallandschap tunnelen. Als men in arrays vlak bij de overgang met het magneetveld steeds meer vortices induceert, treedt ook een supergeleider-isolator faseovergang op. De isolerende toestand wordt hier beschreven als een supergelei-dend zijn van vortices.

Als de vortex een quantummechanisch deeltje is, zal het naast deeltjes-, ook golfeigenschappen vertonen. In een speciaal ontworpen array is een experiment gedaan waarbij vortices interfereren, net als licht wat door twee gaatjes op een scherm valt. Het verschil tussen constructieve en destructieve interferentie wordt gemaakt door een lading via een kleine condensator te induceren op het eiland waar de vortices omheen bewegen. Dit effect is, behalve een indicatie dat vortices inderdaad quantummechanische deeltjes zijn, ook een manifestatie van een fundamenteel fysisch effect van interferentie van magnetische deeltjes om een lading. Naar de wetenschappers die deze interferentie voorspelden, wordt dit het Aharonov-Casher effect genoemd.

De competitie tussen ladings-, en Josephsoneffecten wordt ook veel bestudeerd in kleine systemen van bijvoorbeeld twee juncties in serie. Deze systemen worden niet met vortices beschreven, maar met het tunnelen van Cooperparen. In zo'n dubbele junctie heeft een geïnduceerde lading invloed op de superstroom. De relatie tussen dit effect en de interferentie van vortices in arrays wordt duidelijker door het systeem niet in termen van Cooperparen, maar in termen van fases te analyseren.

Tot slot beschrijven we een experiment waarin nog eens het basisprincipe van de 'Quantum Phenomena' wordt gedemonstreerd. Met een uitbreiding van de dubbele junctie kunnen fluctuaties in de fase op het eiland worden beperkt of vergroot zonder dat er verder iets verandert aan de eigenschappen van de juncties waar de stroom doorheen loopt. Met het verkleinen van de fluctuaties van de fase worden fluctuaties in het aantal Cooperparen groter en dit resulteert in een duidelijke toename van de stroom door de dubbele junctie. Dit effect is een manifestatie van de onzekerheidsrelatie van Heisenberg voor lading en fase in een supergeleider.

Wiveka Elion
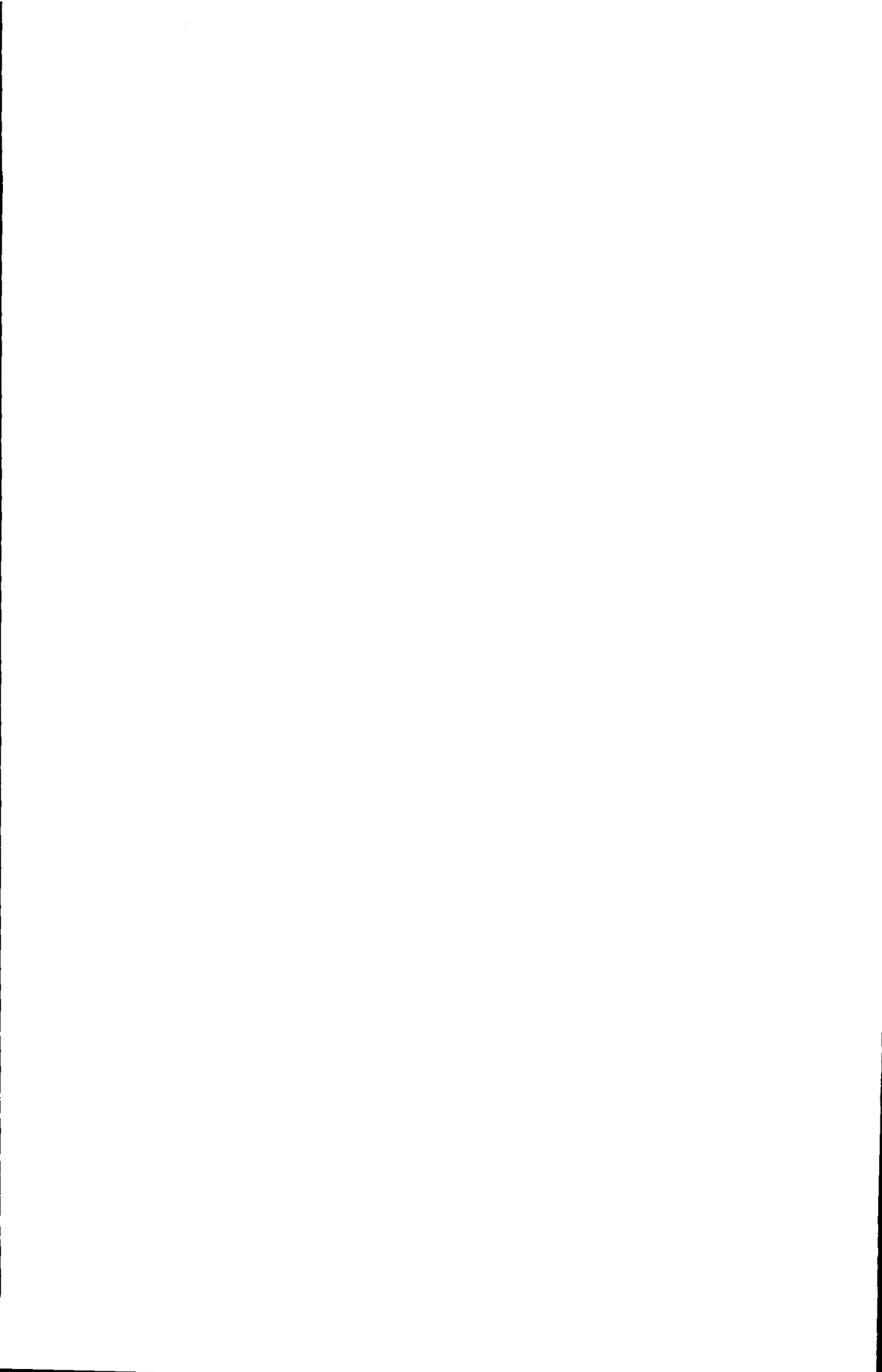
Curriculum Vitae

Wiveka Elion

July 29, 1965   Born in Leiden, the Netherlands

1977–1983   Gymnasium β, at the 'Rijnlands Lyceum', Wassenaar

1983-1984   Preparatory year at Dartington College of Arts, England

1984–1990   Physics at Leiden University
Graduate research in Solid State and Materials group of
prof. dr. L. J. de Jongh
Supervisor: dr. J. van Ruitenbeek
Thermopower of $Bi_2Sr_{2-x}La_xCuO_{6-\delta}$

1990   July-Sept.: traineeship at Calgary research center,
Shell Canada

1991–1995   Ph.D. research at Delft University of Technology, Department of Applied Physics, Solid State / Superconductivity group of prof. dr. ir. J. E. Mooij
Quantum phenomena in networks of Josephson junctions